CHALMERS

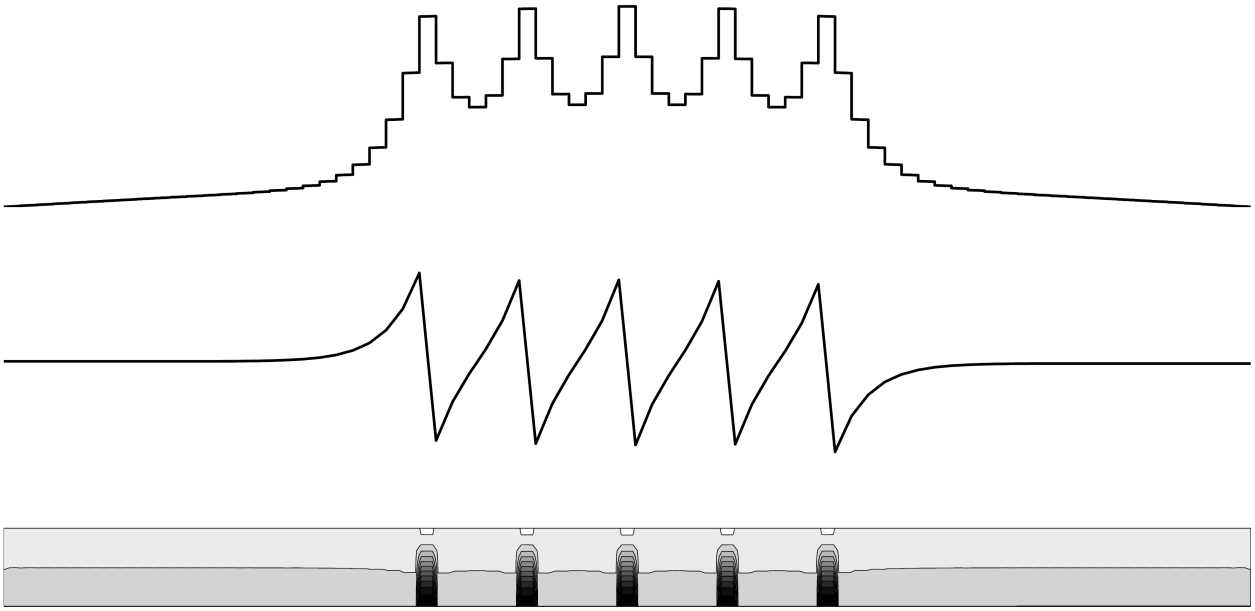

Modelling and simulation of reinforced concrete beams

Coupled analysis of imperfectly bonded reinforcement in fracturing concrete

Master's thesis in Solid and Structural Mechanics

DIMOSTHENIS FLOROS
OLAFUR AGUST INGASON

Department of Applied Mechanics
Division of Solid Mechanics
CHALMERS UNIVERSITY OF TECHNOLOGY
Göteborg, Sweden 2013
Master's thesis 2013:42

MASTER'S THESIS IN SOLID AND STRUCTURAL MECHANICS

Modelling and simulation of reinforced concrete beams

Coupled analysis of imperfectly bonded reinforcement in fracturing concrete

DIMOSTHENIS FLOROS
OLAFUR AGUST INGASON

Department of Applied Mechanics
Division of Solid Mechanics
CHALMERS UNIVERSITY OF TECHNOLOGY

Göteborg, Sweden 2013

Modelling and simulation of reinforced concrete beams
Coupled analysis of imperfectly bonded reinforcement in fracturing concrete
DIMOSTHENIS FLOROS
OLAFUR AGUST INGASON

Master's thesis 2013:42
ISSN 1652-8557
Department of Applied Mechanics
Division of Solid Mechanics
Chalmers University of Technology
SE-412 96 Göteborg
Sweden
Telephone: +46 (0)31-772 1000

Cover:
Results from the developed program not accounting for tension softening. The graphs show from the top, steel stress ,bond-slip and crack pattern

Chalmers Reproservice
Göteborg, Sweden 2013

Modelling and simulation of reinforced concrete beams
Coupled analysis of imperfectly bonded reinforcement in fracturing concrete
Master's thesis in Solid and Structural Mechanics
DIMOSTHENIS FLOROS
OLAFUR AGUST INGASON
Department of Applied Mechanics
Division of Solid Mechanics
Chalmers University of Technology

Abstract

Cracking in reinforced concrete beams is a normal process. It occurs for a small portion of the ultimate load, already in the service state. This kind of local failure in concrete is quantified mainly via crack widths and crack spacing in the tensile zone. Durability, functionality and aesthetics are the main reasons why the aforementioned characteristics should be limited to predefined values. Due to cracking, stiffness redistribution takes place in the flexural member and the reinforced concrete section can no longer be considered to act as a linear elastic, homogeneous material. In addition, the connection between the reinforcement bars and the surrounding concrete is not perfect. A certain slip in the interface between the two materials needs to be considered. Thus, the non-linear constitutive response of concrete and the bond-slip relation need to be incorporated in an accurate model of a reinforced concrete beam under fracture.

This thesis aims to develop a finite element model of a beam that is able to describe the interaction between the reinforcement bars and the cracked concrete. Emphasis is given to the parameter of the two predominant length scales in reinforced concrete structures: the local damage in concrete, which comprises the small scale, and the finite length of the reinforcement bars, which accounts for the large scale. For the development of such a 1D model, advanced beam elements were employed, where the effects of the reinforcement bars were homogenized over the concrete cross-section. The implementation and a non-linear FE analysis of the model were performed in a Matlab code. Outputs from that analysis were compared to (i) experimental results from literature, (ii) analytical calculations of a reinforced concrete beam accounting for tension stiffening, (iii) a 1D beam-type model where fracture of concrete was taken into consideration by the *stiffness adaptation method*, and, (iv) a FE beam-type model considering perfect bond between the constitutive materials developed in the Diana software. The results from the developed model were found to correspond well to the aforementioned methods and the experimental curves. However, further parametric studies are proposed in order to improve the performance of the model.

Keywords: reinforced concrete beam; cracking; bond-slip; length scales

Contents

1 Introduction

Reinforced concrete beams are flexural members which, in the ultimate limit state, are designed allowing for a certain local damage to take place, assuming all tensile forces to be carried by the steel bars. The limit of that damage in a cross-sectional design process is governed by the ultimate compressive strain of concrete so as to avoid crushing when yielding of the reinforcement bars occurs. Hence, the occurrence of cracking in concrete is a rather expected phenomenon for relatively high loads. It should be noted however, that cracks, in cases where no prestressing is applied, are expected to form even for a small portion of the ultimate load, i.e. already in the service state. In addition to the ultimate limit considerations, flexural cracks in reinforced concrete beams, according to a sound design, should be controlled with respect to width and well distributed over the length of the member.

Cracking in concrete is accompanied by overall stiffness reduction, larger deflections, lack of homogeneity of the cross-section, and it is also aesthetically undesired. Furthermore, wide cracks contribute to an increased permeability of the structural member, which under severe environmental conditions could enhance corrosion in the reinforcement, spalling of the concrete cover and local bond deterioration at the interface between the constitutive materials.

Thus, fracture in reinforced concrete beams might be harmful, but on the other hand in most structural engineering applications it cannot be avoided. These considerations highlight the importance for an accurate estimation of the crack widths and the crack pattern in structural engineering.

During the present thesis, a one-dimensional finite element model of a reinforced concrete beam was developed, that is able to describe the interaction between the cracked concrete and the reinforcement bars, while accounting also for the relative slip between the constitutive materials and the different length scales involved in the model. Namely, the microscopic scale induced by fracture of concrete and the finite length of the reinforcement bars. Crack widths and crack pattern were the outputs that the thesis focused mostly on.

After a short literature survey on the existing techniques to model fracture in reinforced concrete beams in Chapter 2, the 'construction' of the model is outlined in Chapter 3. For that purpose, an advanced beam element was applied as it is shown in Section 3.1, accompanied by the derivation of the governing equations of the continuous, as well as, the discrete system in Section 3.2. The concluding FE formulation was a non-linear system of equations, where the factors of non-linearity were induced by the non-linear constitutive models that were employed, so as to account for cracking in concrete, yielding in the steel bars and the bond-slip at the steel/concrete interface. A detailed discussion on the specific constitutive material laws that were used is presented in Section 3.4. The linearization of the non-linear system of equations is described in Section 3.3. The iterative/incremental methods that were used to solve the non-linear system of equations for each load or displacements increment are outlined in Section 3.5, followed by the numerical integration schemes that were employed in order to obtain solutions for the integrals involved in the FE equations. Then, a remedy to the issue of mesh-dependency that sourced from the use of a softening law to take cracking of concrete into consideration is given in Section 3.6. The FE formulation derived in Section 3.2, was applied in a computer program in Matlab environment. The flowchart and a description of the basic steps that were followed in the developed program is presented in Section 3.7.

In Chapter 4, the specific application of a reinforced concrete beam subjected to 'four-point bending' is examined. A comparison is provided in Section 4.4 on the load-displacement

diagrams, the maximum crack-widths and the crack-pattern obtained from the developed model and from (i) experimental results from literature, (ii) analytical calculations of a reinforced concrete beam accounting for tension stiffening, (iii) a 1D beam-type model where fracture of concrete was taken into consideration by the *stiffness adaptation method*, and, (iv) a FE beam-type model considering perfect bond between the constitutive materials developed in the Diana software. The general conclusion that was drawn was that the curves obtained from the developed model fitted well with the ones obtained from the other methods. Details on the experimental set up are given in Section 4.1. The beam theory that was used for the analytical solution of a reinforced concrete beam is outlined in Section 4.2, while the in-data that were provided in the developed model are given in Section 4.3. The present thesis sums up with a discussion on the conclusions from the modelling process in Chapter 5. At the end of the same chapter, proposals for future work are also given.

2 Modelling techniques

2.1 Modelling of the behaviour of reinforced concrete beams

Reinforced concrete beams are flexural members employed in a vast majority of civil engineering applications. For the prediction of their response, various methods are being used, either analytical or numerical. Analytical calculations of an externally statically determinate homogeneous beam with a rather simple geometry may be considered as a very familiar and easy-to-implement process, especially, as long as the concrete remains uncracked. However, if the 'problem' is to be fully defined, sources of heterogeneity in the cross-section, such as the effect of the reinforcement, material non-linearities induced by cracking of concrete and the relative slip between the constitutive materials need to be accounted for. In such cases, the problem is no longer statically determinate, nor linear elastic, thus equilibrium and compatibility conditions, as well as constitutive material laws need to occupied in a non-linear analysis for the determination of the beam characteristic figures. It can be understood that facing situations as the aforementioned analytically is restricted to very fundamental applications, due to the complexity of the nature of the problem, usually for verification of other solution strategies chosen at beforehand.

On the other hand, the difficulties in obtaining a predictive solution for cumbersome structural cases like the one just described, together with the development of very powerful computers and sophisticated non-linear numerical analysis software have promoted the implementation of numerical methods for most of the engineering applications. Among others, the finite element method is, nowadays, the most widely used numerical procedure. If it is applied correctly, it provides fast, efficient solution schemes, of accuracy specified by the user, depending on the specific case.

The finite element method that needs to be employed in a specific investigation depends on several factors, namely:

1. The scale of the structure (single member or entire structure)
2. The complexity of the problem (1D, 2D or 3D)
3. The outputs sought for (features on the global or local scale)
4. The level of accuracy
5. The limitations of the model (material or geometric non-linearities, computational tools available)

In general, when a finite element analysis is to be performed, the main issue the analyst has to face is that of the balance between the accuracy and the computational cost. For the global analysis of a relatively large structure, a detailed model would probably be computationally 'expensive' or even unnecessary. On the other hand, in the examination of structural members or simple geometries, the development of a refined model that is able to describe more complex phenomena is, often, feasible and essential. Such complex phenomena may include various

kinds of non-linearities, arising either from the material behaviour or the specimen's geometry, as well as local scale effects.

As regards to cracking in reinforced concrete structures, it belongs to local damage effects. Together with another phenomenon, that of the relative slip between concrete and reinforcing steel, they form two main sources of non-linearity in the composite material. For the aforementioned characteristics to be captured, advanced computational methods need to be developed. The term, advanced, may stand for more sophisticated constitutive models for the materials, or for special elements that need to be implemented apart from the structural elements out of which the main part of the model is comprised of.

2.1.1 3D modelling

Beams are usually not modelled with 3D solid elements since it requires more computational effort than 1D structural elements or 2D continuum elements. There are some advantages of using 3D elements. They can capture failure modes that are not available with other type of elements e.g. spalling and anchorage failure in support regions. The reinforcement in 3D solid elements can be modelled in different ways. As a 3D solid element, where each bar is modelled with separate 3D solid elements with different constitutive relations. With this analysis it is possible to insert an interface layer between the concrete and steel or to model the reinforcement as embedded, i.e. full interaction between the two materials. The interface layer can prescribe the bond-slip action between the two materials and needs to be predefined with a constitutive model. The reinforcement can also be modelled as 2D plane, assigning an equivalent thickness of the reinforcement layer, or as 1D truss, with the cross section of each bar defined within the 3D solid. In both cases, it is available in commercial software to model the bond-slip relation with special interface elements , line-solid interface for 1D and plane-solid interface for 2D, or as embedded reinforcement. Smeared crack model is often used to model the cracking phenomena in the concrete (Lykidis et al., 2008 [22]). It is convenient to use the smeared crack approach since it does not require special elements to describe the cracks, like e.g. discrete crack approach.[31]

This type of modelling is not appropriate when predicting crack widths and crack patterns because of the unnecessary complexity and additional computational effort needed.

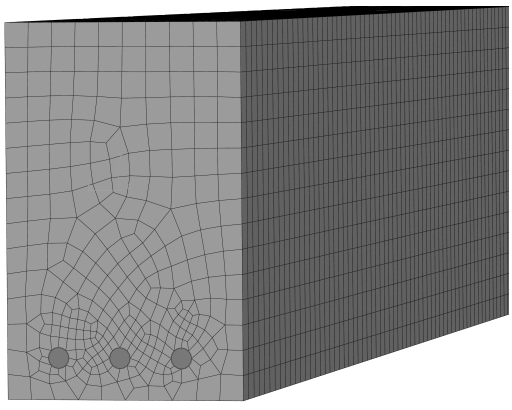

Figure 2.1: *3D modelling of a reinforced concrete beam*

2.1.2 2D modelling

Like with 3D modelling, 2D modelling of beams is usually not carried out when looking at a global behavior of a beam. However when looking at cracking, i.e. crack widths and crack patterns, the 2D analysis can be feasible.

Since the beam is relatively long compared to its width plane stress elements are commonly used to model beams in 2D analysis. The reinforcement can be modelled with 2D and 1D elements as embedded reinforcement or with slip, with line-plane interface for 2D reinforcement and line for bar reinforcement [5]. Like with 3D models, the smeared crack approach is often used to account for cracking.

2.2 Beam models

In general, an one-dimensional element is represented by a line, in which a certain cross-sectional area is assigned. It can be comprised either of only one material, a fact that would characterize it as *homogeneous*, or of many additional ones, which are then homogenized over the cross-section. The simplest FE model that can be implemented is made of two-node *bar*, or else, *truss* elements, having one or two translational degrees of freedom per node (Figure 2.2). Higher order 1D elements are used as well when more complicate phenomena are to be captured, which then contain more than two nodes and approximating functions of higher order. A special place in the 'family' of 1D elements is held by the so-called *beam* or *structural* elements.

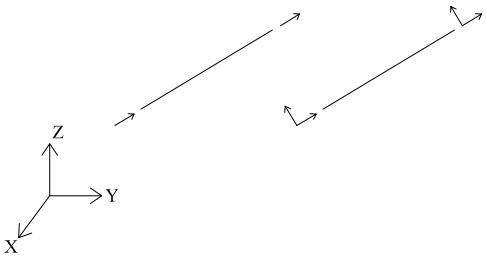

Figure 2.2: *Simplest possible finite elements*

In their simplest form, as shown in Figure 2.3, they are met as two-node elements, with a vertical translational and a rotational degree of freedom per node. It is probably the most widely known and used finite element, mainly due to the simplifications that usually lie behind its constitutive theories and the low computational cost, factors that are making it very user-friendly. Substantial realm of such theories is covered by the principle that 'plane sections remain plane and perpendicular to the reference axis of the beam', known also as the *Euler-Bernoulli* beam theory (Ottosen and Petersson, 1992 [29]). Examples of their use are when the global response of a whole structure is sought for, or, when structural cases of profound bending are examined.

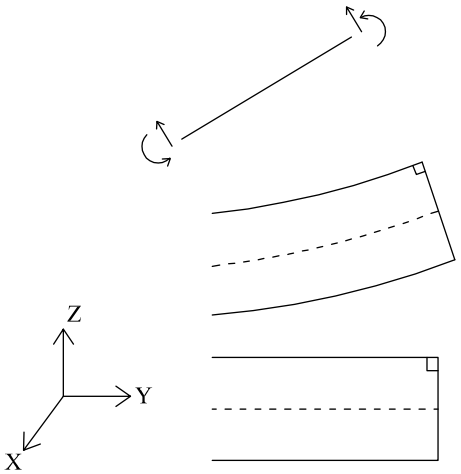

Figure 2.3: *Euler-Bernoulli beam theory*

Another popular theory, that 'plane sections remain plane but not necessarily perpendicular to the reference axis', or else, the *Timoshenko* beam theory is often employed (Hjelmstad, 2005 [14]). Models comprised of *Timoshenko* beam elements are also used for the global structural analysis, they have similar advantages as the *Euler-Bernoulli* elements, but their main use is in cases where shear action is considered to be important for the prediction of the response of the member under consideration (Figure 2.4).

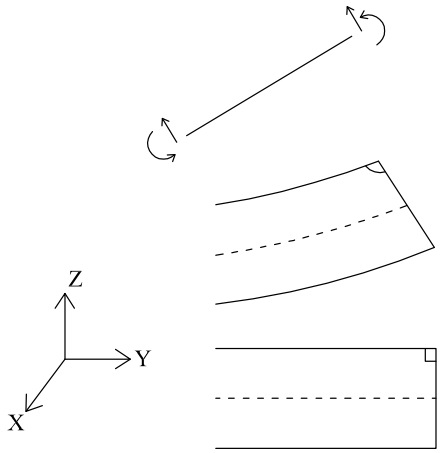

Figure 2.4: *Timoshenko beam theory*

The next one-dimensional element to be described is also known as *plane-frame* element. It can be combined with both beam theories mentioned before, while it also accounts for the axial displacement of the reference axis of the element (Figure 2.5). The pertinent element is used in simulations of plane frame structures and, in general, in applications where the axial motion of the system is of importance. As it will be shown in Section 2.2.1, the consideration of the axial displacement degree of freedom is very useful for modelling effects and geometries that take place and exist, respectively, in the axial direction of the model, as is the effect of the reinforcement and the bold-slip in reinforced concrete members.

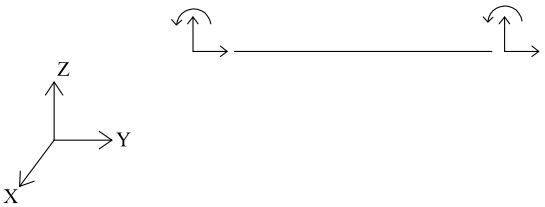

Figure 2.5: *Plane-frame element*

Furthermore, apart from the aforementioned fundamental structural elements, more advanced 1D beam-type models have been developed. These are usually comprised of more than one material, homogenized over the cross-section and they employ more specialized modelling techniques. The construction of such models was motivated from the need to cover in a simplified, but nevertheless, representative manner more complicated tasks, which may involve several localized phenomena that would not be feasible to capture by using the *Euler-Bernoulli* or the *Timoshenko* beam theory alone. Examples of such elements are outlined in Section 2.2.1.

2.2.1 Multi-fibre beam model

As mentioned earlier, the simulation of large civil engineering structures, might prove to be a cumbersome process. For that reason, a simplified method has been introduced (Spacone et al., 1996 [36], Mazars et al., 2004 [23], Kotronis and Mazars, 2005 [19]). Namely, the assembly into consideration is discretized into beam elements that comply with the *Euler-Bernoulli* or the *Timoshenko* beam theory. Usually, flexural members, such as beams, are analysed according to the *Euler-Bernoulli* beam theory. In cases where shear phenomena are more pronounced, the *Timoshenko* theory for beams is employed. What is new in the pertinent method is the division of the cross-section into fibers (Figure 2.6). Each fiber, represents a finite area of the cross-section, as well as, it is made of one of the constitutive materials, concrete and steel.

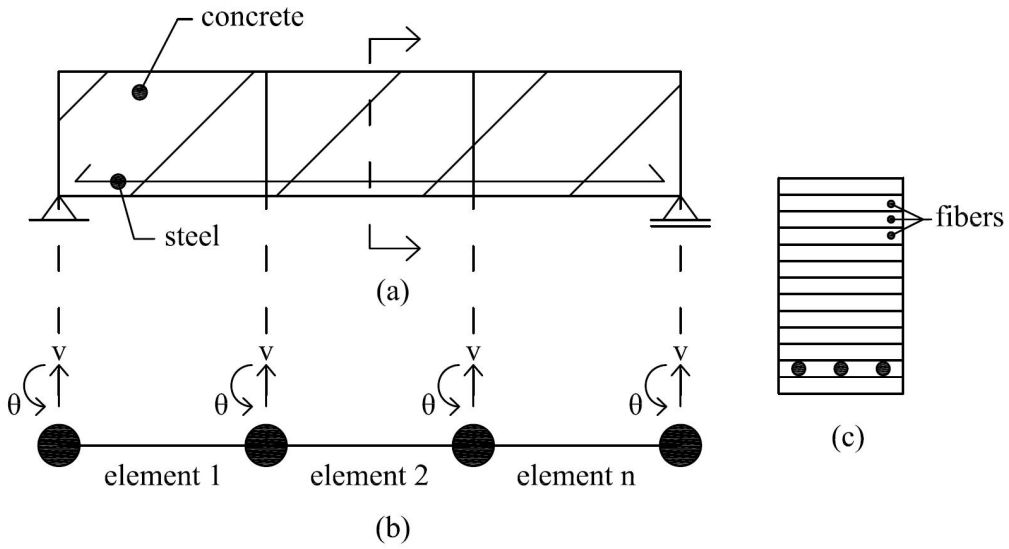

Figure 2.6: *Multi-fiber beam model (a) Reinforced concrete specimen (b) Discretization into elements, nodes, degrees of freedom (c) Separation of the cross-section into fibers*

In the implementation scheme of the proposed method, the main assumption that plain sections remain plane holds. Based on that assumption, the well-known beam theories mentioned in the previous paragraph are applicable. The calculation of the model is realized in three levels, a) the element, b) the sectional and c) the fiber level. Through the fundamental beam theories, the nodal displacements of the simulated member are related to the normal strains (in the case of the *Euler-Bernoulli* beam theory) via a relationship of the form

$$\varepsilon_{xx} = \frac{\partial u^o}{\partial x} + z\frac{\partial^2 w}{\partial x^2} \tag{2.1}$$

where, $\partial u^o/\partial x$, accounts for the axial deformation of the reference axis of the beam, $\partial^2 w/\partial x^2$, is the curvature, and, z, denotes the position of the fiber along the cross-section of the beam. As a next step, the sectional strain of each fiber obtained from (2.1) is inserted into the constitutive law that is assigned for the material of the fiber, in order to derive the stress at the point where the fiber lies along the cross-sectional height.

2.2.2 Applications accounting for the damaged concrete

Early stage applications of the simplified method are attributed to Spacone et al., 1996 [36], Mazars et al., 2004 [23], Kotronis and Mazars, 2005 [19]. Common characteristic of the cited works is that they do not include any relevant slip between the steel and the concrete fibers. Thus, full bond conditions are considered between the constitutive materials. The fibers in this case, depending on their position along the cross-sectional height, represent either concrete in tension/compression or the steel bars. In that sense, two material laws are implemented.

In their article on simplified dynamic analysis of reinforced concrete walls, Kotronis and Mazars [19] depict two examples of the multi-fiber approach on reinforced concrete walls. In these applications, beam elements complying with either the *Euler-Bernoulli* or the *Timoshenko* beam theory were used for the discretization of the member in the global scale. Non-linearities resulting from fracture and cyclic loading were inserted into the analysis via the material constitutive models in the fibers scale. Uni-axial continuum damage mechanics stress-strain relation was employed for concrete. Two damage variables, one for tension and one for compression (dynamic loading conditions are accompanied by sign reversal of the load) were introduced in the concrete material law, ranging from one to zero. By means of these two variables, the stiffness properties of concrete, namely Young's modulus, E, and Poisson's ratio, ν, were degrading through each load cycle. As regards to steel, a uni-axial plasticity law including non-linear kinematic hardening was applied (Armstrong and Frederick, 1966 [10]).

A general conclusion that was drawn by the use of the aforementioned model for concrete is the difficulty to obtain results in extensively damaged regions, for instance crack spacing and crack-widths, outputs that were of major interest in the present thesis. It would take an advanced 3D constitutive law to capture localized fracture more accurately. Another disadvantage that should be noted is the mesh-dependency of the results due to the strain softening law in tension that was used in the concrete model. One solution to that problem is obtained by the use of non-local constitutive models, as described by Pijaudier-Cabot and Bazant, 1987 [30]. The theory recommends to separate the total strain into an elastic part, which would follow a local material law, and an inelastic part, that would be attributed to cracking and the variables associated to that part of the strain, they would be treated by non-local damage model. Another way to get rid of the obstacle of mesh-dependency is provided in Kotronis et al., 2005 [20] by local second gradient theory. However, as it was also applied by the authors in the present thesis, an efficient way to 'tackle' mesh-dependency upon mesh refinement is to scale the stress-strain softening law expressed in terms of the crack width, w, with the area where each crack is expected to localize, as explained in Section 3.6.

In Mazars et al., 2004 [23] the benefits of using two simplified approaches are exposed on two reinforced concrete wall specimens under seismic excitation. The first model is comprised of *Euler-Bernoulli* beam elements on the global scale and each cross-section is divided into fibers. La Borderie uni-axial model [21] is employed for concrete, so as to account for all the non-linear effects arising from dynamic loading such as earthquake. The same plasticity law as in Kotronis and Mazars, 2005 [19] is used for steel (Armstrong and Frederick, 1966 [10]). Next, the second model is realized via *Timoshenko* beam elements. The Pontiroli-Rouquand-Mazars (PRM [34]) constitutive relation is applied for concrete, whereas the elasto-plastic material law available in Abaqus CAE is implemented for steel.

The two simplified models presented in the latter article are computationally efficient and they are able to represent global phenomena, as well as some fundamental local ones, in a satisfactory way. However, more advanced 3D modelling, as stated by the authors, would be necessary in order to describe localized fracture in more accurate manner.

2.2.3 Applications accounting for cracking and bond-slip

As it has already been outlined, the inclusion of the properties of the steel/concrete interface is important for an appropriate description of the response of reinforced concrete structures, together with the consideration of local scale effects, like fracture of concrete. Towards this necessity, significant contribution has been the work by Monti and Spacone, 2000 [26]. The basic formulation at the element and the sectional scale is similar to the one described in Section 2.2.1.

However, in Monti and Spacone, 2000 [26], in order to account for the relative slip, the perfect bond assumption is no longer valid. Instead, in the fibers scale, the total strain of the steel fiber is divided into a part which accounts for the deformation of the reinforcing bar and a second part that considers the relative slip between the constitutive materials. So, the deformations compatibility condition is stated this time between the surrounding concrete strain and the total steel fiber strain.

For the purpose of such an analysis, a multi-fiber finite element model has been developed. *Timoshenko* beam elements have been used for the discretization of the members, so as to account for shear phenomena. Following the same procedure with the fiber-models presented in the previous sections, the cross-section of the beam elements was subdivided into fibers. Depending on the position of the fibers along the cross-section, the appropriate constitutive laws have been implemented for the materials. Namely, the Hognestad model [15] was occupied for concrete (Figure 2.7.a), while the Menegotto-Pinto model was applied for steel [25] (Figure 2.7.b). Eligehausen's bond-slip law was used to describe the behavior of the model at the interface, as it was introduced in [6] and proposed in [3] (Figure 2.7.c).

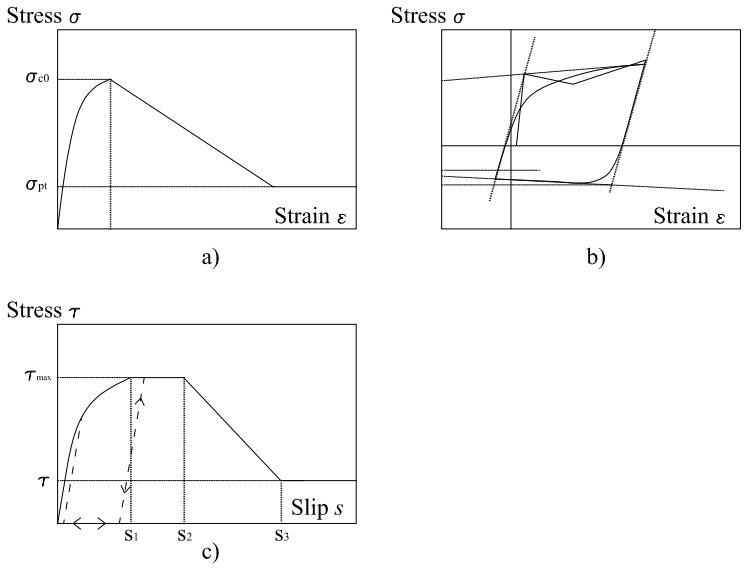

Figure 2.7: *Constitutive material models (a) Hognestad law for concrete (b) Menegotto-Pinto law for steel (c) Eligehausen law for bond-slip*

3 A model for reinforced concrete beams

To develop a simplified one-dimensional reinforced concrete beam model, that should be able to describe the interaction between the cracked concrete and the rebars, a standard procedure was followed regarding the establishment of the finite element model. According to that process, a derivation took place first, which started from stating the *strong form* for the 'problem' of a reinforced concrete beam subjected to transverse and longitudinal distributed loading. Then, the *weak form* of the differential equations that cover the pertinent problem was obtained. Later on, the finite element formulation of the non-linear problem was derived, together with the linearization of the non-linear relationships. Finally, appropriate iterative/incremental procedures and integration schemes were employed for the numerical solution of the non-linear finite element form.

The theoretical foundations of the derivation mentioned in the previous paragraph was the basis for the finite element code constructed at the next step. The outputs from the developed computer program were then used for comparison with relevant tests from literature, figures obtained from analytical calculations, the finite element stiffness adaptation method, as well as with a 'perfect bond' model performed using the Diana software.

Furthermore, the fundamental problem solved in the present thesis was that of a reinforced concrete beam with vertical distributed load. The definition of the beam and the loading conditions can be seen in Figure 3.1.

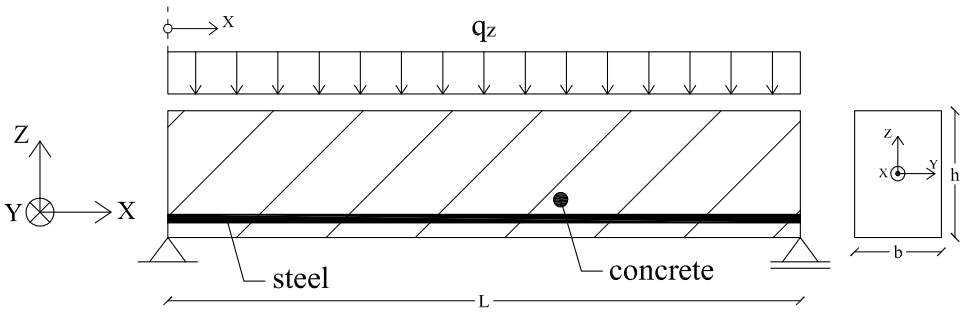

Figure 3.1: *Example of a simply supported reinforced concrete beam*

3.1 Derivation of the non-linear continuous formulation

3.1.1 Cross sectional forces

At the cross-section scale, by definition, the following equations hold for the internal forces $\overline{M}$, $\overline{V}$, $\overline{N}$ and $\overline{N}_i$, whereas, the contribution of the steel bars is taken into account in (3.1) and (3.3), apart from the concrete contribution for a typical homogeneous cross-section.

The axial force $\overline{N}$ is defined by

$$\overline{N} = \int_A \sigma_{xx}^{conc}\, dA + \sum_i A_i \sigma_{si} \tag{3.1}$$

where σ_{xx}^{conc}, is the axial concrete stress across the cross-section A. The shear force $\overline{V}$ is given by

$$\overline{V} = \int_A \sigma_{xz}\, dA \tag{3.2}$$

where, σ_{xz}, is the shear stress across the concrete cross-section. The bending moment $\overline{M}$ is calculated as

$$\overline{M} = \int_A z \cdot \sigma_{xx}^{conc}\, dA + \sum_i A_i \cdot z_i \sigma_{si} \tag{3.3}$$

and, for each layer of n-reinforcement bars, the axial force of each layer is returned by

$$\overline{N}_i = A_i \cdot \sigma_{si} \tag{3.4}$$

where, A_i, denotes the total area of the n_{bars} within the i-st layer of reinforcement, n_{bars} accounts for the number of bars contained in the i-st layer, and, σ_{si}, is the axial steel stress of the i-st layer. Finally, the definition of the bond force between the i-st layer of reinforcement and the surrounding concrete is introduced here, according to the relationship

$$f_i = \tau_{xx}^{bond} \cdot s_i \tag{3.5}$$

where, τ_{xx}^{bond}, is the longitudinal bond stress between the constitutive materials and, s_i, is the sum of the circumference of the n_{bars} that comprise the i-st steel layer.

3.1.2 Equilibrium conditions

As a next step, the equilibrium conditions that are applicable for the beam under consideration are outlined. First, consider an infinitesimal part of the beam, as shown in Figure 3.2.

From equilibrium in the vertical direction (over the height of the cross-section), it can be stated

$$\sum F_z = 0 \Rightarrow -\overline{V} + \overline{V} + \partial\overline{V} + q_z \cdot \partial x = 0$$

$$\Rightarrow -\frac{\partial \overline{V}}{\partial x} = q_z \tag{3.6}$$

A bending moment equation around the left-most point of the reference axis of the beam can be written as

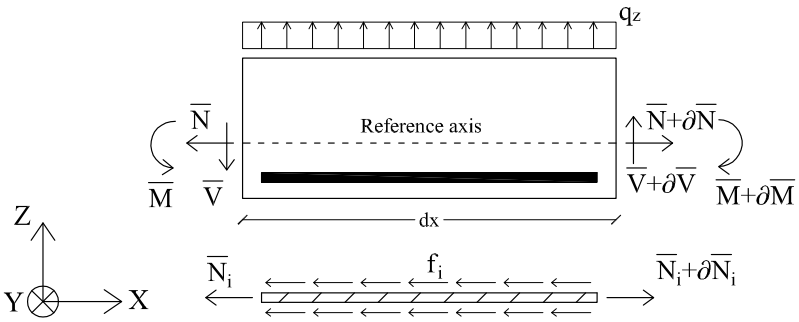

Figure 3.2: *Internal forces of an infinitely small part of a reinforced concrete beam*

$$\sum M_{left} = 0 \Rightarrow (\overline{M} + \partial\overline{M}) - (\overline{V} + \partial\overline{V})\partial x + q_z \cdot \partial x \cdot \frac{\partial x}{2} - \overline{M} = 0$$

$$\Rightarrow \frac{\partial\overline{M}}{\partial x} - \overline{V} - \underbrace{\partial\overline{V} + q_z \cdot \frac{\partial x}{2}}_{infinitesimal} = 0$$

$$\Rightarrow \frac{\partial\overline{M}}{\partial x} - \overline{V} = 0 \tag{3.7}$$

Equilibrium between the forces in the horizontal (longitudinal) direction requires

$$\sum F_x = 0 \Rightarrow \overline{N} + \partial\overline{N} - \overline{N} = 0$$

$$\Rightarrow \frac{\partial\overline{N}}{\partial x} = 0 \tag{3.8}$$

Now, from equilibrium between the longitudinal stress of the i-st layer of reinforcement and the relevant bond stress coming from the surrounding concrete, it can be derived (lower part of Figure 3.2)

$$\sum F_x^{bar} = 0 \Rightarrow \overline{N}_i + \partial\overline{N}_i - \overline{N}_i - f_i \cdot \partial x = 0$$

$$\Rightarrow -\frac{\partial\overline{N}_i}{\partial x} + f_i = 0 \tag{3.9}$$

Next, inserting (3.6) into (3.7) it is obtained

$$-\frac{\partial^2\overline{M}}{\partial x^2} = q_z \tag{3.10}$$

3.1.3 Kinematic relations

The basic principle of *Bernoulli's* theory, namely that *plane sections remain plane and perpendicular to the reference axis of the beam* is considered. From that assumption, fundamental kinematic relations can be derived for the small deformations of the flexural member in the x- and z- axis (Figure 3.3).

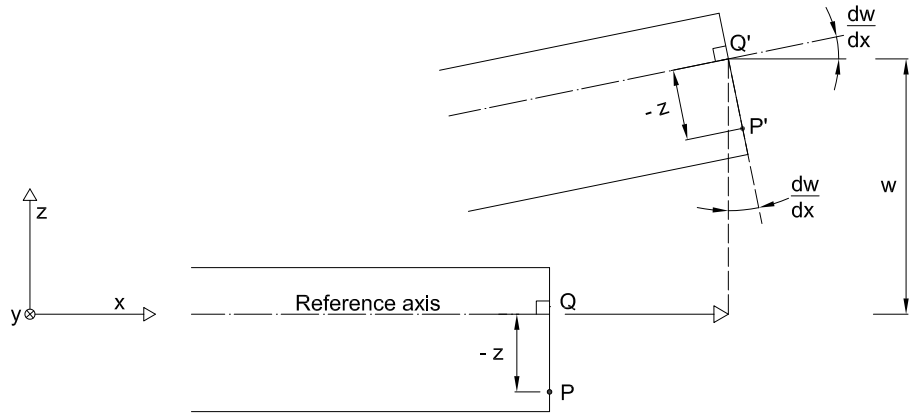

Figure 3.3: *Deformation of an Euler-Bernoulli beam (adopted from Ottesen and Petersson [29])*

To begin with, exploiting *Bernoulli's* principle, the axial displacement u_x of a point P, which is situated below the reference axis of the beam, as it can be seen from Figure 3.3, is described by (3.11.a). Moreover, the assumptions of no *Poisson's* effect in the transverse y-y direction across the width of the cross-section (3.11.b), as well as the hypothesis that u^o and w are functions of x (3.11.c) and (3.11.d), limit the problem into an one-dimensional formulation with dependency only on the axial direction (longitudinal stresses). In the mathematical fields that are to follow, the notation used in [29] is employed.

$$a)\ u_x = u^o - z\frac{\partial w}{\partial x}, \quad b)\ u_y = 0, \quad c)\ u^o = u^o(x), \quad d)\ w = w(x) \tag{3.11}$$

Having defined the displacements field, then it is straightforward to derive the strains field, by using the very well-known equations

$$\begin{aligned} \varepsilon_{xx} &= \frac{\partial u_x}{\partial x} \quad , \quad \gamma_{xy} = \frac{\partial u_x}{\partial y} + \frac{\partial u_y}{\partial x} \\ \varepsilon_{yy} &= \frac{\partial u_x}{\partial y} \quad , \quad \gamma_{xz} = \frac{\partial u_x}{\partial z} + \frac{\partial u_z}{\partial x} \\ \varepsilon_{zz} &= \frac{\partial u_z}{\partial z} \quad , \quad \gamma_{yz} = \frac{\partial u_y}{\partial z} + \frac{\partial u_z}{\partial y} \end{aligned} \tag{3.12}$$

Combining (3.11) and (3.12), the normal strain of the concrete beam and the i-st layer of steel can be determined, as

$$\varepsilon_{xx}^{conc}(x,z) = \frac{\partial u^o}{\partial x} - z\frac{\partial^2 w}{\partial x^2} \tag{3.13}$$

$$\varepsilon_{xx,i}^{bar}(x) = \frac{\partial u^o}{\partial x} - z_i\frac{\partial^2 w}{dx^2} + \frac{\partial \Delta_i}{\partial x} \tag{3.14}$$

where u^o is the axial displacement at the reference axis
Δ_i is the bond-slip between the i-st layer of reinforcement and the surrounding concrete

As it can be seen from (3.13), the axial strain of any point at the concrete beam is a function of the horizontal translation, $u^o(x)$, of the reference axis at the section where the point belongs, and the curvature, $\kappa = \partial^2 w/\partial x^2$. As for the axial strain of the i-st layer of reinforcement (3.14), the deformation of the steel layer equals to the deformation of concrete at the height of the reinforcement layer, plus the contribution from the relative slip, Δ_i, between the constitutive materials.

In other words, the compatibility condition that holds between the i-st layer of reinforcement and the surrounding concrete can be expressed in a more appropriate manner, in the displacements field, as

$$\Delta_i(x) = u_i(x) - u^o(x) + z_i\frac{\partial w(x)}{\partial x} \tag{3.15}$$

where, $u_i(x)$, denotes the axial displacement of the i-st steel layer.

3.2 FE formulation

3.2.1 Differential equations and boundary conditions

Equations (3.8), (3.9) and (3.10) are the equilibrium equations which along with the boundary conditions (Table 3.1) make up the strong form of the problem. In these equations, there are $(2n+2)$ unknown sectional forces $(\overline{N}, \overline{M}, \overline{N}_n, \overline{f}_n)$, while only $(n+2)$ equilibrium equations exist. Thus, compatibility conditions and constitutive relations are needed for the solution of such an internally statically indeterminate member.

$$\frac{\partial \overline{N}}{\partial x} = 0 \quad , \quad 0 \leq x \leq L \tag{3.16}$$

$$-\frac{\partial^2 \overline{M}}{\partial x^2} = q_z \quad , \quad 0 \leq x \leq L \tag{3.17}$$

$$-\frac{\partial \overline{N}_i}{\partial x} + f_i = 0 \quad , \quad a_i \leq x \leq b_i \tag{3.18}$$

where, L, is the length of the beam, and, a_i, b_i, are the starting and the ending points, respectively, of the i-st layer of reinforcement in the longitudinal direction of the beam.

3.2.2 Weak form

After 'constructing' the strong form of the problem (Section 3.2.1), and, in order to 'get rid' of the derivatives accompanying the internal variables, the weak, or variational, form of the equations needs to be employed.

The first step on the way to extract the weak form is to multiply (3.16), (3.17) and (3.18) by arbitrary test-functions δu^0, δw and $\delta \Delta_i$, respectively, and integrate over the appropriate for each variable domain

$$\int_L \delta u^o \frac{\partial \overline{N}}{\partial x} \, dx = 0 \tag{3.19}$$

$$-\int_L \delta w \frac{\partial^2 \overline{M}}{\partial x^2} \, dx = \int_L \delta w \cdot q_z \, dx \tag{3.20}$$

$$-\int_{a_i}^{b_i} \delta \Delta_i \frac{\partial \overline{N}_i}{\partial x} \, dx + \int_{a_i}^{b_i} \delta \Delta_i \cdot f_i \, dx = 0 \tag{3.21}$$

and, secondly, to perform integration by parts once for (3.19) and (3.21), and twice for (3.20). In that sense, (3.19) becomes

$$\int_L \frac{\partial \delta u^o}{\partial x} \overline{N} \, dx = \left[\delta u^o \overline{N}\right]_0^L \tag{3.22}$$

while, (3.20) takes the form

$$-\int_L \frac{\partial^2 \delta w}{\partial x^2} \overline{M} \, dx = \int_L \delta w \cdot q_z \, dx - \left[\frac{\partial \delta w}{\partial x} \overline{M}\right]_0^L + \left[\delta w \cdot \overline{V}\right]_0^L \tag{3.23}$$

and, similarly, (3.21) reforms to

$$\int_{a_i}^{b_i} \left(\frac{\partial \delta \Delta_i}{\partial x} \overline{N}_i + \delta \Delta_i \cdot f_i\right) \, dx = \left[\delta \Delta_i \cdot \overline{N}_i\right]_{a_i}^{b_i} \tag{3.24}$$

At this point, as a by-product of the integration by parts, the boundary terms of the load vector have appeared at the RHS of (3.22), (3.23) and (3.24). These terms lie upon the points of the domain, where either the forces and the moments are prescribed as 'natural' boundary conditions or the displacements are prescribed as 'essential' boundary conditions. Thus, where the 'natural' boundary vector is known, the relevant boundary terms can be determined, while at the points where the essential boundary conditions are defined, the respective boundary terms vanish simply by setting the pertinent test-function to zero. The equations (3.22), (3.23) and (3.24) along with the boundary conditions comprise the weak form of the differential equations. Examples of possible boundary conditions, as well as, the specific boundary conditions that need to applied in order to avoid rigid body motion of the reinforced concrete beam under consideration are given in Section 3.2.3.

3.2.3 Boundary conditions

A beam element accounting for bond-slip has 4 degrees of freedom in each node, horizontal translation (x-direction), vertical translation (z-direction), rotation around y-axis and slip in the interface between concrete and steel. That means for the simplest case a straight beam supported in two nodes at the ends needs 8 boundary conditions essential, natural or convective. Convective boundary conditions are a combination of essential and natural.

Table 3.1: Possible essential (Dirichlet) and natural (Neumann) boundary conditions for the reinforced beam element accounting for bond-slip

Degree of freedom	Essential	Natural
Horizontal translation	u^o	Normal force $\overline{N}$
Vertical translation	w	Shear force $\overline{V}$
Rotation	θ_y	Moment $\overline{M}$
Slip	Δ_i	Normal (anchoring) force $\overline{N}_i$

In Table 3.1 the possible boundary conditions are listed. However there are certain limitations to what boundary conditions combinations give unique solutions. To avoid rigid body motion both the criteria below need to be fulfilled:

- at least one degree of freedom in the horizontal direction has to be prescribed.
- one vertical translational degree of freedom and one rotational or two vertical translational degrees of freedom need to be prescribed

3.2.4 Constitutive equations

So far, the internal variables $(\overline{N}, \overline{M}, \overline{N}_n, \overline{f}_n)$ in the strong form were inserted in the relevant equations as forces. In the subsequent chapters, the pertinent forces are restated, using the definitions of (3.1), (3.3), (3.4) and (3.5), thus introducing the relevant constitutive operators, that represent the constitutive models of the materials. Symbolically, the substitutions just described take the form

$$\sigma_{xx}^{conc} = \sigma_{xx}^{conc}(\varepsilon_{xx}^{conc}(x,z))$$

$$\sigma_{xx}^{bar} = \sigma_{xx}^{bar}(\varepsilon_{xx}^{bar}(x))$$

$$\tau_{xx}^{bond} = \tau_{xx}^{bond}(\Delta_i(x))$$

In that manner, the force-displacement relations of the strong form of (3.16), (3.17) and (3.18) are to be turned into stress-deformation relations in the sections that come next. As it will be shown, with the strains already defined in a typical step of the chosen solution scheme, the stresses are then obtained through the constitutive law set for each material. The material laws just mentioned, can be chosen, so far, arbitrarily by the programmer, due to the general form that is kept for the derivation of the finite element equations outlined in the present chapter.

3.2.5 Introduce the constitutive relations into the weak form

At the current section, the semi-linear $a(u;v)$ form and the load vector $L(v)$ of the problem are to be defined, a notation that is adopted here in order to facilitate the rest of the derivation process. For that purpose, the equations of the weak form, (3.22), (3.23) and (3.24) can be restated as

$$a_{u^o}(u^o, w, \Delta_i; \delta u^o) = L_{u^o}(\delta u^o) \tag{3.25}$$

$$a_w(u^o, w, \Delta_i; \delta w) = L_w(\delta w) \tag{3.26}$$

$$a_{\Delta_i}(u^o, w, \Delta_i; \delta \Delta_i) = L_{\Delta_i}(\delta \Delta_i) \tag{3.27}$$

respectively, where, a_{u^o}, L_{u^o} are defined as

$$a_{u^o}(u^o, w, \Delta_i; \delta u^o) = \int_L \frac{\partial \delta u^o}{\partial x} \left[\int_A \sigma_{xx}^{conc}(\varepsilon_{xx}^{conc})\, dA + \sum_i A_i \cdot \sigma_{si}(\varepsilon_{xx}^{bar}) \right] dx =$$

$$= \int_L \frac{\partial \delta u^o}{\partial x} \left[\int_A \sigma_{xx}^{conc} \left(\frac{\partial u^o}{\partial x} - z \frac{\partial^2 w}{\partial x^2} \right) dA + \sum_i A_i \cdot \sigma_{si} \left(\frac{\partial u^o}{\partial x} - z_i \frac{\partial^2 w}{\partial x^2} + \frac{\partial \Delta_i}{\delta x} \right) \right] dx \tag{3.28}$$

and,

$$L_{u^o}(\delta u^o) = \left[\delta u^o \overline{N} \right]_0^L \tag{3.29}$$

while, a_w, L_w stand for

$$a_w(u^o, w, \Delta_i; \delta w) = \int_L \frac{\partial^2 \delta w}{\partial x^2} \left\{ - \left[\int_A z \cdot \sigma_{xx}^{conc} \left(\varepsilon_{xx}^{conc} \right) dA + \sum_i A_i \cdot z_i \cdot \sigma_{si} \left(\varepsilon_{xx}^{bar} \right) \right] \right\} dx =$$

$$= \int_L \frac{\partial^2 \delta w}{\partial x^2} \left\{ - \left[\int_A z \cdot \sigma_{xx}^{conc} \left(\frac{\partial u^o}{\partial x} - z \frac{\partial^2 w}{\partial x^2} \right) dA + \right. \right.$$

$$\left. \left. + \sum_i A_i \cdot z_i \cdot \sigma_s \left(\frac{\partial u^o}{\partial x} - z_i \frac{\partial^2 w}{\partial x^2} + \frac{\partial \Delta_i}{\delta x} \right) \right] \right\} dx \tag{3.30}$$

and,

$$L_w(\delta w) = \int_L \delta w \cdot q_z \; dx - \left[\frac{\partial \delta w}{\partial x} \overline{M} \right]_0^L + \left[\delta w \cdot \overline{V} \right]_0^L \tag{3.31}$$

whereas, a_{Δ_i}, L_{Δ_i} account for

$$a_{\Delta_i}(u^o, w, \Delta_i; \delta \Delta_i) = \int_{a_i}^{b_i} \left[\frac{\partial \delta \Delta_i}{\partial x} A_i \cdot \sigma_{si} \left(\varepsilon_{xx}^{bar} \right) - \delta \Delta_i \cdot s_i \cdot \tau_{xx}^{bond} \left(\Delta_i(x) \right) \right] dx \tag{3.32}$$

and,

$$L_{\Delta_i}(\delta \Delta_i) = \left[\delta \Delta_i \cdot \overline{N}_i \right]_{a_i}^{b_i} \tag{3.33}$$

where, s_i, is the sum of the circumference of the reinforcement bars used at the i-st steel layer.

3.2.6 Discretization of the continuous displacements field

Until this point, the equations used in the strong form (3.16), (3.17) and (3.18), as well as, in the weak form of the problem (3.22), (3.23) and (3.24), are continuous over the respective domain of each internal variable. In order to transmit the aforementioned relations into finite element equations, they need to be discretized. For that purpose, the approximations on u^o, w and Δ_i have to be introduced, according to

$$\begin{array}{lcll} u^o & \approx & \boldsymbol{u_h^o}(x) & = \boldsymbol{N_{u^o}}(x) \cdot \boldsymbol{a_{u^o}} \\ w & \approx & \boldsymbol{w_h}(x) & = \boldsymbol{N_w}(x) \cdot \boldsymbol{a_w} \\ \Delta_i & \approx & \boldsymbol{\Delta_{i,h}}(x) & = \boldsymbol{N_{\Delta_i}}(x) \cdot \boldsymbol{a_{\Delta_i}} \end{array}$$

where, $\boldsymbol{N_{u^o}}$, $\boldsymbol{N_w}$ and $\boldsymbol{N_{\Delta_i}}$ are shape functions, while $\boldsymbol{a_{u^o}}, \boldsymbol{a_w}$ and $\boldsymbol{a_{\Delta_i}}$ contain the nodal values of u^o, w and Δ_i.

Then, the axial displacement of the reference axis of the beam can be written as

$$u^o(x) \approx \boldsymbol{N_{u^o}}(x) \boldsymbol{a_{u^o}} \Rightarrow \frac{\partial u^o}{\partial x} \approx \frac{\partial \boldsymbol{N_{u^o}(x)}}{\partial x} \boldsymbol{a_{u^o}} = \boldsymbol{B_{u^o}}(x) \boldsymbol{a_{u^o}} \tag{3.34}$$

In a finite element, the shape functions that are to be used for the approximation of the expected deformed shape of the beam in the longitudinal direction take the form

$$\boldsymbol{N_{u^o}^e}(x) = [N_1^e, N_2^e] = \left[-\frac{1}{L^e} (x - x_2) \, , \frac{1}{L^e} (x - x_1) \right]$$

Similarly, the continuous field of the deflections of the beam after discretization becomes

$$w \approx \boldsymbol{N_w}(x)\boldsymbol{a_w} \Rightarrow \frac{\partial^2 w}{\partial x^2} \approx \frac{\partial^2 \boldsymbol{N_w}(x)}{\partial x^2}\boldsymbol{a_w} = \boldsymbol{B_w}\boldsymbol{a_w} \tag{3.35}$$

The approximating functions that describe the deflected form of the beam in the i-st finite element are given by

$$\boldsymbol{N_w^e}(x) = [N_1^e, N_2^e, N_3^e, N_4^e] =$$

$$= \left[1 - \frac{3x^2}{L^{e2}} + \frac{2x^3}{L^{e3}}, x\left(1 - \frac{2x}{L^e} + \frac{x^2}{L^{e2}}\right), \frac{x^2}{L^{e2}}\left(3 - \frac{2x}{L^e}\right), \frac{x^2}{L^e}\left(\frac{x}{L^e} - 1\right)\right]$$

Finally, for the the field of the relative slip between the constitutive materials it is deduced

$$\Delta_i \approx \boldsymbol{N_{\Delta_i}}(x)\boldsymbol{a_{\Delta_i}} \Rightarrow \frac{\partial \Delta_i(x)}{\partial x} \approx \frac{\partial \boldsymbol{N_{\Delta_i}}(x)}{\partial x}\boldsymbol{a_{\Delta_i}} = \boldsymbol{B_{\Delta_i}}\boldsymbol{a_{\Delta_i}} \tag{3.36}$$

The shape functions that are to be occupied to describe the anticipated slip relation between the concrete and the rebars in the finite element have the form

$$\boldsymbol{N_{\Delta_i}^e}(x) = [N_1^e, N_2^e] = \left[-\frac{1}{L^e}(x - x_2), \frac{1}{L^e}(x - x_1)\right]$$

3.2.7 Galerkin's method

Referring back at Section 3.2.2, the term *test-functions* was mentioned. This term, or else the *weight-functions*, symbolically stated as δu^o, δw and $\delta\Delta_i$ is used to denote the virtual displacements of the system in the directions of u^o, w and Δ_i, respectively. As it has already been stated, the pertinent functions can be chosen arbitrarily. However, there have been developed different methods for the choice of the test-functions, and one which is very functional is *Galerkin's method*. It belongs to the 'family' of *weighted residual methods*, together with other ones, as the *Point collocation method*, the *Subdomain collocation method* and the *Least-squares method*, as described in [29].

In the present thesis, *Galerkin's method* is followed for the appropriate choice of the test-functions. The basic idea behind it is to choose the weight-functions the same as the shape functions. For instance, the first weight-function δu^o is taken as

$$\delta u^o \approx \boldsymbol{N_{u^o}}(x)\boldsymbol{c_{u^o}} = \boldsymbol{c_{u^o}^T}\boldsymbol{N_{u^o}^T}(x) \ (\delta u^o \text{ is scalar})$$

$$\Rightarrow \frac{\partial \delta u^o}{\partial x} \approx \frac{\partial \boldsymbol{N_{u^o}}(x)}{\partial x}\boldsymbol{c_{u^o}} = \boldsymbol{B_{u^o}}\boldsymbol{c_{u^o}} = \boldsymbol{c_{u^o}^T}\boldsymbol{B_{u^o}^T} \tag{3.37}$$

whereas, δw, is chosen as

$$\delta w \approx \boldsymbol{N_w}(x)\boldsymbol{c_w} = \boldsymbol{c_w^T}\boldsymbol{N_w^T}(x) \ (\delta w \text{ is scalar})$$

$$\Rightarrow \frac{\partial^2 \delta w}{\partial x^2} \approx \frac{\partial^2 \boldsymbol{N_w}(x)}{\partial x^2}\boldsymbol{c_w} = \boldsymbol{B_w}\boldsymbol{c_w} = \boldsymbol{c_w^T}\boldsymbol{B_w^T} \tag{3.38}$$

and, in the same manner, $\delta\Delta_i$ is replaced by

$$\delta\Delta_i \approx \boldsymbol{N_{\Delta_i}}(x)\boldsymbol{c_{\Delta_i}} = \boldsymbol{c_{\Delta_i}^T}\boldsymbol{N_{\Delta_i}^T}(x) \ (\delta\Delta_i \text{ is scalar})$$

$$\Rightarrow \frac{\partial \delta\Delta_i}{\partial x} \approx \frac{\partial \boldsymbol{N}_{\boldsymbol{\Delta_i}}(x)}{\partial x}\boldsymbol{c}_{\boldsymbol{\Delta_i}} = \boldsymbol{B}_{\boldsymbol{\Delta_i}}\boldsymbol{c}_{\boldsymbol{\Delta_i}} = \boldsymbol{c}^{\boldsymbol{T}}_{\boldsymbol{\Delta_i}}\boldsymbol{B}^{\boldsymbol{T}}_{\boldsymbol{\Delta_i}} \tag{3.39}$$

In the equations above, $\boldsymbol{c_{u^o}}$, $\boldsymbol{c_w}$ and $\boldsymbol{c_{\Delta_i}}$ are column matrices of arbitrary coefficients.

3.2.8 Formulation of the internal force vector

After defining the approximations on u_o, w, Δ_i in (3.34), (3.35) and (3.36) at Section 3.2, and the weight-functions δu_o, δw, $\delta\Delta_i$ in (3.37), (3.38) and (3.39) at Section 3.2.7, the internal force vector, $\boldsymbol{f_{int}}$, can be deduced, by introducing them into the variational form of the problem stated in (3.28) to (3.33).

Replacing, first, the approximated displacement fields and test-functions into (3.25), (3.28) and (3.29), it is derived

$$\boldsymbol{c}^{\boldsymbol{T}}_{\boldsymbol{u^o}} \left\{ \int_L \boldsymbol{B}^{\boldsymbol{T}}_{\boldsymbol{u^o}} \left[\int_A \sigma^{con}_{xx}(\boldsymbol{B}_{\boldsymbol{u^o}}\boldsymbol{a}_{\boldsymbol{u^o}} - z\boldsymbol{B}_{\boldsymbol{w}}\boldsymbol{a}_{\boldsymbol{w}})dA + \right.\right.$$

$$\left.\left. + \sum_i A_i \cdot \sigma_{si}(\boldsymbol{B}_{\boldsymbol{u^o}}\boldsymbol{a}_{\boldsymbol{u^o}} - z_i\boldsymbol{B}_{\boldsymbol{w}}\boldsymbol{a}_{\boldsymbol{w}} + \boldsymbol{B}_{\boldsymbol{\Delta_i}}\boldsymbol{a}_{\boldsymbol{\Delta_i}}) \right] dx \right\} = \boldsymbol{c}^{\boldsymbol{T}}_{\boldsymbol{u^o}} \left\{ \left[\boldsymbol{N}^{\boldsymbol{T}}_{\boldsymbol{u^o}} \overline{N} \right]^L_0 \right\}$$

$$\Rightarrow \boldsymbol{c}^{\boldsymbol{T}}_{\boldsymbol{u^o}} \boldsymbol{f}_{\boldsymbol{int,u^o}}(\boldsymbol{a}_{\boldsymbol{u^o}}, \boldsymbol{a}_{\boldsymbol{w}}, \boldsymbol{a}_{\boldsymbol{\Delta_i}}) = \boldsymbol{c}^{\boldsymbol{T}}_{\boldsymbol{u^o}} \boldsymbol{f}_{\boldsymbol{u^o}} \tag{3.40}$$

Similarly, upon introduction of the discretized displacements and weight-functions into (3.26), (3.30) and (3.31), it is obtained

$$\boldsymbol{c}^{\boldsymbol{T}}_{\boldsymbol{w}} \int_L \boldsymbol{B}^{\boldsymbol{T}}_{\boldsymbol{w}} \left\{ - \left[\int_A z \cdot \sigma^{con}_{xx}(\boldsymbol{B}_{\boldsymbol{u^o}}\boldsymbol{a}_{\boldsymbol{u^o}} - z\boldsymbol{B}_{\boldsymbol{w}}\boldsymbol{a}_{\boldsymbol{w}})dA + \right.\right.$$

$$\left.\left. + \sum_i A_i \cdot z_i \cdot \sigma_{si}(\boldsymbol{B}_{\boldsymbol{u^o}}\boldsymbol{a}_{\boldsymbol{u^o}} - z_i\boldsymbol{B}_{\boldsymbol{w}}\boldsymbol{a}_{\boldsymbol{w}} + \boldsymbol{B}_{\boldsymbol{\Delta_i}}\boldsymbol{a}_{\boldsymbol{\Delta_i}}) \right] \right\} dx =$$

$$\boldsymbol{c}^{\boldsymbol{T}}_{\boldsymbol{w}} \left\{ \int_L \boldsymbol{N}^{\boldsymbol{T}}_{\boldsymbol{w}} q_z dx - \left[\frac{\partial \boldsymbol{N}^{\boldsymbol{T}}_{\boldsymbol{w}}}{\partial x} \overline{M} \right]^L_0 + \left[\boldsymbol{N}^{\boldsymbol{T}}_{\boldsymbol{w}} \overline{V} \right]^L_0 \right\}$$

$$\Rightarrow \boldsymbol{c}^{\boldsymbol{T}}_{\boldsymbol{w}} \boldsymbol{f}_{\boldsymbol{int,w}}(\boldsymbol{a}_{\boldsymbol{u^o}}, \boldsymbol{a}_{\boldsymbol{w}}, \boldsymbol{a}_{\boldsymbol{\Delta_i}}) = \boldsymbol{c}^{\boldsymbol{T}}_{\boldsymbol{w}} \boldsymbol{f}_{\boldsymbol{w}} \tag{3.41}$$

Following the same procedure for (3.27), (3.32) and (3.33), results in

$$\boldsymbol{c}^{\boldsymbol{T}}_{\boldsymbol{\Delta_i}} \int_{a_i}^{b_i} \left[\boldsymbol{B}^{\boldsymbol{T}}_{\boldsymbol{\Delta_i}} \cdot A_i \cdot \sigma_{si} \left(\boldsymbol{B}_{\boldsymbol{u^o}}\boldsymbol{a}_{\boldsymbol{u^o}} - z_i\boldsymbol{B}_{\boldsymbol{w}}\boldsymbol{a}_{\boldsymbol{w}} + \boldsymbol{B}_{\boldsymbol{\Delta_i}}\boldsymbol{a}_{\boldsymbol{\Delta_i}} \right) + \right.$$

$$\left. + \boldsymbol{N}^{\boldsymbol{T}}_{\boldsymbol{\Delta_i}} \cdot s_i \cdot \tau^{bond}_{xx} \left(\boldsymbol{N}_{\boldsymbol{\Delta_i}}\boldsymbol{a}_{\boldsymbol{\Delta_i}} \right) \right] dx = \boldsymbol{c}^{\boldsymbol{T}}_{\boldsymbol{\Delta_i}} \left[\boldsymbol{N}^{\boldsymbol{T}}_{\boldsymbol{\Delta_i}} \overline{N_i} \right]^{b_i}_{a_i}$$

$$\Rightarrow \boldsymbol{c}^{\boldsymbol{T}}_{\boldsymbol{\Delta_i}} \boldsymbol{f}_{\boldsymbol{int,\Delta_i}}(\boldsymbol{a}_{\boldsymbol{u^o}}, \boldsymbol{a}_{\boldsymbol{w}}, \boldsymbol{a}_{\boldsymbol{\Delta_i}}) = \boldsymbol{c}^{\boldsymbol{T}}_{\boldsymbol{\Delta_i}} \boldsymbol{f}_{\boldsymbol{\Delta_i}} \tag{3.42}$$

Assembling the components $\boldsymbol{f_{int,u^o}}$, $\boldsymbol{f_{int,w}}$, and $\boldsymbol{f_{int,\Delta_i}}$ determined in (3.40), (3.41) and (3.42), respectively, into the total internal force vector $\boldsymbol{f_{int}}$, it can be written

$$\boldsymbol{c}^{\boldsymbol{T}} \boldsymbol{f}_{\boldsymbol{int}}(\boldsymbol{a}) = \boldsymbol{c}^{\boldsymbol{T}} \boldsymbol{f} \tag{3.43}$$

where

$$\boldsymbol{f_{int}}(\boldsymbol{a}) = \begin{bmatrix} \boldsymbol{f_{int,u^o}}(\boldsymbol{a}) \\ \boldsymbol{f_{int,w}}(\boldsymbol{a}) \\ \boldsymbol{f_{int,\Delta_i}}(\boldsymbol{a}) \end{bmatrix}, \ \boldsymbol{a} = \begin{bmatrix} \boldsymbol{a_{u^o}} \\ \boldsymbol{a_w} \\ \boldsymbol{a_{\Delta_i}} \end{bmatrix}, \ \boldsymbol{f} = \begin{bmatrix} \boldsymbol{f_{u^o}} \\ \boldsymbol{f_w} \\ \boldsymbol{f_{\Delta_i}} \end{bmatrix}, \ \boldsymbol{c} = \begin{bmatrix} \boldsymbol{c_{u^o}} \\ \boldsymbol{c_w} \\ \boldsymbol{c_{\Delta_i}} \end{bmatrix}$$

3.2.9 Involve essential boundary conditions

In order to obtain a solution for the displacements, $\boldsymbol{a}$, that satisfies (3.43), it is convenient to discretize the full vector, $\boldsymbol{a}$, into *free* and *constrained* degrees of freedom, according to

$$\boldsymbol{a} = \begin{bmatrix} \boldsymbol{a_F} \\ \boldsymbol{a_C} \end{bmatrix}, \quad \text{where} \quad \boldsymbol{a_F} = \begin{bmatrix} a_1 \\ a_2 \\ \vdots \\ a_{N_{free}} \end{bmatrix}, \ \boldsymbol{a_C} = \begin{bmatrix} a_{N_{free}+1} \\ a_{N_{free}+2} \\ \vdots \\ a_{N_{dof}} \end{bmatrix} \tag{3.44}$$

where, $\boldsymbol{a_C}$, is a vector containing the prescribed degrees of freedom, while, $\boldsymbol{a_F}$, are the unknown ones.

Similarly, the same categorization can be done for the shape functions, as well

$$\boldsymbol{N} = \begin{bmatrix} \boldsymbol{N_F} & \boldsymbol{N_C} \end{bmatrix} \tag{3.45}$$

The approximated non-linear system is fully defined at this stage, and, it can be stated as the problem of finding $u_h^o \in \mathbb{V}_h$, $w_h \in \mathbb{W}_h$ and $\Delta_{i,h} \in \mathbb{D}_h$ such that

$$a(u_h^o; \delta u_h^o) = L(\delta u_h^o) \tag{3.46}$$

$$a(w_h; \delta w_h) = L(\delta w_h) \tag{3.47}$$

$$a(\Delta_{i,h}; \delta \Delta_{i,h}) = L(\delta \Delta_{i,h}) \tag{3.48}$$

where, the trial spaces are set as follows

$$\mathbb{V}_h = \left\{ u_h^o : \ u^o = \boldsymbol{N_{u^o,F}} \boldsymbol{a_{u^o,F}} + \boldsymbol{N_{u^o,C}} \boldsymbol{a_{u^o,C}} \ \text{ for any } \ \boldsymbol{a_{u^o,F}} \in \mathbb{R}^{N_{u^o,free}} \right\}$$

$$\mathbb{W}_h = \left\{ w_h : \ w = \boldsymbol{N_{w,F}} \boldsymbol{a_{w,F}} + \boldsymbol{N_{w,C}} \boldsymbol{a_{w,C}} \ \text{ for any } \ \boldsymbol{a_{w,F}} \in \mathbb{R}^{N_{w,free}} \right\}$$

$$\mathbb{D}_h = \left\{ \Delta_{i,h} : \ \Delta_i = \boldsymbol{N_{\Delta_i,F}} \boldsymbol{a_{\Delta_i,F}} + \boldsymbol{N_{\Delta_i,C}} \boldsymbol{a_{\Delta_i,C}} \ \text{ for any } \ \boldsymbol{a_{\Delta_i,F}} \in \mathbb{R}^{N_{\Delta_i,free}} \right\}$$

while, the FE test spaces are defined as

$$\mathbb{V}_h^o = \left\{ u_h^o : \ u^o = \boldsymbol{N_{u^o,F}} \boldsymbol{c_{u^o,F}} \ \text{ for any } \ \boldsymbol{c_{u^o,F}} \in \mathbb{R}^{N_{u^o,free}} \right\}$$

$$\mathbb{W}_h^o = \left\{ w_h : \ w = \boldsymbol{N_{w,F}} \boldsymbol{c_{w,F}} \ \text{ for any } \ \boldsymbol{c_{w,F}} \in \mathbb{R}^{N_{w,free}} \right\}$$

$$\mathbb{D}_h^o = \left\{ \Delta_{i,h} : \ \Delta_i = \boldsymbol{N_{\Delta_i,F}} \boldsymbol{c_{\Delta_i,F}} \ \text{ for any } \ \boldsymbol{c_{\Delta_i,F}} \in \mathbb{R}^{N_{\Delta_i,free}} \right\}$$

Referring back to the non-linear system of equations in (3.43), after the separation accomplished in (3.44) and (3.45), the unknown displacements $\boldsymbol{a_F}$ can be determined via the solution of a reduced system of equations, which takes into account only the free degrees of freedom. The pertinent approach is realized by setting all the arbitrary coefficients contained in $\boldsymbol{c_C^T}$ equal to zero in (3.43). Thus, the system takes the form

$$\begin{bmatrix} \boldsymbol{c_F^T} & \boldsymbol{0} \end{bmatrix} \begin{bmatrix} \boldsymbol{f_{int,F}} \\ \boldsymbol{f_{int,C}} \end{bmatrix} = \begin{bmatrix} \boldsymbol{c_F^T} & \boldsymbol{0} \end{bmatrix} \begin{bmatrix} \boldsymbol{f_F} \\ \boldsymbol{f_C} \end{bmatrix} \tag{3.49}$$

while,

$$\boldsymbol{f_C} = \boldsymbol{f_{l,C}} + \boldsymbol{f_{b,C}} = \boldsymbol{f_{int,C}}(\boldsymbol{a}) \tag{3.50}$$

In (3.50), $\boldsymbol{f_{l,C}}$, denotes the *external force vector* and, $\boldsymbol{f_{b,C}}$, accounts for the *boundary load vector*. The reduced system of equations becomes

$$\boldsymbol{f_{int,F}}(\boldsymbol{a}) = \boldsymbol{f_F}$$

$$\Rightarrow \boldsymbol{g}(\boldsymbol{a_F}) = \boldsymbol{0} \tag{3.51}$$

where, $\boldsymbol{g}$, is known as the *out-of-balance* force vector, numerically defines the *residual* of the finite element equations and is given by

$$\boldsymbol{g}(\boldsymbol{a_F}) = \boldsymbol{f_{int,F}}\left(\begin{bmatrix} \boldsymbol{a_F} \\ \boldsymbol{a_C} \end{bmatrix}\right) - \boldsymbol{f_F} \tag{3.52}$$

After solving (3.51) for $\boldsymbol{a}$, it is possible to define $\boldsymbol{f_{int,C}}$ in (3.50) and, thereafter, to solve (3.50) for the boundary vector $\boldsymbol{f_{b,C}}$. The latter column matrix represents the 'reaction forces' that arise from the application of the constraints at the relevant degrees of freedom.

3.3 Linearization of the non-linear problem

The system of equations (3.51) is a system of $\mathbb{N}_{free}$ non-linear equations. The factor of non-linearity originates directly from the constitutive laws that are to be implemented for the materials. Thus, in order to obtain a solution for the unknown displacements in the iterative solution scheme that is to be used later on, a linearization of the system should be performed first, as described in the following derivation.

For that purpose, the *residuals* of the continuous system in question, namely (3.25), (3.26) and (3.27) are defined, as

$$R_{u^o} = L_{u^o}(\delta u^o) - a_{u^o}(u^o, w, \Delta_i; \delta u^o) \tag{3.53}$$

$$R_w = L_w(\delta w) - a_w(u^o, w, \Delta_i; \delta w) \tag{3.54}$$

$$R_{\Delta_i} = L_{\Delta_i}(\delta \Delta_i) - a_{\Delta_i}(u^o, w, \Delta_i; \delta \Delta_i) \tag{3.55}$$

At this point, a function a^* reasonably close to the true solution of the system of (3.53), (3.54) and (3.55) is assumed. Then, for the latter equations it can be written

$$R(a^*; v) = L(v) - a(a^*, v) \tag{3.56}$$

Employing the linearization of (3.25), (3.26) and (3.27), which comprise the *semi-linear form*, the residual in (3.56) is linearized according to

$$R(a^* + \Delta a; v) \approx R(a^*; v) - a'(a^*; v, \Delta a) \tag{3.57}$$

where, $R(a^*; v)$, is given by (3.56) and, $a'(a^*; v, \Delta a)$, is the *directional derivative* of $a(a^*; v)$ in the direction of Δa.

3.3.1 Linearization of the FE-equations

As it was described for the continuous system in the previous section, a similar linearization scheme is performed for the discrete equations (3.51). Namely, a 'good' guess $\boldsymbol{a^*}$ of the approximate solution $\boldsymbol{a}$ is assumed. In matrix form it can be stated as

$$\boldsymbol{a^*} \approx \boldsymbol{a} \Rightarrow \boldsymbol{a^*} = \begin{bmatrix} \boldsymbol{u^{o*}} \\ \boldsymbol{w^*} \\ \boldsymbol{\Delta_i^*} \end{bmatrix} \approx \boldsymbol{a} = \begin{bmatrix} \boldsymbol{u^o} \\ \boldsymbol{w} \\ \boldsymbol{\Delta_i} \end{bmatrix}$$

In (3.52), the *out-of-balance* force vector was defined as

$$\boldsymbol{g}(\boldsymbol{a}) = \boldsymbol{f_{int}}(\boldsymbol{a}) - \boldsymbol{f}$$

Considering then a small change $\Delta \boldsymbol{a_F}$ in $\boldsymbol{a^*}$, then, expanding $\boldsymbol{g}(\boldsymbol{a_F^*} + \Delta \boldsymbol{a_F})$ in Taylor series, it is obtained

$$\boldsymbol{g}(\boldsymbol{a_F^*} + \Delta \boldsymbol{a_F}) \approx \boldsymbol{g}(\boldsymbol{a_F^*}) + \frac{d\boldsymbol{g}}{d\boldsymbol{a_F^*}}(\boldsymbol{a_F^*}) \Delta \boldsymbol{a_F} \tag{3.58}$$

where, $\boldsymbol{g}(\boldsymbol{a}_{\boldsymbol{F}}^*)$, is the value of function $\boldsymbol{g}$ evaluated at $\boldsymbol{a}_{\boldsymbol{F}}^*$ and $d\boldsymbol{g}/d\boldsymbol{a}_{\boldsymbol{F}}^*$ is the derivative of $\boldsymbol{g}$ in terms of $\boldsymbol{a}_{\boldsymbol{F}}^*$, or else, the *tangent stiffness* matrix.

Finally, comparing the linearized *residual* of the continuous equations (3.57) and the linearized *out-of-balance* force vector in (3.58), it can be observed by term-wise identification the correspondence between $R(a^*;v)$ and $\boldsymbol{g}(\boldsymbol{a}_{\boldsymbol{F}}^*)$, as well as, between, $-a'(a^*;v,\Delta a)$, and $d\boldsymbol{g}/d\boldsymbol{a}_{\boldsymbol{F}}^*(\boldsymbol{a}_{\boldsymbol{F}}^*)\Delta\boldsymbol{a}_{\boldsymbol{F}}$. Next, the directional derivatives of the semi-linear form of (3.25), (3.26) and (3.27) in the direction of Δu^o, Δw and $\Delta\Delta_i$ are to be derived. Thus, having three equations and three directions each, results in nine equations for the derivatives, which after introducing the approximations on u^o, w and Δ_i, the nine components-submatrices of the tangent stiffness matrix will be defined.

To begin with, the directional derivative of (3.25) in the direction of Δu^o is given by

$$
\begin{aligned}
a'_{u^o u^o}(u^{o*},w^*,\Delta_i^*;\delta u^o,\Delta u^o) &= \frac{\partial}{\partial\varepsilon}a_{u^o}(u^{o*}+\varepsilon\Delta u^o,w^*,\Delta_i^*;\delta u^o)\Big|_{\varepsilon=0} = \\
&= \frac{\partial}{\partial\varepsilon}\left\{\int_L \frac{\partial\delta u^o}{\partial x}\left[\int_A \sigma_{xx}^{con}\left(\frac{\partial(u^{o*}+\varepsilon\Delta u^o)}{\partial x}-z\frac{\partial^2 w^*}{\partial x^2}\right)dA+\right.\right. \\
&\left.\left.+\sum_i A_i\sigma_{si}\left(\frac{\partial(u^{o*}+\varepsilon\Delta u^o)}{\partial x}-z_i\frac{\partial^2 w^*}{\partial x^2}+\frac{\partial\Delta_i^*}{\partial x}\right)\right]dx\right\}\Bigg|_{\varepsilon=0} = \\
&= \int_L \frac{\partial\delta u^o}{\partial x}\left[\int_A \frac{\partial\sigma_{xx}^{con}}{\partial\varepsilon}dA+\sum_i A_i\frac{\partial\sigma_{si}}{\partial\varepsilon}\right]\frac{\partial\Delta u^o}{\partial x}dx
\end{aligned}
\tag{3.59}
$$

Introducing the approximations on u^{o*}, w^*, Δ_i^* and $\delta u^o, \Delta u^o$ into (3.59) leads to

$$
\begin{aligned}
a'_{u^o u^o}(\boldsymbol{N}\boldsymbol{a}^*;\boldsymbol{N}_{\boldsymbol{u^o}}\boldsymbol{c}_{\boldsymbol{u^o}},\boldsymbol{N}_{\boldsymbol{u^o}}\Delta\boldsymbol{a}_{\boldsymbol{u^o}}) &= \boldsymbol{c}_{\boldsymbol{u^o}}^{\boldsymbol{T}}\int_L \boldsymbol{B}_{\boldsymbol{u^o}}^{\boldsymbol{T}}\left[\int_A \frac{\partial\sigma_{xx}^{con}}{\partial\varepsilon}dA+\sum_i A_i\frac{\partial\sigma_{si}}{\partial\varepsilon}\right]\boldsymbol{B}_{\boldsymbol{u^o}}dx\Delta\boldsymbol{a}_{\boldsymbol{u^o}} = \\
&= \boldsymbol{c}_{\boldsymbol{u^o}}^{\boldsymbol{T}}\boldsymbol{K}_{\boldsymbol{u^o u^o}}\Delta\boldsymbol{a}_{\boldsymbol{u^o}}
\end{aligned}
\tag{3.60}
$$

where

$$
\boldsymbol{K}_{\boldsymbol{u^o u^o}} = \int_L \boldsymbol{B}_{\boldsymbol{u^o}}^{\boldsymbol{T}}\left[\int_A \frac{\partial\sigma_{xx}^{con}}{\partial\varepsilon}dA+\sum_i A_i\frac{\partial\sigma_{si}}{\partial\varepsilon}\right]\boldsymbol{B}_{\boldsymbol{u^o}}dx \tag{3.61}
$$

Similarly, the derivative of (3.25) in the direction of Δw becomes

$$
\begin{aligned}
a'_{u^o w}(u^{o*},w^*,\Delta_i^*;\delta u^o,\Delta w) &= \frac{\partial}{\partial\varepsilon}a_{u^o}(u^{o*},w^*+\varepsilon\Delta w,\Delta_i^*;\delta u^o)\Big|_{\varepsilon=0} = \\
&= \frac{\partial}{\partial\varepsilon}\left\{\int_L \frac{\partial\delta u^o}{\partial x}\left[\int_A \sigma_{xx}^{con}\left(\frac{\partial u^{o*}}{\partial x}-z\frac{\partial^2(w^*+\varepsilon\Delta w)}{\partial x^2}\right)dA+\right.\right. \\
&\left.\left.+\sum_i A_i\sigma_{si}\left(\frac{\partial u^{o*}}{\partial x}-z_i\frac{\partial^2\left(w^*+\varepsilon\Delta w\right)}{\partial x^2}+\frac{\partial\Delta_i^*}{\partial x}\right)\right]dx\right\}\Bigg|_{\varepsilon=0} = \\
&= \int_L \frac{\partial\delta u^o}{\partial x}\left\{-\left[\int_A z\frac{\partial\sigma_{xx}^{con}}{\partial\varepsilon}dA+\sum_i A_i z_i\frac{\partial\sigma_{si}}{\partial\varepsilon}\right]\right\}\frac{\partial^2\Delta w}{\partial x^2}dx
\end{aligned}
\tag{3.62}
$$

Introducing the approximations on u^{o*}, w^*, Δ_i^* and $\delta u^o, \Delta w$ into (3.62) results in

$$a'_{u^o w}(\boldsymbol{N a^*}; \boldsymbol{N_{u^o} c_{u^o}}, \boldsymbol{N_w \Delta a_w}) = \boldsymbol{c_{u^o}^T} \int_L \boldsymbol{B_{u^o}^T} \left\{ - \left[\int_A z \frac{\partial \sigma_{xx}^{con}}{\partial \varepsilon} dA + \sum_i A_i z_i \frac{\partial \sigma_{si}}{\partial \varepsilon} \right] \right\} \boldsymbol{B_w} dx \Delta \boldsymbol{a_w} =$$

$$= \boldsymbol{c_{u^o}^T K_{u^o w}} \Delta \boldsymbol{a_w} \tag{3.63}$$

where

$$\boldsymbol{K_{u^o w}} = \int_L \boldsymbol{B_{u^o}^T} \left\{ - \left[\int_A z \frac{\partial \sigma_{xx}^{con}}{\partial \varepsilon} dA + \sum_i A_i z_i \frac{\partial \sigma_{si}}{\partial \varepsilon} \right] \right\} \boldsymbol{B_w} dx \tag{3.64}$$

Furthermore, the derivative of (3.25) in the direction of $\Delta\Delta_i$ is determined by

$$a'_{u^o \Delta_i}(u^{o*}, w^*, \Delta_i^*; \delta u^o, \Delta\Delta_i) = \frac{\partial}{\partial \varepsilon} a_{u^o}(u^{o*}, w^*, \Delta_i^* + \varepsilon \Delta\Delta_i; \delta u^o) \Big|_{\varepsilon=0} =$$

$$= \frac{\partial}{\partial \varepsilon} \left\{ \int_L \frac{\partial \delta u^o}{\partial x} \left[\int_A \sigma_{xx}^{con} \left(\frac{\partial u^{o*}}{\partial x} - z \frac{\partial^2 w^*}{\partial x^2} \right) dA + \right. \right.$$

$$\left. \left. + \sum_i A_i \sigma_{si} \left(\frac{\partial u^{o*}}{\partial x} - z_i \frac{\partial^2 w^*}{\partial x^2} + \frac{\partial \left(\Delta_i^* + \varepsilon \Delta\Delta_i \right)}{\partial x} \right) \right] dx \right\} \Big|_{\varepsilon=0} =$$

$$= \int_L \frac{\partial \delta u^o}{\partial x} \left[\sum_i A_i \frac{\partial \sigma_{si}}{\partial \varepsilon} \right] \frac{\partial \Delta\Delta_i}{\partial x} dx \tag{3.65}$$

Introducing the approximations on u^{o*}, w^*, Δ_i^* and $\delta u^o, \Delta\Delta_i$ gives

$$a'_{u^o \Delta_i}(\boldsymbol{N a^*}; \boldsymbol{N_{u^o} c_{u^o}}, \boldsymbol{N_{\Delta_i} \Delta a_{\Delta_i}}) = \boldsymbol{c_{u^o}^T} \int_L \boldsymbol{B_{u^o}^T} \left[\sum_i A_i \frac{\partial \sigma_{si}}{\partial \varepsilon} \right] \boldsymbol{B_{\Delta_i}} dx \Delta \boldsymbol{a_{\Delta_i}} =$$

$$= \boldsymbol{c_{u^o}^T K_{u^o \Delta_i}} \Delta \boldsymbol{a_{\Delta_i}} \tag{3.66}$$

where

$$\boldsymbol{K_{u^o \Delta_i}} = \int_L \boldsymbol{B_{u^o}^T} \left[\sum_i A_i \frac{\partial \sigma_{si}}{\partial \varepsilon} \right] \boldsymbol{B_{\Delta_i}} dx \tag{3.67}$$

To continue with the derivation process, for the derivative of (3.26) in the direction of Δu^o, it can written

$$a'_{w u^o}(u^{o*}, w^*, \Delta_i^*; \delta w, \Delta u^o) = \frac{\partial}{\partial \varepsilon} a_w(u^{o*} + \varepsilon \Delta u^o, w^*, \Delta_i^*; \delta w) \Big|_{\varepsilon=0} =$$

$$= \frac{\partial}{\partial \varepsilon} \left\{ \int_L \frac{\partial^2 \delta w}{\partial x^2} \left\{ - \left[\int_A z \cdot \sigma_{xx}^{con} \left(\frac{\partial (u^{o*} + \varepsilon \Delta u^o)}{\partial x} - z \frac{\partial^2 w^*}{\partial x^2} \right) dA + \right. \right. \right.$$

$$\left. \left. \left. + \sum_i A_i z_i \sigma_{si} \left(\frac{\partial (u^{o*} + \varepsilon \Delta u^o)}{\partial x} - z_i \frac{\partial^2 w^*}{\partial x^2} + \frac{\partial \Delta_i^*}{\partial x} \right) \right] \right\} dx \right\} \Big|_{\varepsilon=0} =$$

$$= \int_L \frac{\partial^2 \delta w}{\partial x^2} \left\{ - \left[\int_A z \frac{\partial \sigma_{xx}^{con}}{\partial \varepsilon} dA + \sum_i A_i z_i \frac{\partial \sigma_{si}}{\partial \varepsilon} \right] \right\} \frac{\partial \Delta u^o}{\partial x} dx \tag{3.68}$$

Replacing the approximations on u^{o*}, w^*, Δ_i^* and $\delta w, \Delta u^o$ into (3.68) gives

$$a'_{wu^o}(\boldsymbol{N a^*}; \boldsymbol{N_w c_w}, \boldsymbol{N_{u^o}} \Delta \boldsymbol{a_{u^o}}) = \boldsymbol{c_w^T} \int_L \boldsymbol{B_w^T} \left\{ - \left[\int_A z \frac{\partial \sigma_{xx}^{con}}{\partial \varepsilon} dA + \sum_i A_i z_i \frac{\partial \sigma_{si}}{\partial \varepsilon} \right] \right\} \boldsymbol{B_{u^o}} dx \Delta \boldsymbol{a_{u^o}} =$$

$$= \boldsymbol{c_w^T K_{wu^o}} \Delta \boldsymbol{a_{u^o}} \tag{3.69}$$

where

$$\boldsymbol{K_{wu^o}} = \int_L \boldsymbol{B_w^T} \left\{ - \left[\int_A z \frac{\partial \sigma_{xx}^{con}}{\partial \varepsilon} dA + \sum_i A_i z_i \frac{\partial \sigma_{si}}{\partial \varepsilon} \right] \right\} \boldsymbol{B_{u^o}} dx \tag{3.70}$$

At this point, it is useful to observe the symmetry that holds between the relevant components of the tangent stiffness matrix. For instance, from (3.64) and (3.70) it is straightforward to observe that

$$\boldsymbol{K_{u^o w}} = \boldsymbol{K'_{wu^o}} \tag{3.71}$$

In the same manner, the concept of symmetry can be exploited in the derivation process of the rest components of the stiffness matrix $\boldsymbol{K}$.

Likewise, the derivative of (3.26) in the direction of Δw is determined by

$$a'_{ww}(u^{o*}, w^*, \Delta_i^*; \delta w, \Delta w) = \frac{\partial}{\partial \varepsilon} a_w(u^{o*}, w^* + \varepsilon \Delta w, \Delta_i^*; \delta w) \Big|_{\varepsilon=0} =$$

$$= \frac{\partial}{\partial \varepsilon} \left\{ \int_L \frac{\partial^2 \delta w}{\partial x^2} \left\{ - \left[\int_A z \sigma_{xx}^{con} \left(\frac{\partial u^{o*}}{\partial x} - z \frac{\partial^2 (w^* + \varepsilon \Delta w)}{\partial x^2} \right) dA + \right. \right. \right.$$

$$\left. \left. \left. + \sum_i A_i z_i \sigma_{si} \left(\frac{\partial u^{o*}}{\partial x} - z_i \frac{\partial^2 (w^* + \varepsilon \Delta w)}{\partial x^2} + \frac{\partial \Delta_i^*}{\partial x} \right) \right] \right\} dx \right\} \Big|_{\varepsilon=0} =$$

$$= \int_L \frac{\partial^2 \delta w}{\partial x^2} \left[\int_A z^2 \frac{\partial \sigma_{xx}^{con}}{\partial \varepsilon} dA + \sum_i A_i z_i^2 \frac{\partial \sigma_{si}}{\partial \varepsilon} \right] \frac{\partial^2 \Delta w}{\partial x^2} dx \tag{3.72}$$

Introducing the approximations on u^{o*}, w^*, Δ_i^* and $\delta w, \Delta w$ into (3.72) results in

$$a'_{ww}(\boldsymbol{N a^*}; \boldsymbol{N_w c_w}, \boldsymbol{N_w} \Delta \boldsymbol{a_w}) = \boldsymbol{c_w^T} \int_L \boldsymbol{B_w^T} \left[\int_A z^2 \frac{\partial \sigma_{xx}^{con}}{\partial \varepsilon} dA + \sum_i A_i z_i^2 \frac{\partial \sigma_{si}}{\partial \varepsilon} \right] \boldsymbol{B_w} dx \Delta \boldsymbol{a_w} =$$

$$= \boldsymbol{c_w^T K_{ww}} \Delta \boldsymbol{a_w} \tag{3.73}$$

where

$$\boldsymbol{K_{ww}} = \int_L \boldsymbol{B_w^T} \left[\int_A z^2 \frac{\partial \sigma_{xx}^{con}}{\partial \varepsilon} dA + \sum_i A_i z_i^2 \frac{\partial \sigma_{si}}{\partial \varepsilon} \right] \boldsymbol{B_w} dx \tag{3.74}$$

To continue with the derivative of (3.26) in the direction of $\Delta\Delta_i$, it can be stated

$$a'_{w\Delta_i}(u^{o*}, w^*, \Delta_i^*; \delta w, \Delta\Delta_i) = \frac{\partial}{\partial\varepsilon} a_w(u^{o*}, w^*, \Delta_i^* + \varepsilon\Delta\Delta_i; \delta w)\Big|_{\varepsilon=0} =$$

$$= \frac{\partial}{\partial\varepsilon}\left\{\int_L \frac{\partial^2\delta w}{\partial x^2}\left\{-\left[\int_A z\sigma_{xx}^{con}\left(\frac{\partial u^{o*}}{\partial x} - z\frac{\partial^2 w^*}{\partial x^2}\right)dA + \right.\right.\right.$$

$$\left.\left.\left. + \sum_i A_i z_i \sigma_{si}\left(\frac{\partial u^{o*}}{\partial x} - z_i\frac{\partial^2 w^*}{\partial x^2} + \frac{\partial\left(\Delta_i^* + \varepsilon\Delta\Delta_i\right)}{\partial x}\right)\right]\right\} dx\right\}\Bigg|_{\varepsilon=0} =$$

$$= \int_L \frac{\partial^2\delta w}{\partial x^2}\left[-\sum_i A_i z_i \frac{\partial\sigma_{si}}{\partial\varepsilon}\right]\frac{\partial\Delta\Delta_i}{\partial x}dx \tag{3.75}$$

Introducing the approximations on u^{o*}, w^*, Δ_i^* and $\delta w, \Delta\Delta_i$ into (3.75), it is obtained

$$a'_{w\Delta_i}(\boldsymbol{N a^*}; \boldsymbol{N_w c_w}, \boldsymbol{N_{\Delta_i}}\Delta\boldsymbol{a_{\Delta_i}}) = \boldsymbol{c_w^T}\int_L \boldsymbol{B_w^T}\left[-\sum_i A_i z_i \frac{\partial\sigma_{si}}{\partial\varepsilon}\right]\boldsymbol{B_{\Delta_i}}dx\Delta\boldsymbol{a_{\Delta_i}} =$$

$$= \boldsymbol{c_w^T K_{w\Delta_i}}\Delta\boldsymbol{a_{\Delta_i}} \tag{3.76}$$

where,

$$\boldsymbol{K_{w\Delta_i}} = \int_L \boldsymbol{B_w^T}\left[-\sum_i A_i z_i \frac{\partial\sigma_{si}}{\partial\varepsilon}\right]\boldsymbol{B_{\Delta_i}}dx \tag{3.77}$$

As it was the case for the previous relevant components of the stiffness matrix, accounting for symmetry, the following hold

$$\boldsymbol{K_{\Delta_i u^o}} = \boldsymbol{K'_{u^o\Delta_i}} \tag{3.78}$$

and,

$$\boldsymbol{K_{\Delta_i w}} = \boldsymbol{K'_{w\Delta_i}} \tag{3.79}$$

where, $\boldsymbol{K_{u^o\Delta_i}}$ and $\boldsymbol{K_{w\Delta_i}}$ are determined in (3.67) and (3.77), respectively.

The last component to be calculated is $\boldsymbol{K_{\Delta_i\Delta_i}}$, according to

$$a'_{\Delta_i\Delta_i}(u^{o*}, w^*, \Delta_i^*; \delta\Delta_i, \Delta\Delta_i) = \frac{\partial}{\partial\varepsilon} a_{\Delta_i}(u^{o*}, w^*, \Delta_i^* + \varepsilon\Delta\Delta_i; \delta\Delta_i)\Big|_{\varepsilon=0} =$$

$$= \frac{\partial}{\partial\varepsilon}\left[\int_{a_i}^{b_i}\frac{\partial\delta\Delta_i}{\partial x}A_i\sigma_{si}\left(\frac{\partial u^{o*}}{\partial x} - z_i\frac{\partial^2 w^*}{\partial x^2} + \frac{\partial\left(\Delta_i^* + \varepsilon\Delta\Delta_i\right)}{\partial x}\right)dx + \right.$$

$$\left. + \int_{a_i}^{b_i}\delta\Delta_i \cdot s_i \cdot \tau_{xx}^{bond}\left(\Delta_i^* + \varepsilon\Delta\Delta_i\right)dx\right]\Bigg|_{\varepsilon=0} =$$

$$\int_{a_i}^{b_i}\frac{\partial\delta\Delta_i}{\partial x}\left[\sum_i A_i\frac{\partial\sigma_{si}}{\partial\varepsilon}\right]\frac{\partial\Delta\Delta_i}{\partial x}dx + \int_{a_i}^{b_i}\delta\Delta_i\left[\sum_i s_i\frac{\partial\tau_{xx}^{bond}}{\partial\varepsilon}\right]\Delta\Delta_i dx =$$

$$\int_{a_i}^{b_i}\left\{\frac{\partial\delta\Delta_i}{\partial x}\left[\sum_i A_i\frac{\partial\sigma_{si}}{\partial\varepsilon}\right]\frac{\partial\Delta\Delta_i}{\partial x} + \delta\Delta_i\left[\sum_i s_i\frac{\partial\tau_{xx}^{bond}}{\partial\varepsilon}\right]\Delta\Delta_i\right\}dx \tag{3.80}$$

Introducing the approximations on u^{o*}, w^*, Δ_i^* and $\delta\Delta_i, \Delta\Delta_i$ into (3.80) gives

$$a'_{\Delta_i\Delta_i}(\boldsymbol{N}\boldsymbol{a}^*; \boldsymbol{N}_{\boldsymbol{\Delta}_i}\boldsymbol{c}_{\boldsymbol{\Delta}_i}, \boldsymbol{N}_{\boldsymbol{\Delta}_i}\boldsymbol{\Delta}\boldsymbol{a}_{\boldsymbol{\Delta}_i}) = \boldsymbol{c}^{\boldsymbol{T}}_{\boldsymbol{\Delta}_i} \int_{a_i}^{b_i} \left\{ \boldsymbol{B}^{\boldsymbol{T}}_{\boldsymbol{\Delta}_i} \left[\sum_i A_i \frac{\partial \sigma_{si}}{\partial \varepsilon} \right] \boldsymbol{B}_{\boldsymbol{\Delta}_i} + \right.$$

$$\left. + \boldsymbol{N}^{\boldsymbol{T}}_{\boldsymbol{\Delta}_i} \left[\sum_i s_i \frac{\partial \tau^{bond}_{xx}}{\partial \varepsilon} \right] \boldsymbol{N}_{\boldsymbol{\Delta}_i} \right\} dx \Delta\boldsymbol{a}_{\boldsymbol{\Delta}_i} = \boldsymbol{c}^{\boldsymbol{T}}_{\boldsymbol{\Delta}_i} \boldsymbol{K}_{\boldsymbol{\Delta}_i\boldsymbol{\Delta}_i} \Delta\boldsymbol{a}_{\boldsymbol{\Delta}_i} \tag{3.81}$$

where

$$\boldsymbol{K}_{\boldsymbol{\Delta}_i\boldsymbol{\Delta}_i} = \int_{a_i}^{b_i} \left\{ \boldsymbol{B}^{\boldsymbol{T}}_{\boldsymbol{\Delta}_i} \left[\sum_i A_i \frac{\partial \sigma_{si}}{\partial \varepsilon} \right] \boldsymbol{B}_{\boldsymbol{\Delta}_i} + \boldsymbol{N}^{\boldsymbol{T}}_{\boldsymbol{\Delta}_i} \left[\sum_i s_i \frac{\partial \tau^{bond}_{xx}}{\partial \varepsilon} \right] \boldsymbol{N}_{\boldsymbol{\Delta}_i} \right\} dx \tag{3.82}$$

In conclusion, the resulting linearized equation (3.58) can be written

$$\boldsymbol{c}^{\boldsymbol{T}} \boldsymbol{f}_{\boldsymbol{int}}(\boldsymbol{a}^* + \Delta\boldsymbol{a}) \approx \boldsymbol{c}^{\boldsymbol{T}} \boldsymbol{f}_{\boldsymbol{int}}(\boldsymbol{a}^*) + \boldsymbol{c}^{\boldsymbol{T}} \boldsymbol{K}(\boldsymbol{a}^*) \Delta\boldsymbol{a} \tag{3.83}$$

or, in terms of the reduced *out-of-balance* force vector

$$\boldsymbol{c}^{\boldsymbol{T}}_{\boldsymbol{F}} \boldsymbol{g}(\boldsymbol{a}^*_{\boldsymbol{F}} + \Delta\boldsymbol{a}_{\boldsymbol{F}}) \approx \boldsymbol{c}^{\boldsymbol{T}}_{\boldsymbol{F}} \boldsymbol{g}(\boldsymbol{a}^*_{\boldsymbol{F}}) + \boldsymbol{c}^{\boldsymbol{T}}_{\boldsymbol{F}} \boldsymbol{K}(\boldsymbol{a}^*_{\boldsymbol{F}}) \Delta\boldsymbol{a}_{\boldsymbol{F}} \tag{3.84}$$

In the latter equations, the internal and external force vectors, $\boldsymbol{f}_{\boldsymbol{int}}$ and $\boldsymbol{f}$, are defined by (3.40), (3.41) and (3.42), while the tangent stiffness matrix, denoted as $\boldsymbol{K}$ is assembled employing (3.61)-(3.82), into the global stiffness matrix, schematically shown as

$$\boldsymbol{K} = \begin{bmatrix} \boldsymbol{K}_{\boldsymbol{u}^o\boldsymbol{u}^o} & \boldsymbol{K}_{\boldsymbol{u}^o\boldsymbol{w}} & \boldsymbol{K}_{\boldsymbol{u}^o\boldsymbol{\Delta}_i} \\ \boldsymbol{K}_{\boldsymbol{w}\boldsymbol{u}^o} & \boldsymbol{K}_{\boldsymbol{w}\boldsymbol{w}} & \boldsymbol{K}_{\boldsymbol{w}\boldsymbol{\Delta}_i} \\ \boldsymbol{K}_{\boldsymbol{\Delta}_i\boldsymbol{u}^o} & \boldsymbol{K}_{\boldsymbol{\Delta}_i\boldsymbol{w}} & \boldsymbol{K}_{\boldsymbol{\Delta}_i\boldsymbol{\Delta}_i} \end{bmatrix} \tag{3.85}$$

3.4 Constitutive models

The aim of the project, as it has already been described in the introduction of Chapter 3, was to develop a simplified FE model that should be able to describe the interaction between the cracked concrete and the reinforcement bars, accounting for the relative slip at the steel/concrete interface, as well as, the different length scales involved in the model. Significant contribution into the accomplishment of the goals just outlined was the implementation of the appropriate non-linear material laws.

3.4.1 Concrete

The post-cracking behaviour of concrete was taken into consideration by a *smeared-crack* model, following a purely linear law for strains lower than the *cracking strain*. The main idea in the *smeared-crack* approach is to assume one crack to exist within the finite domain h pertaining to, e.g., a finite element. We thus divide the total strain, ε, into an elastic, ε^e, and an inelastic part, according to (3.86).

$$\varepsilon = \varepsilon^e + \frac{w}{h} \tag{3.86}$$

where, ε^e, is used to denote the deformation of the uncracked regions of the continuum (Figure 3.4), which are been loaded and unloaded elastically, and, w/h, accounts for the part of the total strain that is attributed to cracking. In (3.86), w, is the crack-width, while, h, is the part of the loaded body over which the pertinent crack is smeared.

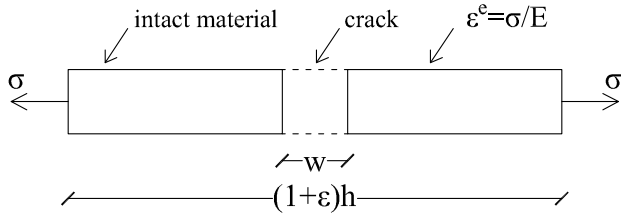

Figure 3.4: *Division of the total strain*

The uni-axial softening law employed was the *Hordjik* curve (Figure 3.5), which in terms of local coordinates is given by

$$\sigma = f_w(w) \equiv f_t \left\{ \left[1 + \left(\frac{c_1 w}{w_c} \right)^3 \right] exp(-\frac{c_2 w}{w_c}) - e^{-c_2} \left(1 + c_1^3 \right) \frac{w}{w_c} \right\} \tag{3.87}$$

where	σ	is the stress component normal to the crack plane
	f_t	is the tensile strength of concrete
	w	is the crack-width
	w_c	is the critical crack opening
	c_1, c_2	are material constants

The constants are usually given the default values of $c_1 = 3.0$ and $c_2 = 6.93$. The *critical crack opening*, which is the value of the *crack-width* for which the stress vanishes, is calculated

by

$$w_c = \frac{5.136 G_F}{f_t} \tag{3.88}$$

where, G_F, is the *fracture energy* of concrete. As it can be seen, (3.87) is expressed in terms of the crack-width, w. In order to state the aforementioned relation in terms of strains, the crack-width, w, must be divided by an appropriate length, h, as it was also shown in (3.86). Concerning the choice of h, or else, the *crack band-width*, and the *fracture energy*, G_F, as it will be shown in Section 3.6, they are related to issues of mesh-dependency and strain localization.

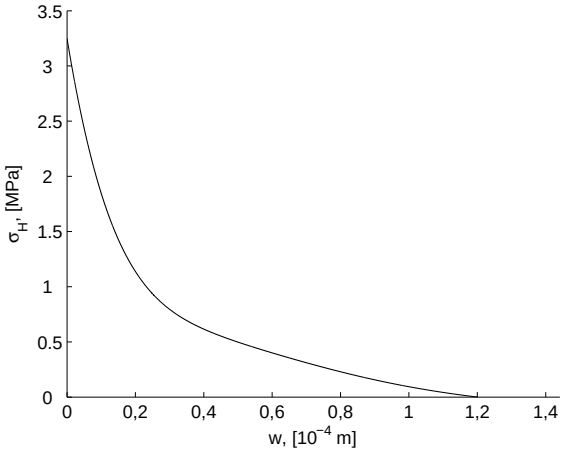

Figure 3.5: *Hordjik softening law*

Another issue met during the modelling process was unloading. Although, only monotonic loading conditions were considered, unloading was also induced due to opening and closure of existing cracks. For that reason, an appropriate *history* variable was introduced, in which the maximum previously converged strain state reached in any cracked point was 'recorded'. In that sense, in case of unloading of a cracked section, the decrease in stress would follow the secant stiffness curve from the maximum strain state point to the origin of the coordinate system. If reloading takes place, then the stress increase would follow the secant stiffness line, until 'meeting' the basic softening curve at the maximum previously converged strain state. The discussion just outlined, expressed in total strain, is shown schematically in Figure 3.6.

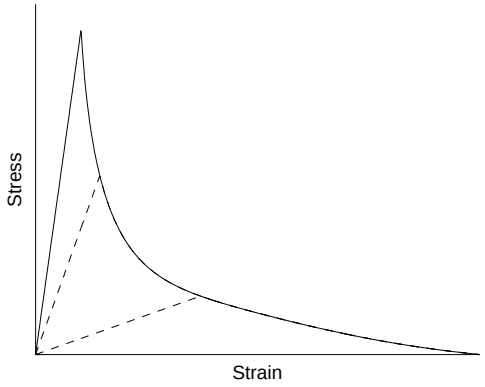

Figure 3.6: *Damage model*

In more detail, in the iterative scheme within each load increment, the crack-width, w, in a cracked integration point was compared to the relevant maximum previously converged crack-width stored in the *history* variable, w_p, at the same point. The appropriate value for the concrete tensile stress, σ_c, and the tangent stiffness, $\partial\sigma_c/\partial w$, at the current iterative step were then determined by (3.89) and (3.90), as

$$\sigma_c(w_{n+1}) = \begin{cases} \dfrac{\sigma_H(w_p)}{w_p} w_{n+1} & , \quad w_{n+1} < w_p \\ \sigma_H(w_{n+1}) & , \quad w_{n+1} >= w_p \end{cases} \tag{3.89}$$

$$\frac{\partial\sigma_c}{\partial w} = \begin{cases} \dfrac{\sigma_H(w_p)}{w_p} & , \quad w_{n+1} < w_p \\ \dfrac{\partial\sigma_H}{\partial w}(w_{n+1}) & , \quad w_{n+1} >= w_p \end{cases} \tag{3.90}$$

where, σ_H, was determined by the *Hordjik* curve defined by (3.87) and shown in Figure 3.5, and, the subscript, $n+1$, denotes the current iterative step.

Next, the history variable in any cracked point was updated with the condition (3.91). Namely, the maximum value of the crack-width, w, between the converged value of w in the current iterative step and the one previously stored in the pertinent 'position' of the history variable.

$$w_{p,n+1} = max(w_{n+1}, w_{p,n}) \tag{3.91}$$

Regarding the response of concrete in compression, the fully non-linear law described in [3] was adopted (Figure 3.7), until the compressive strain where the curve exhibits a peak. The curve is given by

$$\frac{\sigma_c}{f_{cm}} = -\left(\frac{k\cdot\eta - \eta^2}{1 + (k-2)\cdot\eta}\right) \; for \; \|\varepsilon_c\| < \|\varepsilon_{c1}\| \tag{3.92}$$

where, η $= \varepsilon_c/\varepsilon_{c1}$
k $= E_{ci}/E_{c1}$
σ_c is the uni-axial concrete stress
f_{cm} is the mean compressive strength
ε_{c1} is the strain at the mean compressive strength
E_{c1} is the secant modulus at $\varepsilon_c = 0$
E_{ci} is the mean modulus of elasticity
k is the plasticity number

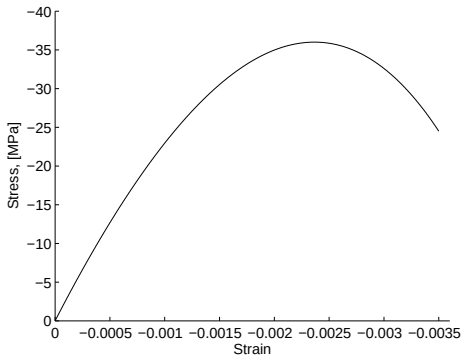

Figure 3.7: *Constitutive law of concrete in compression*

After the peak, at the compressive softening region, as is the case for the tension softening, the area under the curve, or else, the *fracture energy* in compression should be scaled in order to avoid objectivity and mesh-dependence of the results upon mesh refinement. For that purpose, the method described in [28] was adopted. The principle for such a procedure can be seen in Figure 3.8. The parameter, h, accounts for the element length, while the *fracture energy* in compression was taken as $G_c = 250G_F$.

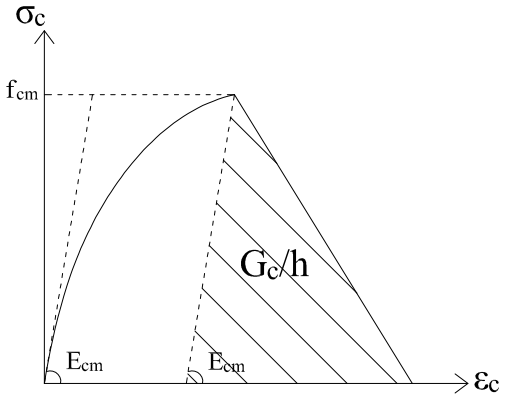

Figure 3.8: *Mesh-independent softening*

The complete uni-axial constitutive model used for concrete can be seen in Figure 3.9.

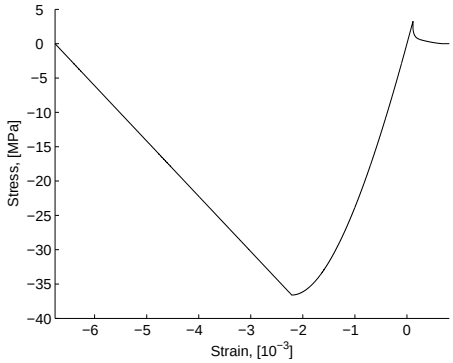

Figure 3.9: *Constitutive law of concrete*

3.4.2 Reinforcement steel

As regards the steel bars, a 'simple' elasto-plastic law was occupied, as shown in Figure 3.10. The curve is fully defined by the *Young's* modulus $E_s = 200GPa$, which is a rather standard value for reinforcement steel, and the tensile yield strength of $f_y = 500GPa$.

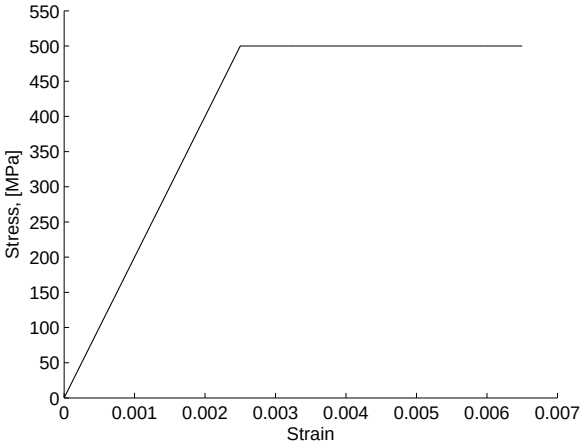

Figure 3.10: *Elasto-plastic constitutive law of reinforcement steel*

3.4.3 Bond-slip

Much discussion took place during the modelling phase regarding the bond-slip law that should be inserted in the analysis. The 'classic' *Eligehausen's* law was considered to be the most suitable, as it is also recommended in [3]. The graph of the model is drawn in Figure 3.11.

Four distinct regions can be recognized in the graph, which are described by (3.93).

$$\tau(s) = \begin{cases} \tau_{max}\left(\dfrac{s}{s_1}\right)^{\alpha} & , \quad 0 \leq s \leq s_1 \\ \tau_{max} & , \quad s_1 < s \leq s_2 \\ \dfrac{\tau_f - \tau_{max}}{s_3 - s_2}s + \left[\tau_f - \dfrac{\tau_f - \tau_{max}}{s_3 - s_2}\right] & , \quad s_2 < s \leq s_3 \\ \tau_f & , \quad s \geq s_3 \end{cases} \tag{3.93}$$

where, $\tau_{max} = 2.5\sqrt{f_{cm}}\ [MPa]$ (f_{cm} *in* MPa)
$\tau_f = 0.4\tau_{max}$
$s_1 = 0.001m$
$s_2 = 0.005m$
$s_3 = 0.009m$
$\alpha = 0.4$

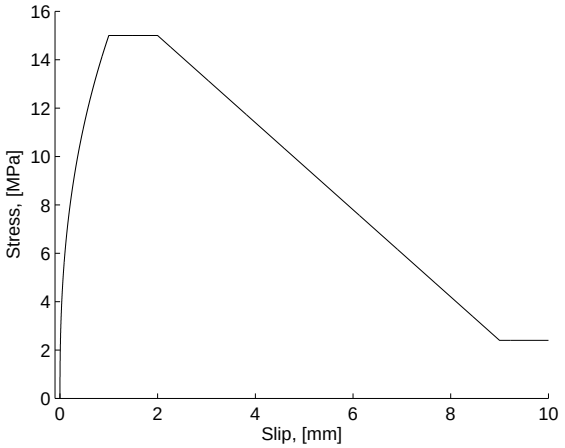

Figure 3.11: *Constitutive law of bond-slip between the concrete and reinforcement*

Details on the values of $\tau_{max},\ \tau_f, s_1,\ s_2,\ s_3$ and α can be found in [3]. According to (3.93), *Eligehausen's* law exhibits infinite initial stiffness, which comprised a source of computational difficulties upon using the inverse tangent stiffness matrix at the first step of the incremental/iterative procedure (see also Section 3.5). For that reason, the actual initial exponential part of the model was approximated by a linear segment. The influence of the stiffness of the initial linear segment on the crack widths and the crack pattern is proposed as a parametric study for further work by the authors.

3.5 Numerical schemes

3.5.1 Newton's method

The reduced system of $\mathbb{N}_{Free}$ non-linear equations described symbolically in (3.51) can be solved iteratively, employing numerous methods. In the present, the widely used *Newton's method* was chosen. A schematic description of the iterative process within each load step is given in Figure 3.12, where, λ, is used to denote the applied load, and, $\boldsymbol{a}$, accounts for the displacements vector.

As a start, for a certain load step (for convenience, the initial step, n_o, can be assumed here), an appropriate guess, $\boldsymbol{a_i^{(o)}}$, of the displacements field is made. Note that, a choice of the initial guess not close enough to the expected true solution, might lead to difficult or even lack of convergence. Considering a small change in, $\boldsymbol{a_i^{(o)}}$, namely, $\boldsymbol{\Delta a_{i+1}^{(o)}}$, and setting the linearized *residual* at, $\boldsymbol{a_i^{(o)}} + \boldsymbol{\Delta a_{i+1}^{(o)}}$, equal to zero in (3.84), a closer value towards the desired solution is most probably captured, after updating the displacements vector, $\boldsymbol{a_i^{(o)}}$, by the change, $\boldsymbol{\Delta a_{i+1}^{(o)}}$. The solution is assumed that has been reached when the 'norm' of the *residual* evaluated from (3.51) tends to 'zero'. In matrix form, it can be written

$$\boldsymbol{K}(\boldsymbol{a_{i,F}^{(o)}})\Delta\boldsymbol{a_{i+1,F}^{(o)}} = -\boldsymbol{g}(\boldsymbol{a_{i,F}^{(o)}}) \tag{3.94}$$

where, the subscript, *i*, or, *i+1*, denote the number of the iterative step, the superscript, *(o)*, accounts for the number of the incremental step and, *F*, symbolizes the free/unconstrained degrees of freedom. According to the *Newton's method* , the next iterative step, *i+1*, is taken as the displacements vector from the previous step, $\boldsymbol{a_{i,F}^{(o)}}$, plus the change, $\Delta\boldsymbol{a_{i+1,F}^{(o)}}$, calculated from the previous step, *i*, from (3.94) , namely

$$\boldsymbol{a_{i+1,F}^{(o)}} = \boldsymbol{a_{i,F}^{(o)}} + \Delta\boldsymbol{a_{i+1,F}^{(o)}} \tag{3.95}$$

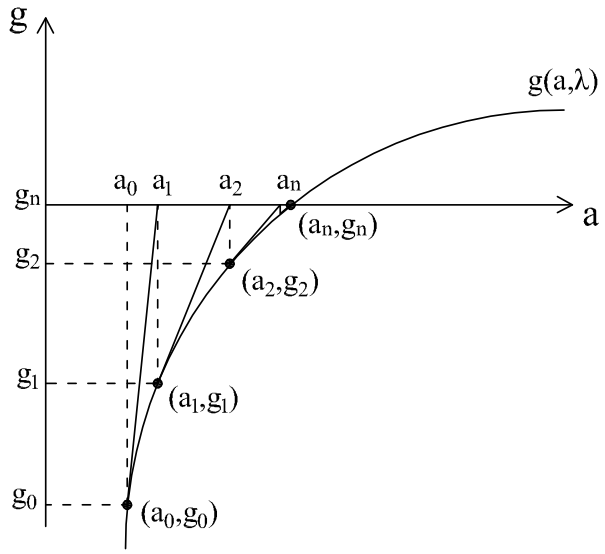

Figure 3.12: *Newton iterative procedure*

3.5.2 Incremental methods

The iterative procedure described at Section 3.5.1 is repeated until convergence at the current iterative step is reached. The convergence criterion used was that $\|\boldsymbol{g}\|$ should be less than a predefined tolerance. So, for a certain load step, the solution vector has been obtained following *Newton's method*. What comes next, is the incremental process. In other words, to calculate the new displacements vector when adding one load step, n_1, to the previous converged load step, n_o. For that purpose, the starting 'guessed' displacements vector, $\boldsymbol{a}_{\boldsymbol{1,F}}^{\boldsymbol{(1)}}$, would be the converged solution of the previous step, $\boldsymbol{a}_{\boldsymbol{n,F}}^{\boldsymbol{(o)}}$, where, n, denotes the number of iterations needed for the desired tolerance to be met in the previous step, n_o.

It can be stated that three major categories of incremental methods exist, the *load-control*, the *displacement-control* and the *arc-length-control method*. All of them were applied in the present thesis, in order for the numerical issues that arose to be 'tackled'. As an example, for the displacement-control method to be realized at a *three-point bending* problem, it is enough to prescribe, apart from the appropriate *simple support* essential and natural boundary conditions, also the deflection at the position where the point load is applied (Figure 3.13). That would generate a *reaction force* at this point, which would account for the applied point load.

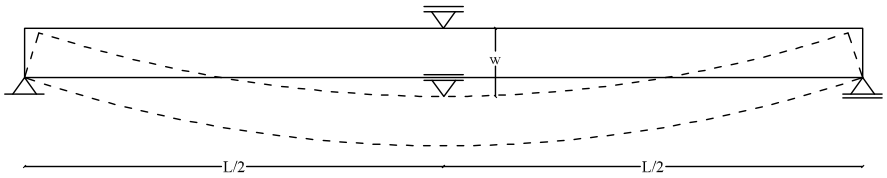

Figure 3.13: *Displacement-control method*

And if most analysts are more familiar with the *load-control* and the *displacement-control* method, then it is interesting to follow the *arc-length-control method* within one incremental step, as shown in principle in Figure 3.14, where, λ, is a load multiplier and, $\boldsymbol{a}$, denotes the displacements vector. Details on the application of the latter method are given in [4]. In short, the *arc-length-control* method, in a usual *Newton* iterative step, makes use of a constraint equation that is employed so as by defining an arc-length, to be able to control both the load and the displacements increment. The method assumes that the external force vector is applied in increments, which are defined by a load multiplier, λ, according to

$$\boldsymbol{f_{ext}}(\lambda) = \boldsymbol{f_o} + \lambda \boldsymbol{f} \tag{3.96}$$

where, $\boldsymbol{f}$, is a reference load vector, λ, is the load parameter and, $\boldsymbol{f_o}$, is a constant external load. Thus, the *out-of-balance* force vector can be written as

$$\boldsymbol{g}(\boldsymbol{a}, \lambda) = \boldsymbol{f_{int}}(\boldsymbol{a}) - \boldsymbol{f_o} - \lambda \boldsymbol{f} \tag{3.97}$$

At this point, as was shown for a typical *Newton's* iterative step at Section 3.5.2, the k-st incremental step, $(\boldsymbol{a_i^{(k)}}, \lambda_i^{(k)})$, can be assumed. Then, considering a small change in, $(\boldsymbol{a_i^{(k)}}, \lambda_i^{(k)})$, namely, $(\delta \boldsymbol{a_{i+1}^{(k)}}, \delta \lambda_{i+i}^{(k)})$, and evaluating the residual from (3.97) at that point employing Taylor series, it is obtained

$$\boldsymbol{g}(\boldsymbol{a_i^{(k)}} + \delta \boldsymbol{a_{i+1}^{(k)}}, \lambda_i^{(k)} + \delta \lambda_{i+1}^{(k)}) = \boldsymbol{f_{int}}(\boldsymbol{a_i^{(k)}}) - \boldsymbol{f_o} - \lambda_i^{(k)} \boldsymbol{f} + \boldsymbol{K}(\boldsymbol{a_i^{(k)}}) \delta \boldsymbol{a_{i+1}^{(k)}} - \delta \lambda_{i+1}^{(k)} \boldsymbol{f} \tag{3.98}$$

Setting (3.98) equal to 'zero' the following relationship is derived

$$\boldsymbol{K}(\boldsymbol{a_i^{(k)}})\delta\boldsymbol{a_{i+1}^{(k)}} = -\boldsymbol{f_{int}}(\boldsymbol{a_i^{(k)}}) + \boldsymbol{f_o} + \lambda_i^{(k)}\boldsymbol{f} + \delta\lambda_{i+1}^{(k)}\boldsymbol{f} \tag{3.99}$$

In (3.98) and (3.99), as well as, in the equations that are to follow, the subscripts, i, or, $i+1$, are used to denote the number of the iterative step, while the superscript, (k), symbolizes the number of the incremental step. Furthermore, a separation of, $\delta\boldsymbol{a_{i+1}^{(k)}}$, takes place as

$$\begin{cases} \boldsymbol{K}(\boldsymbol{a_i^{(k)}})\boldsymbol{\delta_{g,i+1}^{(k)}} &= -\boldsymbol{f_{int}}(\boldsymbol{a_i^{(k)}}) + \boldsymbol{f_o} + \lambda_i^{(k)}\boldsymbol{f} \\ \boldsymbol{K}(\boldsymbol{a_i^{(k)}})\boldsymbol{\delta_{T,i+1}^{(k)}} &= \boldsymbol{f} \end{cases} \tag{3.100}$$

where

$$\delta\boldsymbol{a_{i+1}^{(k)}} = \boldsymbol{\delta_{g,i+1}^{(k)}} + \delta\lambda_{i+1}^{(k)}\boldsymbol{\delta_{T,i+1}^{(k)}} \tag{3.101}$$

Through the additional/constraint equation, the solution for the incremental step, k, can be found as the point where the arc defined by (3.101) intersects the *out-of-balance* force vector, $\boldsymbol{g}$, and, simultaneously, the *norm* of the *out-of-balance* force vector becomes lower than the predefined tolerance. The pertinent equation has the form

$$g_{con}(\Delta\boldsymbol{a}, \Delta\lambda) = \Delta\boldsymbol{a^T C}\Delta\boldsymbol{a} + c^2\Delta\lambda^2\boldsymbol{f^T f} - \Delta l^2 \tag{3.102}$$

where

$$\Delta\boldsymbol{a^{(k)}} = \boldsymbol{a^{(k)} - a^{(k-1)}} \tag{3.103}$$

$$\Delta\lambda^{(k)} = \lambda^{(k)} - \lambda^{(k-1)} \tag{3.104}$$

while, $\boldsymbol{C}$, and, c, are scaling factors, and, Δl, is the prescribed *arc-length*. Employing the same procedure as in (3.98), (3.102) becomes

$$g_{con}(\Delta\boldsymbol{a_i^{(k)}} + \delta\boldsymbol{a_{i+1}^{(k)}}, \Delta\lambda_i^{(k)} + \delta\lambda_{i+1}^{(k)}) = (2\Delta\boldsymbol{a_i^{(k)}}^T C)\boldsymbol{\delta_{g,i+1}^{(k)}} + (2c^2\Delta\lambda_i^{(k)}\boldsymbol{f^T f})\delta\lambda_{i+1}^{(k)} +$$

$$+\Delta\boldsymbol{a_i^{(k)^T}}\boldsymbol{C}\Delta\boldsymbol{a_i^{(k)}} + c^2{\Delta\lambda_i^{(k)}}^2\boldsymbol{f^T f} - \Delta l^2 \tag{3.105}$$

Then, substituting (3.101) into (3.105) and setting the latter equation equal to 'zero', results in

$$\delta\lambda_{i+1}^{(k)} = \frac{-2\Delta\boldsymbol{a_i^{(k)^T}}\boldsymbol{C\delta_{g,i+1}^{(k)}} - \Delta\boldsymbol{a_i^{(k)^T}}\boldsymbol{C}\Delta\boldsymbol{a_i^{(k)}} - c^2{\Delta\lambda_i^{(k)}}^2\boldsymbol{f^T f} + \Delta l^2}{2\Delta\boldsymbol{a_i^{(k)^T}}\boldsymbol{C\delta_{T,i+1}^{(k)}} + 2c^2\Delta\lambda_i^{(k)}\boldsymbol{f^T f}} \tag{3.106}$$

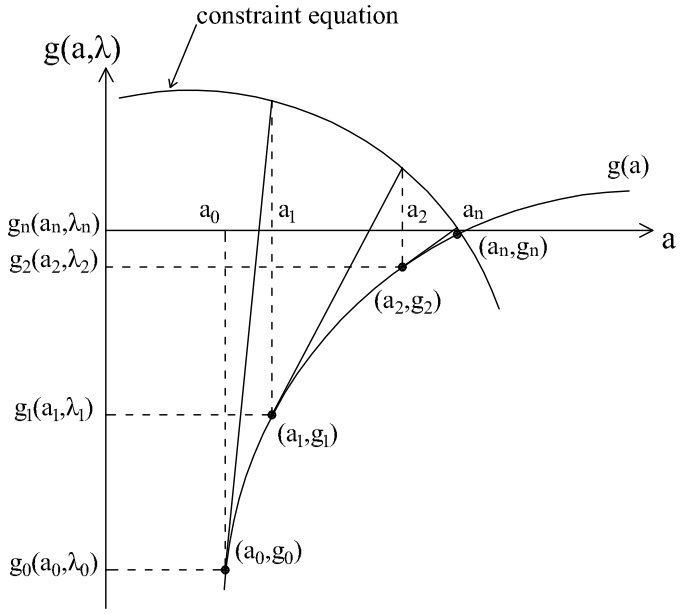

Figure 3.14: *Arc-length-control method*

3.5.3 Numerical integration

From (3.40), (3.41) and (3.42), it can be observed that evaluation of integrals of the form

$$I_{z,\sigma} = \int_A f(z)\sigma(x,z)dA = b\int_{-h/2}^{h/2} f(z)\sigma(x,z)dz \tag{3.107}$$

$$I_{z,d\sigma} = \int_A f(z)\frac{\partial\sigma}{\partial\varepsilon}(x,z)dA = b\int_{-h/2}^{h/2} f(z)\frac{\partial\sigma}{\partial\varepsilon}(x,z)dz \tag{3.108}$$

is needed along the height, where, h, is the height, and, b, is the width of the cross-section, z and x, are the axes along the height and the length of the elements, respectively. Also, from (3.61)-(3.82) it can be observed that evaluation of integrals of the form

$$I_{x,\sigma} = \int_L \boldsymbol{B}^{\boldsymbol{T}}(x)\sigma(x,z)\boldsymbol{B}(x)dx \tag{3.109}$$

$$I_{x,d\sigma} = \int_L \boldsymbol{B}^{\boldsymbol{T}}(x)\frac{\partial\sigma}{\partial\varepsilon}(x,z)\boldsymbol{B}(x)dx \tag{3.110}$$

is needed over the length of the finite elements, where the $\boldsymbol{B}$-matrices were defined in the FE-formulation of the problem, and, ε, denotes the normal strains of the beam. For the evaluation of the pertinent integrals, where, usually, it is difficult to obtain closed-form analytical solutions, suitable numerical methods need to be employed. After performing the transformation from $z \in [-h/2, h/2]$ to $\xi \in [-1, 1]$, (3.107) and (3.108) reform to

$$I_z = \frac{bh}{2}\int_{-1}^{1} g(x,\frac{h}{2}\xi)d\xi = \frac{bh}{2}\sum_{i=1}^{n} w_{z,i}g(x,\frac{h}{2}\xi_i) \tag{3.111}$$

while, from the transformation from $x \in [0, L]$ to $\eta \in [-1, 1]$, (3.109) and (3.110) are restated as

$$I_x = \frac{L}{2} \int_{-1}^{1} h\left(\frac{\eta + 1}{2}, z\right) d\eta = \frac{L}{2} \sum_{i=1}^{n} w_{x,i} h\left(\frac{\eta_i + 1}{2}, z\right) \tag{3.112}$$

In (3.111) and (3.112), $w_{z,i},\ w_{x,i}$, are the integration weights and, $\xi_i,\ \eta_i$, are the integration points.

In the present, it is understood that due to the non-linear response of the outer-most fibers of concrete in tension and compression (see Section 3.4 for further details), there was a necessity of an appropriate *quadrature* over the height of the cross-section, so as to capture satisfactorily as many non-linearities included in the model as possible. A *Gauss-Lobatto*, a *Gauss-Legendre* and a simple *trapezoidal* scheme were the methods this study focused mostly in. The advantage with the *Lobatto* quadrature is the fact that it accounts also for the outer-most points of the cross-section, where most of the non-linearities of the model exist. However, the drawback comparing to the *Gauss* scheme, is that the latter can integrate with n integration points, a polynomial of $2n - 1$ degree exactly, while the relevant *Lobatto* number is $2n - 3$. Thus, the *Gauss* scheme requires, in general, less integration points, a fact that makes it computationally more efficient. The pertinent integration points and the respective weights are depicted in Figure 3.15.

Pertaining to the selected integration schemes along the length of the i-st element, a *Newton-Cotes*, a *Gauss-Legendre* and the user friendly *trapezoidal* quadrature were employed. The number of integration points was chosen as the least possible, so as to describe bending, which uses third order polynomial shape functions. However, due to other parameters, such as the material non-linearities and the bond-slip effect, it was not that straightforward to decide upon the number of integration points that would be enough in that direction, just by considering the bending criterion. The general 'trend' was, though, to choose the least possible integration points, while increasing the number of elements in order to achieve convergence and the desired level of accuracy.

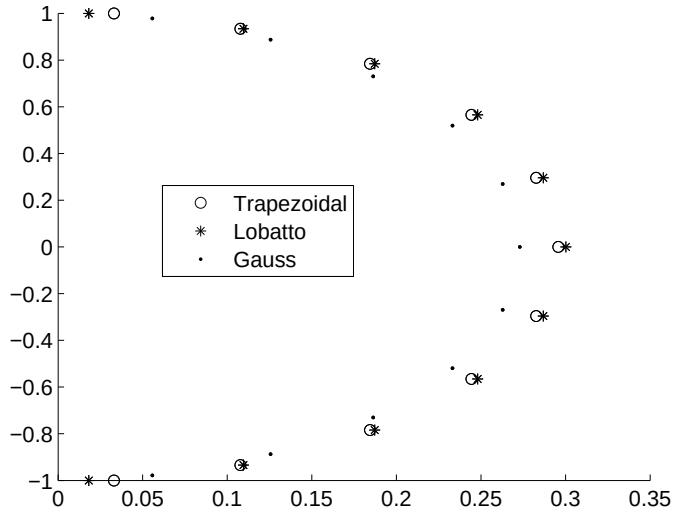

Figure 3.15: *Integration weights and points*

3.5.4 Step control

The appropriate choice of step size was crucial in order to achieve representative results. A factor that influenced the step size was the stiffness of the bond-slip constitutive model. Like discussed in Section 3.4.3 for *Eligehausen's* law, shown in Figure 3.11, a linear branch had to be taken for the first part of the curve from zero slip to a prescribed value, a percentage of s_1 for example. The lower this percentage was taken the stiffer the slip-stress relation and consequently the step length had to be reduced, see Figure 3.16.

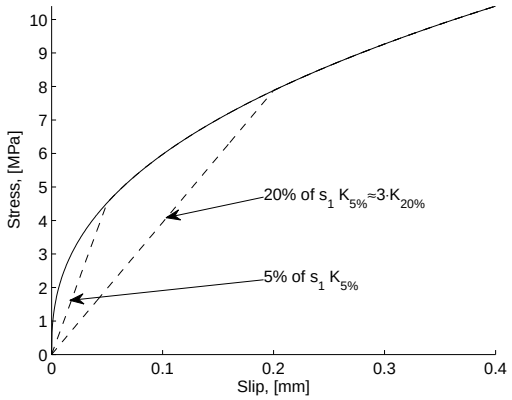

Figure 3.16: *Initial stiffness change when larger portion of the bond-slip law is taken as linear branch*

Other influence on the step size was the scaling of the Hordjik curve. The critical crack opening given by (3.88) is influenced by the tensile strength, f_t, and the *fracture energy*, G_F. The tensile strength is relatively easy to measure and often predefined for concrete mixtures. The *fracture energy* on the other hand has a wider range, from around 50 N/m [33] to 140 N/m [9] for concrete with a mean compressive strength of 36 MPa. The value taken for the fracture energy had significant influence on the *Hordjik* curve, as the lower the *fracture energy* the steeper the branch of the tensile softening curve. It was observed that when the curve was less brittle, i.e. the change in stiffness not as abrupt after the cracking strain was reached, the cracks had a tendency to distribute rather than localizing. This could be avoided to some extent by reducing the step size.

The third large influence on the step size was the number of elements. A crack is considered to localize in one element. To make the problem mesh independent the descending branch was scaled with element length so that the area under the tensile part of the stress-strain constitutive model is always G_f/h, with h being the element length. This had the same influence as discussed in the previous paragraph for the *fracture energy*, i.e. if the number of elements was increased the step had to be reduced.

The consequences of taking a too large step were mainly that too many Gauss-points would go from being uncracked to cracked especially when the solution converged easily. It was observed that this fact produced problems later on, resulting in non-converging displacement steps. There was also another drawback related to the damage model; as mentioned in Section 3.4 a damage model was applied to the tensile constitutive model. The damage strain variable would take larger value than the one returned for a smaller step, giving lower secant stiffness when the strain would be reduced in the i-st Gauss-point.

3.6 Strain localization and mesh dependency

At Section 3.4, the tensile softening law was depicted for concrete (Figure 3.18). As it is described, among numerous sources, in [17] and [1], in order to avoid ill-posedeness of the results upon mesh refinement, the softening law expressed in (3.87) in terms of the crack width, w_c, should be divided by the area where the cracks are expected to localize. In that way, it is accomplished that the same amount of energy is dissipated by a crack that is formed/smeared over the element length of a coarse mesh and another crack that is localizing over the element length of a finer mesh. Then, exploiting the fact that the real, imperfect specimen would crack in a finite region where the section is weaker, it is said that the pertinent region in the model would be the length of one element of an adequately fine mesh.

Schematically (Figure 3.17), starting from the softening law of the form, $\sigma_H = f(w)$, the pertinent diagram is divided by the crack band-width, h. Doing so, two goals are accomplished. Firstly, a stress-strain softening law is obtained, as well as, the desired mesh-independence is realized. Then, it can be understood that by that division, the softening diagram is attributed to the area specified by h, namely the part of the continuum where the crack is expected to localize, so local damage was the expected response of the developed model. Next, employing the separation of the total strain into an elastic, ε^e, and an inelastic, ε^c, part (that accounts for fracture), according to the smeared crack approach, the concluding stress-strain law of Figure 3.17 is at hand.

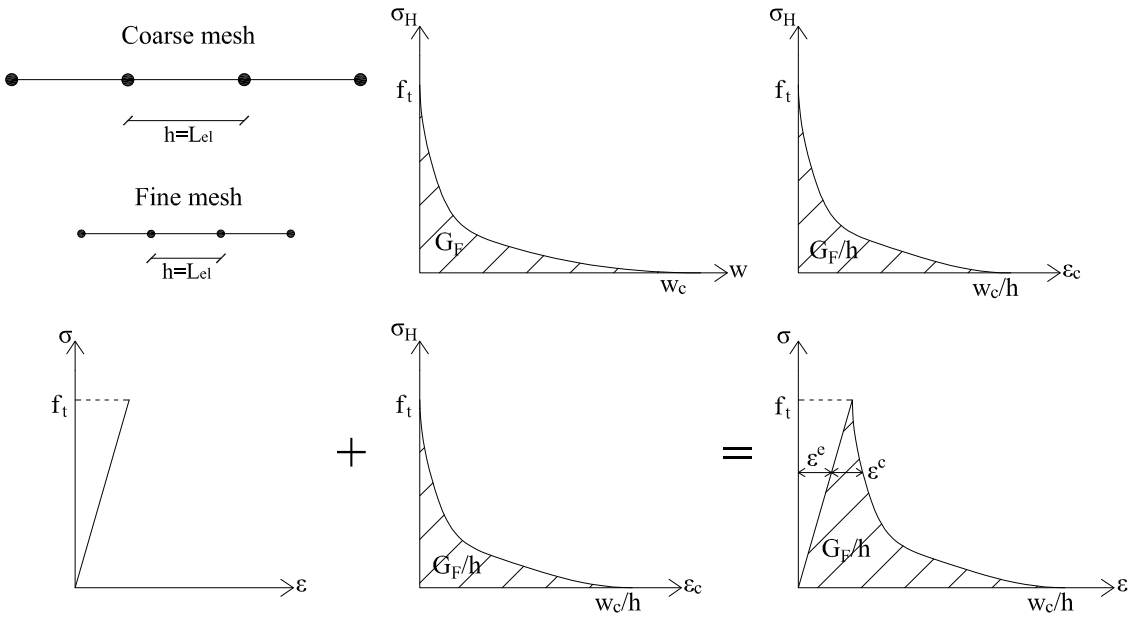

Figure 3.17: *Mesh-independent stress-strain law (inspired by [17])*

After scaling the softening law with the crack band-width, then the form of the curve in the post-cracking region acquires a certain dependence on that parameter. Since, h, was chosen as the element length, it is straight forward to deduce that the finer the mesh, the lower the crack band-width, h. In Figure 3.18 the aforementioned relation is depicted. During the modelling phase, it was observed that the expected localization of fracture in concrete was obtained more difficult as the chosen mesh was finer. In particular, in order to accomplish the goal of localized cracking with a finer mesh, the incremental step size should be decreased significantly.

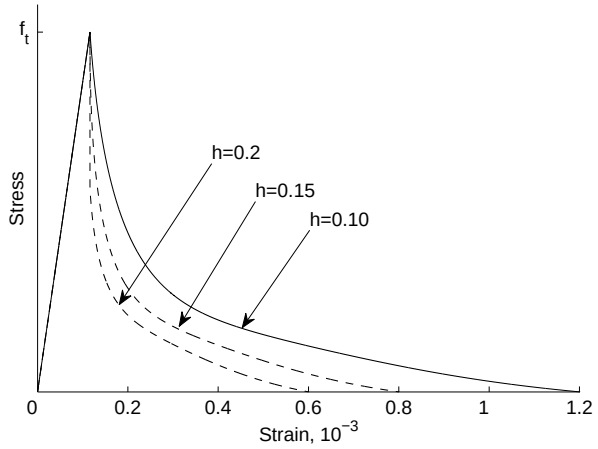

Figure 3.18: *Constitutive law of concrete*

A similar effect on the stress softening law and in the modelling process, as it was described for the crack band-width, h, was observed by the value of the *fracture energy*, G_F, that should be inserted in the model. Many sources and methods are proposed in literature for the proper selection of that parameter, as the pertinent choice is related to many issues of material uncertainties and specimens' size effects. The reader is referred to [27] and [37] for more information. The actual number selected in the present thesis was that of $G_F = 76,\ [N/m]$.

The actual shape of the stress-strain law for concrete after scaling it with the element length, for varying *fracture energy* can be seen in Figure 3.19. As it was noted for the crack band-width for finer meshes, a higher value of *fracture energy* changes significantly the overall shape of the concrete tensile softening law. Namely, for $G_F = 76, [N/m]$, the change in stress in the softening region does not take place as abruptly as is the case for example when $G_F = 15, [N/m]$. This is the reason why it was more difficult to obtain the expected localized fracture of concrete for the higher value of *fracture energy*. Instead, in order to capture local damage, the incremental step had to be reduced to very small values.

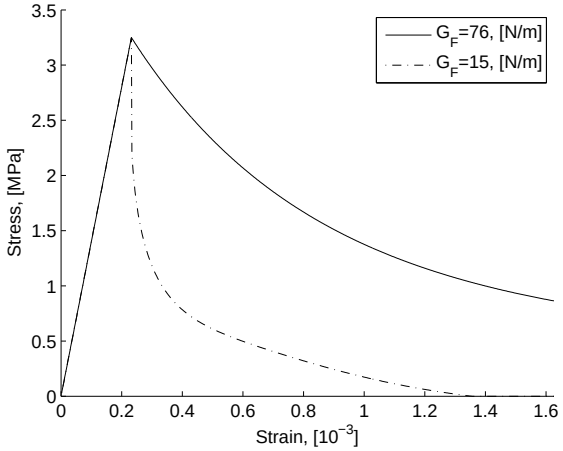

Figure 3.19: *Tensile law for varying fracture energy,* $[N = 100$ *elements*$]$

Furthermore, a bifurcation analysis was performed using the developed model on a reinforced concrete beam subjected to 'four-point bending', with higher *fracture energy* ($G_F = 76,\ [N/m]$),

which if an adequately small incremental step was not chosen, the resulting load-deflection curve would exhibit distributed, rather than localized cracking. If a bifurcation point would exist at the point on the load-deflection diagram where the first localized crack should appear, then one could conclude that the system is following an unstable equilibrium path, since from 'reality' it is known for the specific 'four-point bending' problem that the path which results in localization is the one which releases more energy, the stable one. Then, via the *arc-length-control* method and an appropriate guess, it would be possible to enforce the solution towards the 'real' response which involves localization. However, after checking the lowest eigenvalues of the tangent stiffness matrix right before the possible critical points and after those, no change of sign was observed. Thus, the existence of bifurcation points was excluded, a fact that led to the conclusion that it was most probably the value of the *fracture energy* and the crack band-width, which governed the difficulty of localized cracking to take place.

The aforementioned difficulties in obtaining the expected localized fracture in concrete were overcome, mainly, by using a weaker middle element (i.e. the most stressed one upon adding the self-weight in the applications examined in Chapter 4). That was accomplished by inserting lower tensile strength and *fracture energy* for the middle element, which was the one where the first localized crack was expected to form. Another way to 'trigger' localization was by updating the *history* variable (see also Section 3.4.1 for more details on the *history* variable) using values for the crack width that resulted from 'controlled' non-converged *Newton's* iterative steps, only in critical points, i.e. when cracks were about to form. The term 'controlled' refers to the fact that out of all the non-converged *Newton's* iterative steps that appeared within a critical incremental step, only the values for the crack width from the iterative step with the least divergence were stored in the *history* variable. That measure had a perturbation effect on the stiffness of the most stressed part of the beam, where the first crack was to form, contributing in obtaining the first localized crack, using less integration points than it would be necessary to use if the *history* variable was updated only by converged *Newton's* iterative steps.

3.7 Description and flowchart of the program

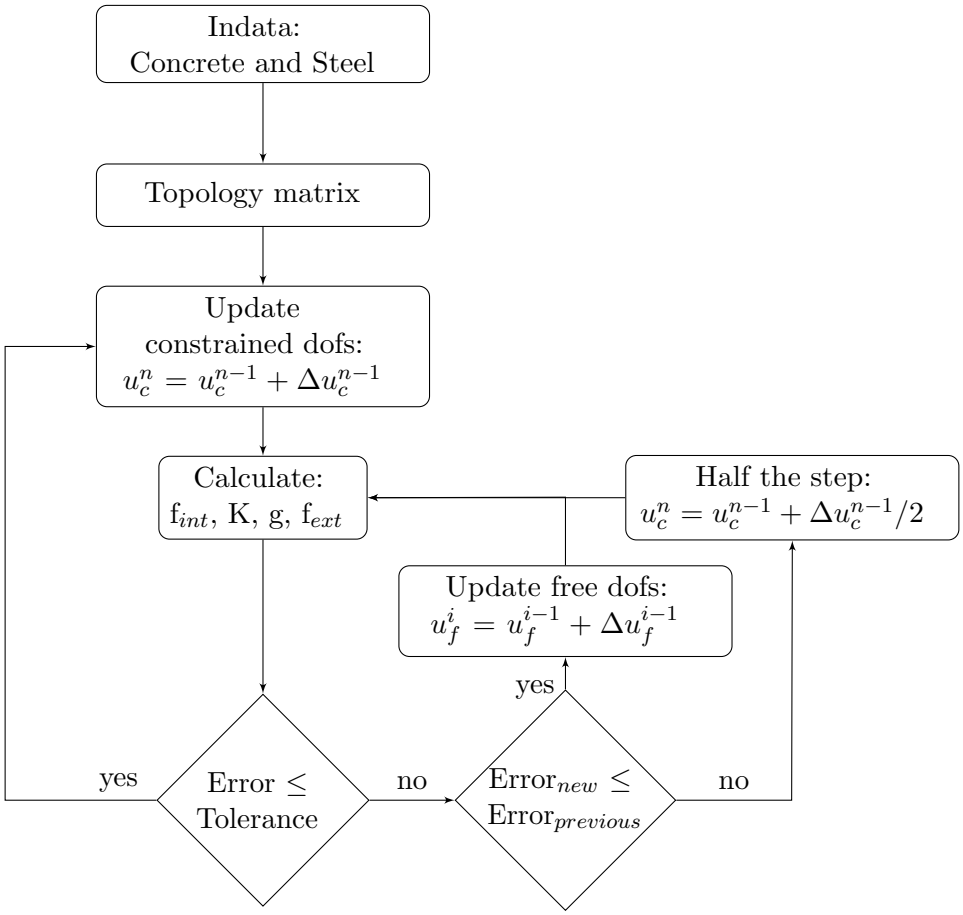

Figure 3.20: *Flowchart showing the algorithm for the reinforced concrete model accounting for the bond-slip*

Figure 3.20 shows in schematic way the basic steps of the developed beam model. After the indata, the geometry and material parameters of the concrete and steel were defined and a topology matrix was established. The topology matrix contains the information on the degrees of freedom belonging to each element. This is used to assemble the global vectors and matrices.

The method used in the model is displacement control. This method is easy to use when dealing with point loads. For that case nodes are locked under the loads and displaced with a predefined step. The solution is then iterated for the displacement vector, u, where the converged vector from the previous step taken as an input for the new iteration and the nodes under the point loads displaced with the predefined step. The tangent stiffness matrix, internal, external (only if distributed load is also applied) and out of balance force vector are calculated. If the error, which is the norm of the out of balance force vector, is smaller than the tolerance set in the beginning, next iteration is performed. Otherwise the free degrees of freedom in the displacement vector are updated according to the Newton iteration scheme but if and only if the error is smaller than the previous error from the same step. If this criterion is not met the step is halved. The load corresponding to each converged solution is taken as the reaction forces in the internal force vector.

The program has also a feature, in which if convergence is not obtained after halving the step for a predefined number of times the program is forced to try the next step with the latest converged displacement vector.

4 Evaluation and comparison with experiments and Eurocode

4.1 Experiments from literature

In the present chapter, methods that will be presented in Section 4.2 are used to calculate beams of the same length, cross-section and material properties as beams tested in the laboratory by Gilbert et al. [12]. In the pertinent study, twelve specimens were cast (six beams and six slabs). With regard to the beams, three different cross-sections were used.

For each cross-section, two identical specimens were made and tested at different concrete ages. The dimensions and the cross-sections of the beams are given in Figure 4.1 and Table 4.1. The material data for the three different configurations of the beams are shown in Table 4.2. Since the values for the steel properties were not given in the experimental results, they were assumed; the characteristic tensile strength, $f_{yk} = 500\ MPa$, and the elastic modulus, $E_s = 200\ GPa$. The concrete properties were interpolated from measured values for appropriate ages. This is reasonable since the change in properties is small. The uniaxial tensile strength was obtained from tensile splitting tests, the used relation is given in Section 4.2.2.

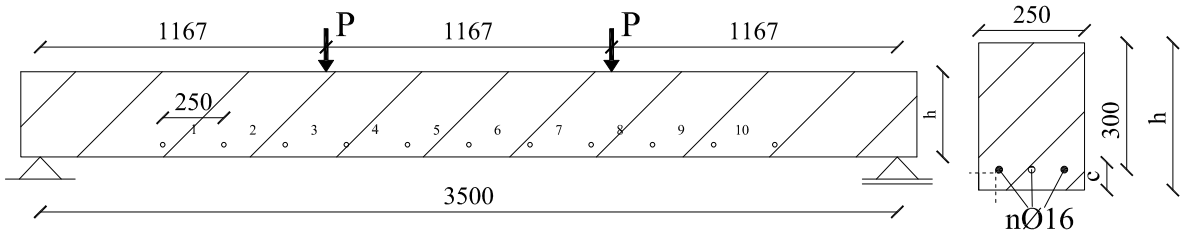

Figure 4.1: *Beams test configuration with dimensions, varying parameters and cross section layout. Test setup from Gilbert et al. [12]*

Table 4.1: Values of varying parameters of the beams

	h [mm]	c [mm]	n [bars]
B1	348	40	2
B2	333	25	2

Table 4.2: Material properties of the tested beams, the numbers in bold represent measured values, the other are interpolated values.

Age [days]	27	28	42	45	48	53	54	55	63	68
f_{cm} [MPa]	36.0	**36.3**	36.5	36.6	**36.6**	37.1	37.2	**37.3**	**39.1**	40.1
f_{ctm} [MPa]	3.05	**3.06**	3.19	3.22	3.25	3.30	3.31	3.31	**3.39**	3.44
E_{cm} [GPa]	**26.9**	27.0	27.7	27.8	28.0	28.2	28.2	28.3	28.7	**28.9**

4.2 Analytical calculations

To verify the developed FEM beam model simple analytical calculations were conducted. They were then compared to experimental results. Furthermore experimental results were used for comparison.

4.2.1 Mid span deflection

Euler-Bernoulli beam theory was used to calculate the moment and deflection resulting from bending.

$$\frac{d^2w}{dx^2} = -\frac{M}{EI} \tag{4.1}$$

The beams were all statically determinate and symmetric, see Figure 4.1. Therefore the sectional forces can be determined by equilibrium equations. This means that globally there is only one solution that fulfills equilibrium, so when the beam cracks there will only be force redistribution locally within the beam cross section. When the beam cracks it looses stiffness gradually until fully cracked[7].

$$\zeta(x) = \left(1 - \left(\frac{M_{cr}}{M(x)}\right)\right) \tag{4.2}$$

$$EI(x) = \zeta(x)EI_I + (1 - \zeta(x))EI_{II} \tag{4.3}$$

where ζ is a distribution coefficient
EI_I is stiffness of the uncracked section
EI_{II} is stiffness of the fully cracked section

The mid point deflection is given by the following equation [7].

$$f(l/2) = l/2 \int_0^{l/2} \kappa(x)dx - \int_0^{l/2} \kappa(x)(l/2 - x)dx \tag{4.4}$$

where κ is the curvature given by Equation (4.1)

4.2.2 Tensile strength

When calculating the crack widths the uniaxial tensile strength, f_{ctm} is needed. In Section 4.1 test results are compared to the EC2 model for crack widths. In the experimental results presented in Gilbert et al.[12] the concrete has been tested by using tensile splitting test. The FIB model code from 2010 [9] recommends that the uniaxial tensile strength is determined from splitting test as

$$f_{ctm} = A_{sp} \cdot f_{ct,sp} \tag{4.5}$$

where A_{sp} is a conversion factor, FIB Model code suggests 1.0
$f_{ct,sp}$ is the mean splitting tensile strength

4.2.3 Steel stress

The steel stress σ_s in a beam in state II, fully cracked was calculated using Naviers formula for bending stress

$$\sigma_s = \frac{M}{I_{II}}(d - x_{II}) \cdot \alpha_c \tag{4.6}$$

where M is the moment in the section
d is the distance from the top edge down to the gravity center of reinforcement
x_{II} is the depth of compressive zone in the reinforced concrete beam in state II
I_{II} is the second moment of area of the fully cracked cross section in state II
α_e is the ratio E_s/E_c

The second moment of area was calculated as

$$I_{II} = \frac{bx_{II}^3}{3} + A_s\alpha_c\left(d - x_{II}\right)^2$$

and the depth of the concrete compressive zone in state II, x_{II}, without compressive reinforcement and linear stress-strain relation can be solved from the following second order polynomial

$$\frac{bx_{II}^2}{2} - A_s \cdot \alpha_c(d - x_{II}) = 0$$

4.2.4 Crack widths

The characteristic crack width was calculated according to the Eurocode standard

$$w_k = s_{r,max}(\varepsilon_{sm} - \varepsilon_{cm}) \tag{4.7}$$

where $s_{r,max}$ is the maximum crack spacing
ε_{sm} is the mean strain in the reinforcement
ε_{cm} is the mean strain in the concrete between cracks

EC 2 gives an empirical expression to calculate the difference between the mean reinforcement and concrete strain.

$$\varepsilon_{sm} - \varepsilon_{cm} = \frac{\sigma_s - k_t \dfrac{f_{ctm}}{\rho_{p,eff}}\left(1 + \alpha_e \rho_{p,eff}\right)}{E_s} \geq 0.6\frac{\sigma_s}{E_s} \tag{4.8}$$

where σ_s is the tensile stress in the cracked section
f_{ctm} is the mean uniaxial tensile strength
α_e is the ratio E_s/E_c
$\rho_{p,eff}$ $\dfrac{A_s}{A_{c,eff}}$
$A_{c,eff}$ is the effective tension concrete area
k_t is a load duration factor, 0.6 is used for short term

For a beam in pure bending and with high bond bars the maximum crack spacing can be assumed from EC2

$$s_{r,max} = 3.4c + \frac{0.17\phi}{\rho_{p,eff}} \tag{4.9}$$

where c is the concrete cover
ϕ the reinforcement bar diameter

4.3 Analysis with the developed beam model

In the analysis with the developed model the dead weight of the beam was applied first, in one step using load control. After that the developed model runs with displacement control of the two nodes under the point loads, as seen in Figure 4.1. Since the nodes have to be positioned directly under the loads and an element in the middle is wanted the choice of number of elements is restricted to 6n+3. This is a simply supported beam and the boundary conditions are the following

Essential or Dirichlet boundary conditions :
i) $u^o = 0 \quad \text{at} \quad x = 0$
ii) $w = 0 \quad \text{at} \quad x = 0 \quad \text{and} \quad x = L$
Natural or Neumann boundary conditions :
i) $\overline{M} = 0 \quad \text{at} \quad x = 0 \quad \text{and} \quad x = L$
ii) $\overline{N} = 0 \quad \text{at} \quad x = L$
iii) $\overline{N}_i = 0 \quad \text{at} \quad x = 0 \quad \text{and} \quad x = L$

The input values are shown in Table 4.3

Table 4.3: Input values for the reinforced concrete model

Concrete	*B1 and B2*
Height of section	348 and 333 mm
Width of section	250 mm
Young's Modulus	28 and 27.7 GPa
Compressive strength	36.6 and 37.5 MPa
Tensile strength	3.25 and 3.3 MPa
Tension softening	Hordjik
Compressive law	Figure 3.7
Fracture energy	76 N/m
Crack approach	Smeared crack
Crack band width	L_{el}
Steel	
Effective depth	300 mm
Yield strength	500 MPa
Young's modulus	200 GPa
Total steel area	400 mm^2
Model specification	
Number of elements	75
Height integration scheme	Lobatto
Number of Lobatto points	15
Length integration scheme	Gauss
Number of Gauss points	3
Maximum step length	$2 \cdot 10^{-7}\ m$
Selfweight	1.5 kN/m
Part of bond-slip linear	20%

In the bond-slip relation, presented in Section 3.4, the stiffness in the beginning is extremely high and does not work with the developed model. The stiffness has to be adapted so that the first 20% of s_1 are taken as a linear branch and the rest of the curve is unchanged.

Since the four point bending case has a large constant moment area, a uniformly distributed load, representing the selfweight, was added to the beam in order to initiate the cracking in the middle element.

A weaker middle element was used in order to initiate the cracking. The parameters that were different in that element were that the tensile strength was 2.75 MPa instead of 3.25 MPa, and the fracture energy was 15 N/m instead of 76 N/m. These values were chosen as the ones that gave cracking and localization in the middle element for the four point bending case.

4.4 Comparison of results

In section 4.2.4 the Eurocode method for calculating crack widths was presented. Equation (4.7) gives the upper characteristic crack width that means that 95% of cracks should be smaller than the values given by the equation. In the experiments, Gilbert et al. [12], all the cracks were measured. The maximum crack opening was compared to the Eurocode model, see Figures 4.2 and 4.4.

4.4.1 Stiffness adaptation method

The stiffness adaptation method was adopted to compare with the load-deflection diagram retrieved from the developed model. Stiffness adaptation is a Finite Element method where the stiffness is changed if a element cracks, i.e. when a element cracks it goes from being uncracked, in state I, to being fully cracked, in state II. The element is determined to be cracked or not from the average moment in each element and if that is higher than the cracking moment. It is obvious that when using this method, the tension stiffening or the influence of the bond slip are not considered in the development of crack and crack positions.

4.4.2 Diana analysis

Models of the beams were set up using the commercial FE program Diana, where all the non-linearities of the material were considered. Classic beam elements, L7BEN, were used where both translational degrees of freedom were locked at the left boundary and on the right side the vertical translation was locked. The beam consisted of 11 nodes and 10 elements. Other input values and parameters are specified in Table 4.4. No bond slip was considered, i.e. the reinforcement was embedded with full interaction between concrete and steel. Therefore the crack band width was choosen as the expected crack spacing calculated from (4.9).

Table 4.4: Diana input for the non-linear FE-analysis

Concrete	*B1 and B2*
Height of section	348 and 333 mm
Width of section	250 mm
Young's Modulus	28 and 27.7 GPa
Compressive strength	36.6 and 37.5 MPa
Tensile strength	3.25 and 3.3 MPa
Tension softening	Hordjik
Compressive law	Thoren
Fracture energy	76 N/m
Crack approach	Smeared crack
Crack band width	0.176 m
Steel	
Effective depth	300 mm
Yield strength	500 MPa
Young's modulus	200 GPa
Yield criterion	Von Mises
Total steel area	400 mm^2

4.4.3 Global deflection and crack widths

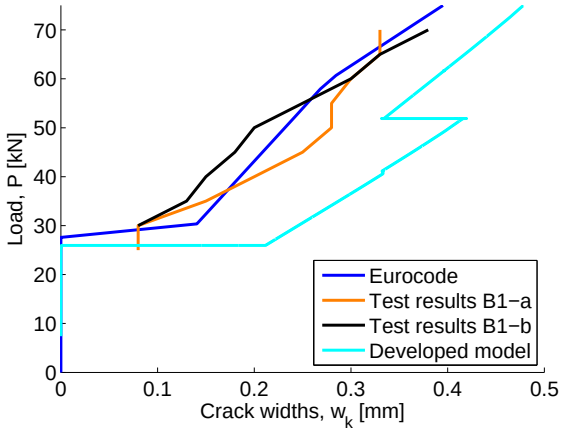

Figure 4.2: *Beam B1, with EC2 crack model and experimental results from Gilbert et al. [12]*

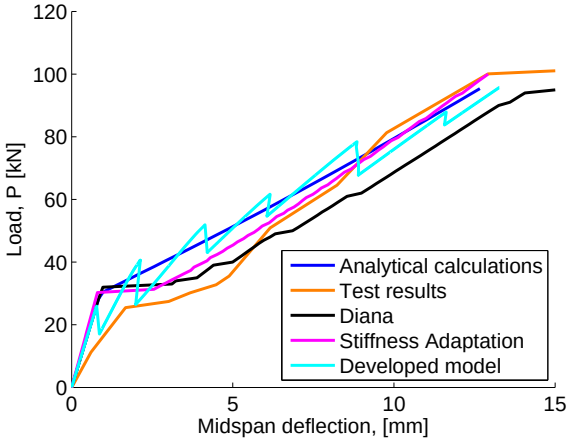

Figure 4.3: *Load deflection curves with different analysis for beam B1*

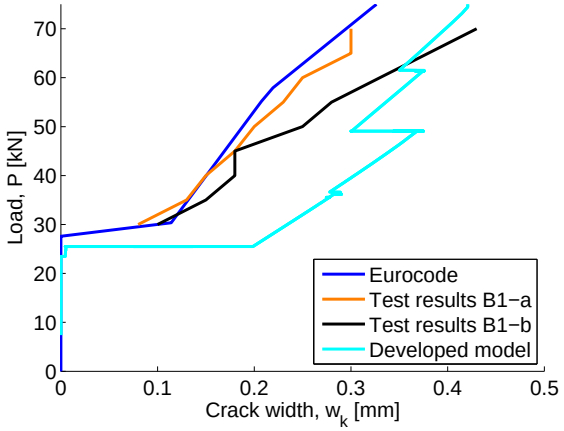

Figure 4.4: *Beam B2, with EC2 crack model and experimental results from Gilbert et al. [12]*

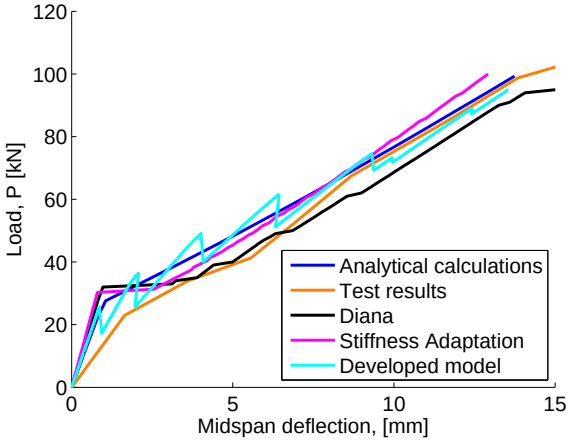

Figure 4.5: *Load deflection curves with different analysis for beam B2*

The results from the developed model can be seen in Figures 4.2 to 4.5. Apart from the regions of the graphs which indicate the occurrence of the first and the subsequent cracks, the values in the history variable (see Section 3.4.1 for the pertinent discussion) where updated keeping the values for the crack opening that resulted only from converged *Newton's* steps. However, in those regions where cracking took place, as another means to trigger localization, also some 'controlled' values of the crack opening resulted from non-converged *Newton's* steps were used to update the history variable.

In the load deflection relation presented in Figure 4.3 and 4.5, cracking in the test results curve started for lower applied load than the calculated. The difference can be partly due the fact that the test results curves, that were taken from Gilbert et al. [12], had to be taken graphically from the report, which might have created errors. This was especially the case for low load and deflections.

For the analytical calculations, stiffness adaptation, and the developed model, failure was assumed to take place when the stress in the reinforcement reached yielding.

The developed model cracked for a lower load than the analytical curve, the stiffness adaptation method and the model 'constructed' in Diana, since a weaker middle element was used to initiate cracking. After the cracking, the curve shows good correlation with the other methods. The crack widths from the developed model showed substantially larger crack widths, seen in Figure 4.2 and 4.4 especially when only one crack had formed, from the cracking load to roughly 50 kN, like mentioned before this is due to the reduction of fracture energy mentioned in Section 4.3. This difference reduces as the cracking progresses and the second and third cracks localize.

4.4.4 Crack pattern

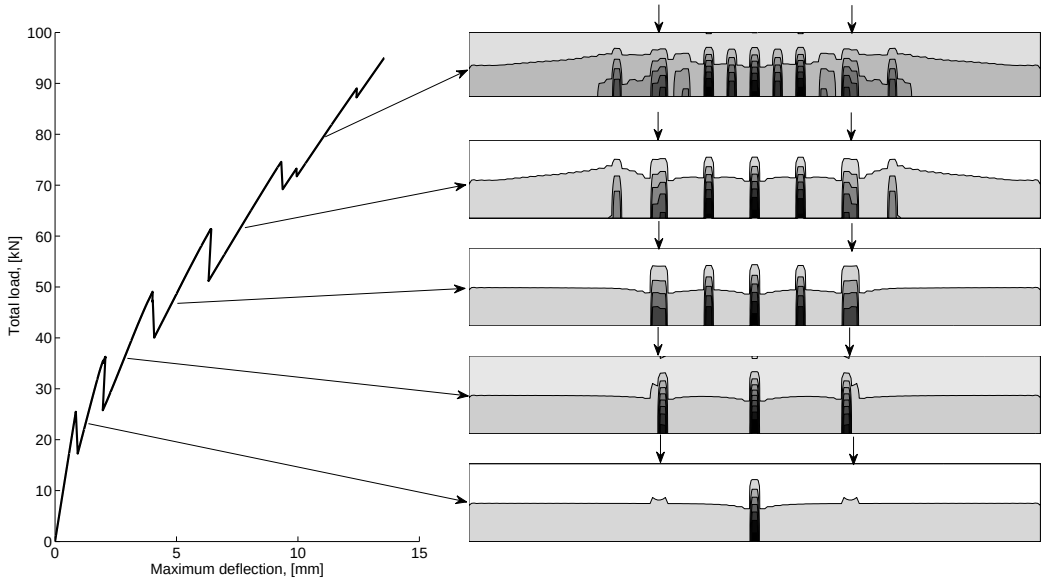

Figure 4.6: *Crack pattern of beam B2 with the load deflection curve on the left*

The crack patterns for different loads can be seen in Figure 4.6. Arrows point to what load level, on the load-deflection curve, each pattern corresponds to. The cracks in the constant moment region were always well defined in all steps, while under the loads, i.e. where cracks 2 and 3 form, the cracks tended to go from localized to distributed cracks as the load increased. A second thing worth to note about crack pattern is the cracking sequence, especially that cracks localized under the concentrated loads rather than in the positions of crack 4 and 5. It was observed that where cracks 4 and 5 localize, those elements the highest strain of all the uncracked elements and the next pair of cracks expected there. However due to some numerical difficulties under the point loads and the fact that some limited values of the crack opening that resulted from non-converged *Newton's* iterative steps were used in the *history* variable (see also Section 3.6 for more details on the non-converged *Newton's* iterative steps), the cracking sequence is rather peculiar as presented in Figure 4.6.

5 Conclusions and suggestions for further work

In the present thesis, a 1D finite element model was developed, that is able to describe the response of a reinforced concrete beam that undergoes local damage, while accounting also for the relative slip at the steel/concrete interface. Three non-linear constitutive laws were implemented for the materials. A softening law was used to account for fracture in concrete; to obtain objectivity of the results upon mesh refinement, it was scaled with the element length. A simple elasto-plastic law was inserted for steel and *Eligehausen's* law was used for the bond-slip. *Newton's* iterative scheme was chosen for the solution of the non-linear system of equations obtained from the FE-formulation of the problem. The pertinent equations were developed for the case of a reinforced concrete beam subjected to transverse distributed loading. Pertaining to the incremental procedures, *load-control*, *displacement-control*, *arc-length-control*, as well as combinations between the aforementioned methods were applied in order to obtain results overcoming numerical problems of various kinds.

The developed model was used in non-linear FE analysis of reinforced concrete beams subjected to 'four-point bending'. Several observations were made: First, initiation of cracking was a crucial parameter in the model. It was found that the combination of a higher value of *fracture energy*, together with the scaling of the stress softening diagram of concrete with the element length resulted in a less steep softening curve. Secondly, it was observed that the less steep the softening curve, the more difficult was for the first localized crack to appear. Only by 'triggering' localization, the first concentrated crack would form. Ways for such 'triggering' were to reduce the tensile strength and the *fracture energy* of the middle element. In that way, a more brittle behaviour in that element was forced.

Furthermore, a certain dependence of the results obtained from the developed model on the chosen incremental step size was observed. This effect was attributed to the influence of the *history* variable introduced in order to account for the unloading of the beam upon opening and closure of existing cracks. A larger step size would lead more integration points to pass beyond the *cracking strain*. These points would, then, upon unloading, instead of following the linear branch of the stress-strain law, unload with the secant stiffness from the point reached in the softening law towards the origin of the coordinate system.

A rather unexpected phenomenon was captured during the analysis for the 'four-point bending' problem. Namely, the first cracking would always tend to appear under the point loads, instead of forming at the middle element, which was the most stressed one, as the self-weight was included. Then, depending on where the first crack/cracks would appear, the sequence of appearance of the next cracks was also affected.

Some comments could also be stated upon the stiffness of the implemented bond-slip relation, *Eligehausen's* law in particular. The first one is related to the initial infinite stiffness of the pertinent exponential law. Upon using the inverse of the tangent stiffness matrix in the *Newton's* iterative scheme, the infinite stiffness of the initial branch of *Eligehausen's* law resulted in an non-invertible matrix. Even when trespassing the stiffness value evaluated for 'zero' slip, the stiffness of the constitutive model is so high, that in order to be implemented, a very low step for the slip should be inserted in the displacements field so as to avoid divergence of the iterative procedure. In order to overcome these objective obstacles pertaining to the bond-slip law, it was decided to use a linear approximation of the initial part of the exponential curve, stiff enough to allow for the expected number of cracks to appear for each specific model application. However, the extent of such an initial branch has a significant influence on the

crack widths and the crack spacing.

As exposed in the previous discussion, many parameters affected the resulting scheme, whether it is the load-deflection response, or the crack widths and crack patterns, as a result of the material non-linearities considered in the developed model. Therefore further work is needed in order to improve the performance of the model, as well as, to broaden its applicability, if possible. A suggestion of profound importance for future work is regarded to be the study on 'triggering' cracking consistently, i.e. updating the *history* variable keeping the values of the crack width that result only from converged *Newton's* iterative steps. Furthermore, a parametric study on the effect of the value of the *fracture energy* on the overall response of the system is considered to be essential.

Also, the influence of the stiffness of the initial linear approximation of the *Eligehausen's* law is a parameter that is worth investigating further, especially the effect that it has on the crack widths and crack pattern. Referring to *Eligehausen's* law, it should be noted that besides the difficulties in its numerical application, there is very limited guidance in the literature to overcome the obstacles just described.

Another interesting investigation is regarded the study upon the phenomenon described earlier regarding the occurrence of the first crack/s under the point loads at the 'four-point bending' problem. It is still not clear why the first crack in the pertinent problem would always tend to form under the point loads instead of appearing in the middle element where the stress had a maximum provided that the self-weight was included. The pertinent obstacle in the analyses performed in the present study was attributed mainly to 'numerical issues'. Possible ways to 'tackle' them, as a proposed future work, are considered to be the study of half the beam, exploiting symmetry appropriately, as well as, increasing the integration points especially over the cross-sectional height and, finally, to perform the analyses with an adequately reduced step size.

Finally, it was observed that the number of integration points along the height of the cross-section, as well as, over the element length had significant influence on whether convergence would be achieved and on the overall performance of the model. Therefore, a study on the number of integration points in both directions is considered of great importance for future work.

References

[1] Z. P. Baiant. "Mechanics of distributed cracking". In: *Appl. Mech. Rev* 39.5 (1986), pp. 675–705.

[2] CEB-FIB. *Model Code 1990*. Vol. 1. Thomas Telford Services Ltd, 1993.

[3] CEN. *Eurocode 2: Design of concrete structures - Part 1-1*. European Commitee for Standardization, 2004.

[4] M. A. Crisfield. "A fast incremental/iterative solution procedure that handles "snap-through"". In: *Computers & Structures* 13.1 (1981), pp. 55–62.

[5] T. Diana. "TNO Diana manual release 9.4.4". 2012.

[6] R. Eligehausen, E. P. Popov, and V. V. Bertero. "Local bond stress-slip relationships of deformed bars under generalized excitations". In: (2012).

[7] B. Engstrom. *Design and analysis of continuous beams and columns*. Chalmers University of Technology, 2011.

[8] B. Engstrom. *Restraint cracking of reinforced concrete structures*. Chalmers University of Technology, 2011.

[9] FIB. *Model Code 2010, Draft model code, Bulletin 55*. International Federation for Structural Concrete, 2010.

[10] C. Frederick and P. Armstrong. "A mathematical representation of the multiaxial Bauschinger effect". In: *Materials at High Temperatures* 24.1 (2007), pp. 1–26.

[11] C. F. Gerd Jan Schreppers and Hee-Jeong. "Prediction of Crack-width and Crack-pattern". 2011.

[12] R. Gilbert et al. *An Experimental Study of Flexural Cracking in Reinforced Concrete Members Under Short Term Loads*. UNICIV report. University of New South Wales, 2004.

[13] L. G.R and Q. S.S. *The finite element method, a practical course*. Butterworth Heinemann, 2003.

[14] K. D. Hjelmstad. *Fundamentals of structural mechanics*. Springer, 2005.

[15] E. Hognestad et al. *A study of combined bending and axial load in reinforced concrete members / [A report of an investigation conducted by the Engineering Experiment Station, University of Illinois, under the auspices of the Engineering Foundation, through the Reinforced Concrete Research Council*. English. University of Illinois, Urbana : 1951, 128 p. :

[16] B. C. Jensen. *Teknisk Stabi*. Vol. 21. Nyt Teknisk Forlag, 2011.

[17] M. Jirásek. "Damage and smeared crack models". In: *Numerical modeling of concrete cracking*. Springer, 2011, pp. 1–49.

[18] M. Jirásek. "Numerical modeling of deformation and failure of materials". In: *Lecture notes* (1999).

[19] P. Kotronis and J. Mazars. "Simplified modelling strategies to simulate the dynamic behaviour of R/C walls". In: *Journal of earthquake engineering* 9.02 (2005), pp. 285–306.

[20] P. Kotronis et al. "Local second gradient models and damage mechanics: application to concrete". In: *11th international conference on fracture, Turin, Italy, Org. ICF, cd, paper*. 5712. 2005, pp. 20–25.

[21] C. La Borderie. "Phénomènes unilatéraux dans un matériau endommageable: modélisation et application à l'analyse de structures en béton". PhD thesis. 1991.

[22] G. C. Lykidis and K. Spiliopoulos. "3D Solid Finite-Element Analysis of Cyclically Loaded RC Structures Allowing Embedded Reinforcement Slippage". In: *Journal of structural engineering* 134.4 (2008), pp. 629–638.

[23] J. Mazars et al. "Numerical modelling for earthquake engineering: the case of lightly RC structural walls". In: *International journal for numerical and analytical methods in geomechanics* 28.7-8 (2004), pp. 857–874.

[24] J. Mazars. "A description of micro-and macroscale damage of concrete structures". In: *Engineering Fracture Mechanics* 25.5 (1986), pp. 729–737.

[25] M. Menegotto. *Method of analysis for cyclically loaded RC plane frames including changes in geometry and non-elastic behaviour of elements under combined normal force and bending*. IABSE, 1973.

[26] G. Monti and E. Spacone. "Reinforced concrete fiber beam element with bond-slip". In: *Journal of Structural Engineering* 126.6 (2000), pp. 654–661.

[27] S Muralidhara et al. "Fracture process zone size and true fracture energy of concrete using acoustic emission". In: *Construction and Building Materials* 24.4 (2010), pp. 479–486.

[28] H. Nakamura and T. Higai. "Compressive fracture energy and fracture zone length of concrete". In: *Modeling of inelastic behavior of RC structures under seismic loads* (2001), pp. 471–487.

[29] N. Ottesen and H. Pettersson. *Introduction to the finite element method*. Pearson Education Limited, 1992.

[30] G. Pijaudier-Cabot and Z. P. Bazant. "Nonlocal damage theory". In: *Journal of Engineering Mechanics* 113.10 (1987), pp. 1512–1533.

[31] M. Plos. *Finite element analyses of reinforced concrete structures*. Chalmers University of Technology, 2000.

[32] B. Richard et al. "A multi-fiber approach for modeling corroded reinforced concrete structures". In: *European Journal of Mechanics-A/Solids* 30.6 (2011), pp. 950–961.

[33] C Rosselló, M Elices, and G. Guinea. "Fracture of model concrete: 2. Fracture energy and characteristic length". In: *Cement and concrete research* 36.7 (2006), pp. 1345–1353.

[34] A. Rouquand and C. Pontiroli. "Some Considerations on Implicit Damage Models Including Crack Closure Effects and Anisotropic Behaviour". In: *Proc. FRAMCOS-2, Ed. FH Wittmann, AEDIFICATIO Publisher, Freiburg, Germany* (1995).

[35] G. J. Schreppers. "Embedded Reinforcement". 2011.

[36] E. Spacone, F. Filippou, and F. Taucer. "Fibre beam-column model for non-linear analysis of R/C frames: Part I. Formulation". In: *Earthquake Engineering and Structural Dynamics* 25.7 (1996), pp. 711–726.

[37] V. Vydra, K. Trtík, and F. Vodák. "Size independent fracture energy of concrete". In: *Construction and Building Materials* 26.1 (2012), pp. 357–361.

[38] F. Wang et al. "Simulation analysis of static and shaking table tests on rc columns with insufficient lap splices". In: *SMIRT 19th Conference*. 2007.

Appendix

```
%-------------------------------------------
%Main file for the solution of the four-point
%bending problem employing linear constitutive
%models for the materials with displacement control
%-------------------------------------------
%Created by: Dimosthenis Floros
%            Olafur Agust Ingason
%-------------------------------------------

clear all
close all
clc

%Concrete cross-section definition

h=0.333;                    %Cross-sectional height [m]
b=0.25;                     %Cross-sectional width  [m]
d=0.3;                      %Distance from top to reinforcement [m]
c=0.04;                     %Concrete cover of reinforcement [m]

%Steel bar cross-section definition

phi=0.016;                  %Diameter of the i-st layer of reinforcement [m]
n_bars=2;                   %Number of rebars at i-st layer [#]
As_i=pi*phi^2/4;            %Area of one bar [m^2]
z_i=h/2-d;                  %Distance of the G.C of the i-st layer of rein-
                            %forcement from reference axis of the beam [m]
s_i=pi*phi;                 %Circuference of one rebar [m]

%Concrete material parameters

f_t=3.3e6;                  %Tensile strength of concrete [Pa]
f_c=36.6e6;                 %Compressive strength of concrete [Pa]
Ec=27.7e9;                  %Elastic modulus of concrete [Pa]
e_t=f_t/Ec;                 %Cracking strain  [-]
G_f=76;                     %Fracture energy  [N/m]

%Steel material parameters

Es=200e9;                   %Steel Youngs modulus [Pa]
fy=500e6;                   %Yield stress [Pa]

%Discretization

num_el=33;                                  %Number of elements
L=3.5;                                      %Length of the beam
L_el=L/num_el;                              %Length of the element

% Topology matrix

Edof=zeros(num_el,9);
```

```
Edof(1,2:end)=1:8;
Edof(2,2:end)=[2 9 5 6 10 11 8 12];
Edof(3,2:end)=[9 13 10 11 14 15 12 16];

Ex=zeros(num_el,2);

for i=0:(num_el-1)

    Edof(i+1,1)=i+1;

    Ex(i+1,1)=L_el*i;
    Ex(i+1,2)=L_el*(i+1);

end

for i=4:num_el

    Edof(i,2:end)=Edof(i-1,2:end)+4*ones(1,8);

end

%Number of int points, guessed displacements

ne_x=3;             %Number of integration points along the element length
u=zeros(max(max(Edof)),1);  %Initial guess for the iterations' scheme
ne_z=15;               %Number of integration points over height of cross sec
[z,w]=lglnodes(ne_z-1); %Possitions and weights of Lobatto integration
z=-z'*h/2;

%Calculate the external force vector
F_ext=f_external(-1.5e3,Edof,L_el,num_el);

%Properties for the f_internal.m
ep_inter=[z_i,Es,fy,Ec,e_t,f_t,b,As_i,f_c,s_i,n_bars,G_f];

dw=-10e-7;
steel_yield=0;
p=0;
e_cr_old=zeros(length(z),ne_x*num_el);

while steel_yield==0
    disp(p)
    p=p+1;
    u_previous=u;

    %Update the constrained degrees of freedom
    bc=[1 0;  3 0; Edof(end,6) 0;....
        Edof(num_el/3,6) u(Edof(num_el/3,6))+dw; ...
        Edof(2*num_el/3,6) u(Edof(2*num_el/3,6))+dw];

    bc_total=(1:max(max(Edof)))';
    Constr=bc(:,1);
    Free=setdiff(bc_total,Constr);

    u(Constr)=bc(:,2);
```

```
Error=100; TOL=1e-4; counter=0; old_Error=1e100; upp=1; temp=0;

while Error>TOL || rcond(K_FF)<1e-14

    counter=counter+1;

    [F_int,K,ec,x_el_out,es,t_di,delta_i,M,N,slip,steel,...
        e_cr_new,s_concrete]=f_internal(num_el,ne_x,ne_z,z,L_el,...
      u,Edof,Ex,ep_inter,e_cr_old,w);

    g_F=F_int(Free)-F_ext(Free);     %Calculate the new out-of-balance
    Error=norm(g_F);                 %Calculate the error
    K_FF=K(Free,Free);               %Extract the Free dofs of the

    %This loop halfs the step if the criteria is met
    while old_Error<=Error || counter==30

        counter=1;
        u=u_previous;

        bc=[1 0;  3 0; Edof(end,6) 0;....
            Edof(num_el/3,6) u(Edof(num_el/3,6))+dw/upp*2; ...
            Edof(2*num_el/3,6) u(Edof(2*num_el/3,6))+dw/upp*2];

        u(Constr)=bc(:,2);

        upp=upp+1;

        [F_int,K]=f_internal(num_el,ne_x,ne_z,z,L_el,u,Edof,Ex,...
        ep_inter,e_cr_old,w);

        g_F=F_int(Free)-F_ext(Free);  %Calculate the new out-of-balance

        old_Error=norm(g_F);           %Calculate the error
        K_FF=K(Free,Free);            %Extract the Free dofs of the

        Da_F=-K_FF\g_F;

        u(Free)=u(Free)+Da_F;

        [F_int,K,ec_out,x_el_out,es,t_di,delta_i,M,N,...
slip,steel,e_cr_new,s_concrete]=f_internal(num_el,ne_x,ne_z,z,L_el,...
u,Edof,Ex,ep_inter,e_cr_old,w);

        g_F=F_int(Free)-F_ext(Free);

        Error=norm(g_F);

        if old_Error>=Error || upp==5
           break
        end


    end

    old_Error=Error;
```

```
        Da_F=-sparse(K_FF)\g_F;    %Solve g(a+Da)=0 for the update Da_F

        if Error>TOL
            u(Free)=u(Free)+Da_F;     %Update the displacements vector
        elseif Error<TOL

            break
        end

        if upp==5
                u=u_previous;
                u(Edof(num_el/3,6))=u(Edof(num_el/3,6))+dw;
                u(Edof(2*num_el/3,6))=u(Edof(2*num_el/3,6))+dw;
                disp('break')
            break
        end

    end

    for col=1:ne_x*num_el
        for row=1:length(z)
            if e_cr_old(row,col)<e_cr_new(row,col)
                e_cr_old(row,col)=e_cr_new(row,col);
            end
        end
    end

    steel_yield=sum(steel>fy);

end
```

```
%
% [F_int,K,ec_out,x_el_out,es,t_di,delta_i,M,N,...
%    slip,steel,e_cr_new,s_concrete]=f_internal(num_el,ne_x,ne_z,z,L_el,...
%    u,Edof,Ex,ep,e_cr_old,w)
%
%-------------------------------------------------------------------------
% PURPOSE
%  Compute the global internal force vector and the global tangent
%  stiffness matrix
%
% INPUT:  num_el             number of elements
%         ne_x               number of integration point along each element
%         ne_z               number of intergration over the height
%         z                  coordinates of the integration points
%         L_el               length of one element
%         u                  displacement vector
%         Edof               topology matrix
%         Ex                 global x-coordintes
%         ep=[z_i,Es,fy,Ec,e_t,f_t,b,As_i,f_c,s_i,n_bars,G_f];
%                            z_i: distance from reference axis to
%                            reinforcement
%                            Es: steel stiffness
%                            fy: yield stress of the reinforcement
%                            e_t: cracking strain of concrete
%                            f_t: tensile strength of concrrete
%                            b: breadth of beam cross section
%                            As_i: steel area of the reinforcement bar
%                            f_c: compressive concrete strength
%                            s_i: circumference of the steel bar
%                            n_bars: the number of bars in the layer
%                            G_f: fracture energy of the concrete
%        e_cr_old            the highest cocrete strain in each Gauss point
%        w                   weights for integration over height
%
% OUTPUT: F_int              the full internal force vector for the given
%                            displacment vector
%         K                  tangent stiffness for a given displacement
%                            vector
%         ec_out             matrix of concrete strain in integration point
%         x_el_out           global possition of the integration point in x
%         es                 vector of steel strain in intergration points
%         t_di               bond stress
%         delta_i            bond-slip in interface
%         M                  moment
%         N                  normal force
%         slip               slip force
%         steel              steel stress in integration points
%         e_cr_new           the cracking strain for the displacement
%                            vector
%         s_concrete         stress in each integration point
%
%-------------------------------------------------------------------------
%
%Written by: Dimosthenis Floros and Olafur Agust Ingason
%
%-------------------------------------------------------------------------
```

```
function [F_int,K,ec_out,x_el_out,es,t_di,delta_i,M,N,...
    slip,steel,e_cr_new,s_concrete]=f_internal(num_el,ne_x,ne_z,z,L_el,...
    u,Edof,Ex,ep,e_cr_old,w)

z_i=ep(1);
Es=ep(2);
fy=ep(3);
Ec=ep(4);
e_t=ep(5);
f_t=ep(6);
b=ep(7);
As_i=ep(8);
f_c=ep(9);
s_i=ep(10);
n_bars=ep(11);
G_f=ep(12);


%Internal vectors and matrices definition
%-------------------------------------------------------------------

x_el=[-sqrt(3/5) 0 sqrt(3/5)]*L_el/2+L_el/2; %Gauss points
w_gauss=[5/9 8/9 5/9];                       %Gauss weights

a=extract(Edof,u);              %Arrangement of displacement to
                                %the pertinent dofs

f_int=zeros(8,1);               %Internal force vector

ec=zeros(ne_z,ne_x);            %Concrete strain

es=zeros(1,ne_x);               %Steel strain

delta_i=zeros(1,ne_x);          %Slip between concrete and rebars

K_u0w=zeros(2,4);               %Block matricies for the tangent stiffness
K_ww=zeros(4,4);
K_diw=zeros(2,4);
K_didi=zeros(2,2);

K=zeros(max(max(Edof)),max(max(Edof))); %Global tangent stiffness matrix

F_int=zeros(max(max(Edof)),1);          %Internal force vector

ec_out=[];x_el_out=[];M=[];N=[];slip=[];steel=[];e_cr_new=[];s_concrete=[];

%-------------------------------------------------------------------

for i=1:num_el

    %Coordinates of int points along the length of element i
    %-----------------------------------------------------

    ex=Ex(i,:);
    x(i,:)=linspace(ex(1,1),ex(1,2),ne_x);
```

```
%-------------------------------------------------------

%Arrange the pertinent displacements of element i
%-------------------------------------------------

a_u0=[a(i,1);a(i,2)];  %Nodal axial displacement at the reference axis

a_w=[a(i,3);a(i,4);a(i,5);a(i,6)];     %Nodal deflections and rotations
                                       %at the nodes

a_di=[a(i,7);a(i,8)];     %Nodal relative slip


%-------------------------------------------------

%Shape functions for the approximation of the slip
%-------------------------------------------------

N_di_1=-1/L_el*(x(i,:)-ex(2));
N_di_2=1/L_el*(x(i,:)-ex(1));

%-------------------------------------------------

%B_matrices (Derivative of the shape functions)
%-------------------------------------------------

B_u0=1/L_el*[-1 1];

B_w_1=-6/L_el^2+12*x_el/L_el^3;
B_w_2=-4/L_el+6*x_el/L_el^2;
B_w_3=6/L_el^2-12*x_el/L_el^3;
B_w_4=6*x_el/L_el^2-2/L_el;

B_di=1/L_el*[-1 1];

%-------------------------------------------------

%Concrete and steel strains at the network of int points
%(ne_x: Integration points along the length of the element)
%(ne_z: Integration points along the cross-section height)
%-------------------------------------------------------------

for j=1:ne_x

    B_w(1,1:4)=[B_w_1(1,j) B_w_2(1,j) B_w_3(1,j) B_w_4(1,j)];

    N_delta_i(1,1:2)=[N_di_1(1,j) N_di_2(1,j)];

    ec(:,j)=B_u0*a_u0-z'*B_w*a_w;

    es(1,j)=B_u0*a_u0-z_i*B_w*a_w+B_di*a_di;

    delta_i(1,j)=N_delta_i*a_di;

end
```

```
%-------------------------------------------------------

%Concrete and steel stresses at the network of int points
%-------------------------------------------------------

[s_si,D_si]=sigma_si(es,Es,fy,ne_x);

%Make the middle element weaker and with lower fracture energy
if i==ceil(num_el/2)
    f_t_new=f_t-0.5e6;
[s_xx_con,D_con,e_cr_nytt]=sigma_xx_con(ne_x,ne_z,ec,Ec,f_t_new/Ec,...
f_t_new,f_c,L_el,15,e_cr_old(:,3*i-2:3*i));
else
[s_xx_con,D_con,e_cr_nytt]=sigma_xx_con(ne_x,ne_z,ec,Ec,e_t,f_t...
,f_c,L_el,G_f,e_cr_old(:,3*i-2:3*i));
end

%-------------------------------------------------------

%f_int_u0
%-------------------------------------------------------------

%Numerical integration along the height of the cross-section

N_con=b*lobatto(z,s_xx_con,w);

N=[N N_con+n_bars*As_i*s_si];

%Numerical ingration across the length of the element

f_int(1:2,1)=B_u0'*gaussi(L_el,(N_con+n_bars*As_i*s_si),w_gauss');

%-------------------------------------------------------------

%f_int_w
%-------------------------------------------------------------

%Numerical integration along the height of the cross-section

M_con=zeros(1,ne_x); dM_con=zeros(1,ne_x); z_dM_con=zeros(1,ne_x);

for i_m=1:ne_x

    M_con(1,i_m)=b*lobatto(z,s_xx_con(:,i_m).*z',w);
    dM_con(1,i_m)=b*lobatto(z,D_con(:,i_m).*z',w);
    z_dM_con(1,i_m)=b*lobatto(z,D_con(:,i_m).*z'.^2,w);

end

%Numerical ingration across the length of the element

f_int(3:6,1)=[gaussi(L_el,B_w_1.*(-(M_con+n_bars*As_i*z_i*s_si)),...
                w_gauss');
              gaussi(L_el,B_w_2.*(-(M_con+n_bars*As_i*z_i*s_si)),...
                w_gauss');
```

```
              gaussi(L_el,B_w_3.*(-(M_con+n_bars*As_i*z_i*s_si)),...
                w_gauss');
              gaussi(L_el,B_w_4.*(-(M_con+n_bars*As_i*z_i*s_si)),...
                w_gauss')];

%-----------------------------------------------------------------

%f_int_di
%-----------------------------------------------------------------

[t_di,D_ti]=b_slip(delta_i,ne_x,f_c);

%Numerical ingration across the length of the element

f_int(7:8,1)=[gaussi(L_el,B_di(1,1)*n_bars*As_i*s_si+N_di_1.*t_di*...
s_i*n_bars,w_gauss');
              gaussi(L_el,B_di(1,2)*n_bars*As_i*s_si+N_di_2.*t_di*...
          s_i*n_bars,w_gauss')];

%-----------------------------------------------------------------

%Tangent stiffness matrix
%-----------------------------------------------------------------

%Numerical integration along the height of the cross-section

dN_con=b*trapz(z,D_con);

%Numerical ingration across the length of the element

K_u0u0=B_u0'*gaussi(L_el,(dN_con+n_bars*As_i*D_si),w_gauss')*B_u0;

%Numerical ingration across the length of the element

K_u0w(1,1)=gaussi(L_el,B_u0(1,1)*(-(dM_con+n_bars*As_i*z_i*D_si))...
*B_w_1,w_gauss');
K_u0w(1,2)=gaussi(L_el,B_u0(1,1)*(-(dM_con+n_bars*As_i*z_i*D_si))...
.*B_w_2,w_gauss');
K_u0w(2,1)=gaussi(L_el,B_u0(1,2)*(-(dM_con+n_bars*As_i*z_i*D_si))...
    .*B_w_1,w_gauss');
K_u0w(2,2)=gaussi(L_el,B_u0(1,2)*(-(dM_con+n_bars*As_i*z_i*D_si))...
    .*B_w_2,w_gauss');
K_u0w(1,3)=gaussi(L_el,B_u0(1,1)*(-(dM_con+n_bars*As_i*z_i*D_si))...
    .*B_w_3,w_gauss');
K_u0w(2,3)=gaussi(L_el,B_u0(1,2)*(-(dM_con+n_bars*As_i*z_i*D_si))...
    .*B_w_3,w_gauss');
K_u0w(1,4)=gaussi(L_el,B_u0(1,1)*(-(dM_con+n_bars*As_i*z_i*D_si))...
    .*B_w_4,w_gauss');
K_u0w(2,4)=gaussi(L_el,B_u0(1,2)*(-(dM_con+n_bars*As_i*z_i*D_si))...
    .*B_w_4,w_gauss');

%Numerical ingration across the length of the element

K_u0di=B_u0'*gaussi(L_el,n_bars*As_i*D_si,w_gauss')*B_di;

K_wu0=K_u0w';  %Exploit symmetry of the tangent stiffness matrix
```

```
%Numerical ingration across the length of the element

K_ww(1,1)=gaussi(L_el,B_w_1.*(z_dM_con+n_bars*As_i*z_i^2*D_si)...
    .*B_w_1,w_gauss');
K_ww(1,2)=gaussi(L_el,B_w_1.*(z_dM_con+n_bars*As_i*z_i^2*D_si)...
    .*B_w_2,w_gauss');
K_ww(1,3)=gaussi(L_el,B_w_1.*(z_dM_con+n_bars*As_i*z_i^2*D_si)...
    .*B_w_3,w_gauss');
K_ww(1,4)=gaussi(L_el,B_w_1.*(z_dM_con+n_bars*As_i*z_i^2*D_si)...
    .*B_w_4,w_gauss');
K_ww(2,1)=K_ww(1,2);
K_ww(2,2)=gaussi(L_el,B_w_2.*(z_dM_con+n_bars*As_i*z_i^2*D_si)...
    .*B_w_2,w_gauss');
K_ww(2,3)=gaussi(L_el,B_w_2.*(z_dM_con+n_bars*As_i*z_i^2*D_si)...
    .*B_w_3,w_gauss');
K_ww(2,4)=gaussi(L_el,B_w_2.*(z_dM_con+n_bars*As_i*z_i^2*D_si)...
    .*B_w_4,w_gauss');
K_ww(3,1)=K_ww(1,3);
K_ww(3,2)=K_ww(2,3);
K_ww(3,3)=gaussi(L_el,B_w_3.*(z_dM_con+n_bars*As_i*z_i^2*D_si)...
    .*B_w_3,w_gauss');
K_ww(3,4)=gaussi(L_el,B_w_3.*(z_dM_con+n_bars*As_i*z_i^2*D_si)...
    .*B_w_4,w_gauss');
K_ww(4,1)=K_ww(1,4);
K_ww(4,2)=K_ww(2,4);
K_ww(4,3)=K_ww(3,4);
K_ww(4,4)=gaussi(L_el,B_w_4.*(z_dM_con+n_bars*As_i*z_i^2*D_si)...
    .*B_w_4,w_gauss');

%Numerical integration across the length of the element

K_diw(1,1)=gaussi(L_el,B_di(1,1)*(-z_i*n_bars*As_i*D_si)...
    .*B_w_1,w_gauss');
K_diw(1,2)=gaussi(L_el,B_di(1,1)*(-z_i*n_bars*As_i*D_si)...
    .*B_w_2,w_gauss');
K_diw(1,3)=gaussi(L_el,B_di(1,1)*(-z_i*n_bars*As_i*D_si)...
    .*B_w_3,w_gauss');
K_diw(1,4)=gaussi(L_el,B_di(1,1)*(-z_i*n_bars*As_i*D_si)...
    .*B_w_4,w_gauss');
K_diw(2,1)=gaussi(L_el,B_di(1,2)*(-z_i*n_bars*As_i*D_si)...
    .*B_w_1,w_gauss');
K_diw(2,2)=gaussi(L_el,B_di(1,2)*(-z_i*n_bars*As_i*D_si)...
    .*B_w_2,w_gauss');
K_diw(2,3)=gaussi(L_el,B_di(1,2)*(-z_i*n_bars*As_i*D_si)...
    .*B_w_3,w_gauss');
K_diw(2,4)=gaussi(L_el,B_di(1,2)*(-z_i*n_bars*As_i*D_si)...
    .*B_w_4,w_gauss');

%Numerical integration across the length of the element

K_wdi=K_diw';

%Numerical integration across the length of the element

K_diu0=K_u0di';
```

```
    %Numerical integration across the length of the element

    K_didi(1,1)=gaussi(L_el,B_di(1,1)*n_bars*As_i*D_si*B_di(1,1)...
        +N_di_1.*D_ti.*N_di_1*s_i*n_bars,w_gauss');
    K_didi(1,2)=gaussi(L_el,B_di(1,1)*n_bars*As_i*D_si*B_di(1,2)...
        +N_di_1.*D_ti.*N_di_2*s_i*n_bars,w_gauss');
    K_didi(2,1)=gaussi(L_el,B_di(1,2)*n_bars*As_i*D_si*B_di(1,1)...
        +N_di_2.*D_ti.*N_di_1*s_i*n_bars,w_gauss');
    K_didi(2,2)=gaussi(L_el,B_di(1,2)*n_bars*As_i*D_si*B_di(1,2)...
        +N_di_2.*D_ti.*N_di_2*s_i*n_bars,w_gauss');

    %Assemble the element tangent stiffness matrix

    Ke=[K_u0u0  K_u0w  K_u0di;
        K_wu0   K_ww   K_wdi;
        K_diu0  K_diw  K_didi];

    %Assemble the element matrices into the global one

    [K,F_int]=assem(Edof(i,:),K,Ke,F_int,f_int);

    ec_out=[ec_out ec]; x_el_out=[x_el_out x(i,:)]; slip=[slip delta_i];
    steel=[steel s_si]; e_cr_new=[e_cr_new e_cr_nytt];
    s_concrete=[s_concrete s_xx_con]; M=[M M_con+n_bars*As_i*z_i*s_si];
end
end
```

```
%
% [F_ext]=f_external(q,Edof,L_el,num_el)
%
%
%-------------------------------------------------------------------------
% PURPOSE
%  Compute the effect on the degrees of freedom in a beam element from a
%  uniformly distributed load
%
% INPUT:  q                  uniformly distributed load
%         Edof               topology matrix
%         L_el               length of the element
%         num_el             number of elements
%
% OUTPUT: F_ext              the full external force vector from the load
%-------------------------------------------------------------------------
%
%Written by: Dimosthenis Floros and Olafur Agust Ingason
%
%-------------------------------------------------------------------------

function [F_ext]=f_external(q,Edof,L_el,num_el)

F_ext=zeros(max(max(Edof)),1);
f_ext=zeros(8,1);

for k=1:num_el

    f_ext(3,1)=1/2*q*L_el;
    f_ext(4,1)=1/12*q*L_el^2;
    f_ext(5,1)=1/2*q*L_el;
    f_ext(6,1)=-1/12*q*L_el^2;

    F_ext(Edof(k,2:end))=F_ext(Edof(k,2:end))+f_ext;
end

end
```

```
%
% [t_di,D_ti]=b_slip(delta_i,ne_x,f_c)
%
%-------------------------------------------------------------------------
% PURPOSE
%  Compute the shear stress and stiffness in the interface between concrete
%  and reinforcement steel. This model is adopted from FIB model code from
%  2010
%
% INPUT:  delta_i            the slip in the integration points
%         ne_x               number of integration points along the beam
%         f_c                characteristic compressive strength
%
% OUTPUT: t_di               shear stress in interface
%         D_ti               tangent stiffness in interface
%-------------------------------------------------------------------------
%
%Written by: Dimosthenis Floros and Olafur Agust Ingason
%
%-------------------------------------------------------------------------

function [t_di,D_ti]=b_slip(delta_i,ne_x,f_c)

%Model constants for the definition of the curve
%-----------------------------------------------

s0=20e-5;               %To this point the constituitive is linear
s1=0.001;               %Constants from FIB model code for good bond
s2=0.002;
s3=0.009;
a=0.4;
t_max=2.5*sqrt(f_c/1e6)*1e6; %Maximum shear stress in interface
t_f=0.4*sqrt(f_c/1e6)*1e6;   %Final shear stress in interface

%-----------------------------------------------

t_di=zeros(1,ne_x);
D_ti=zeros(1,ne_x);

K_fake=(t_max*abs(s0)^a/s1^a)/s0;


for j=1:ne_x

    %Linear branch of the curve
    if abs(delta_i(1,j))>=0 && abs(delta_i(1,j))<=s0

        t_di(1,j)=K_fake*delta_i(j);
        D_ti(1,j)=K_fake;

        %Non-linear part of the curve
        %-----------------------------------------
    elseif  abs(delta_i(1,j))>s0 && abs(delta_i(1,j))<=s1

        t_di(1,j)=delta_i(j)/abs(delta_i(j))*(t_max*abs(delta_i(1,j))...
            ^a/s1^a);
```

```
        D_ti(1,j)=delta_i(j)/abs(delta_i(j))*(a*t_max/s1^a*...
            abs(delta_i(1,j))^(a-1));



    %-------------------------------------------

    %Higher plateau of the curve
    %-------------------------------------------

    elseif abs(delta_i(1,j))>s1  && abs(delta_i(1,j))<=s2

           t_di(1,j)=delta_i(j)/abs(delta_i(j))*t_max;
           D_ti(1,j)=0;

    %-------------------------------------------

    %Linear degrading part of the curve
    %-------------------------------------------

    elseif abs(delta_i(1,j))>s2  && abs(delta_i(1,j))<=s3

           t_di(1,j)=delta_i(j)/abs(delta_i(j))*(t_max-(t_max-t_f)...
               *(abs(delta_i(1,j))-s2)/(s3-s2));
           D_ti(1,j)=(t_max-t_f)/(s2-s3);

    %-------------------------------------------

    %Lower plateau of the curve
    %-------------------------------------------

    elseif abs(delta_i(1,j))>s3

           t_di(1,j)=delta_i(j)/abs(delta_i(j))*t_f;
           D_ti(1,j)=0;

    end

end
```

```
%
% [s_si,D_si]=sigma_si(es,Es,fy,ne_x)
%
%-------------------------------------------------------------------------
% PURPOSE
%  Compute the steel stress and tangent stiffness from steel strains
%  2010
%
% INPUT:  es                  steel strains in an element
%         ne_x                number of integration points along the beam
%         fy                  characteristic yield strength
%         Es                  Youngs modulus
%
% OUTPUT: s_si                steel stress
%         D_si                tangent stiffness for the steel
%-------------------------------------------------------------------------
%
%Written by: Dimosthenis Floros and Olafur Agust Ingason
%
%-------------------------------------------------------------------------

function [s_si,D_si]=sigma_si(es,Es,fy,ne_x)

s_si=zeros(1,ne_x);
D_si=zeros(1,ne_x);

for j=1:ne_x

    %Elastic part of the curve
    %------------------------------

    if es(1,j)>=0 && es(1,j)<=fy/Es

       s_si(1,j)=Es*es(1,j);
       D_si(1,j)=Es;
    %------------------------------

    %Plastic part of the curve
    %-------------------------

    elseif es(1,j)>fy/Es

           s_si(1,j)=fy;
           D_si(1,j)=0;

    %-------------------------

    end
end
```

```
%
% [s_xx_con,D_con,e_cr_new]=sigma_xx_con(ne_x,ne_z,ec,Ec,e_t...
% ,f_t,f_c,L_el,G_f,e_cr_old)
%
%------------------------------------------------------------------------
% PURPOSE
%  Compute element stress and tangent stiffness from a given total strain
%  values
%
% INPUT:  ne_x               number of integration point along length
%         ne_z               number of integration points over height
%         ec                 total strain
%         Es             concrete stiffness
%     e_t            cracking strain
%         f_t                tensile strength
%         f_c            compressive strength
%         L_el               length of the element
%         G_f            fracture energy
%     e_cr_old           highest cracking strain in each Gauss point
%
% OUTPUT: s_xx_con           concrete stress
%         D_con              Tangent stiffness
%         e_cr_new           new cracking strain
%
%------------------------------------------------------------------------
%
%Written by: Dimosthenis Floros and Olafur Agust Ingason
%
%------------------------------------------------------------------------
function [s_xx_con,D_con,e_cr_new]=sigma_xx_con(ne_x,ne_z,ec,Ec,e_t...
,f_t,f_c,L_el,G_f,e_cr_old)

%Material constants for concrete
%-------------------------------

e_f=5.136*G_f/(L_el*f_t);

k=1.81;
ec1=-2.366*10^(-3);
ec_lim=-3.5*10^(-3);

e_cr_new=zeros(size(e_cr_old));

%-------------------------------

s_xx_con=zeros(ne_z,ne_x);
D_con=zeros(ne_z,ne_x);

for j=1:ne_x     %Loop for i.p. along the length of the i-st element

    for i_z=1:ne_z %Loop for i.p. along the height of the cross-section

        e_cr=0;

        %Linear tensile part of the curve
        %--------------------------------
```

```
if ec(i_z,j)>=0 && ec(i_z,j)<=e_t && e_cr_old(i_z,j)==0

    s_xx_con(i_z,j)=Ec*ec(i_z,j);
    D_con(i_z,j)=Ec;

    %--------------------------------

    %Tension softening part of the curve
    %--------------------------------

elseif (ec(i_z,j)>e_t && ec(i_z,j)<=e_f) || (ec(i_z,j)>=0 ...
    && ec(i_z,j)<=e_t && e_cr_old(i_z,j)>0)

    e_cr=1e-2; %initial guess

    %'Hordjik' curve in local coordinates

    [f_cr,D_c]=hordjik(e_cr,e_cr_old(i_z,j),e_f,f_t);

    %Out-of-balance force function

    g_c=Ec*ec(i_z,j)-Ec*e_cr-f_cr;

    Error_cr=norm(g_c);    %Evaluate the error

    n_cr=0;                %Counter of iterations

    while Error_cr>10^(-8) %Iterations' loop

        J_cr=-Ec-D_c;    %Tangent stiffness function

        De_cr=-J_cr\g_c; %Solve g(e_cr+De_cr) for e_cr

        e_cr=e_cr+De_cr;  %Update the cracking strain e_cr

        [f_cr,D_c]=hordjik(e_cr,e_cr_old(i_z,j),e_f,f_t);

        g_c=Ec*(ec(i_z,j)-e_cr)-f_cr; %Calculate the new
        %o-o-b force function

        Error_cr=norm(g_c); %Evaluate the error

        n_cr=n_cr+1;        %Add one step

    end
    %Material tangent stiffness in Global coordinates
    D=Ec-Ec*(Ec+D_c)^(-1)*Ec;


    %Cracked concrete stress in total deformation
    s_xx_con(i_z,j)=Ec*(ec(i_z,j)-e_cr);

    D_con(i_z,j)=D;

    %--------------------------------------
```

```
            %Stress for strains over the ultimate strain e_f
            %-----------------------------------------------

        elseif ec(i_z,j)>e_f

            s_xx_con(i_z,j)=0;
            D_con(i_z,j)=0;

            e_cr=e_f;

            %-----------------------------------------------

            %Compressive part of the curve
            %-------------------------------------

        elseif ec(i_z,j)<0 && abs(ec(i_z,j))<=abs(ec_lim)

            s_xx_con(i_z,j)=-f_c*(k*ec(i_z,j)/ec1-ec(i_z,j)^2/ec1^2)...
            /(1+(k-2)*ec(i_z,j)/ec1);
            D_con(i_z,j)=f_c*((k/abs(ec1)-2*abs(ec(i_z,j))/ec1^2)...
            *(1+(k-2)*ec(i_z,j)/ec1)-(k*ec(i_z,j)/ec1-ec(i_z,j)^2/ec1^2)...
            *(k-2)/abs(ec1))/(1+(k-2)*ec(i_z,j)/ec1)^2;

        elseif ec(i_z,j)<0 && abs(ec(i_z,j))>abs(ec_lim)

            s_xx_con(i_z,j)=0;
            D_con(i_z,j)=0;


        end

        e_cr_new(i_z,j)=e_cr;

    end

end
end
```

```
%
% [f_cr,D_c]=hordjik(e_cr,e_cr_old,e_f,f_t)
%
%------------------------------------------------------------------------
% PURPOSE
%  Compute element post cracking stress, from a Hordjik tension softening,
%  from a given cracking strain. Has a damage history variable for a secant
%  damage model from the highest provious converged strain.
%
%
% INPUT:  e_cr               cracking strain
%         e_cr_old           highest previously converged strain
%         e_f                minimum strain to give tensile stress
%         f_t                tensile strength
%
% OUTPUT: f_cr               stress
%         D_c                Tangent stiffness
%------------------------------------------------------------------------
%
%Written by: Dimosthenis Floros and Olafur Agust Ingason
%
%------------------------------------------------------------------------

function [f_cr,D_c]=hordjik(e_cr,e_cr_old,e_f,f_t)

c1=3;                           %Constants of the Hordjik curve
c2=6.93;

%Checks if cracking strain is larger then previous value
if e_cr<e_cr_old
    f_cr=e_cr/e_cr_old*(f_t*((1+(c1*e_cr_old/e_f)^3)*exp(-c2*e_cr_old/e_f)-...
        exp(-c2)*(1+c1^3)*e_cr_old/e_f));
    D_c=1/e_cr_old*(f_t*((1+(c1*e_cr_old/e_f)^3)*exp(-c2*e_cr_old/e_f)-...
        exp(-c2)*(1+c1^3)*e_cr_old/e_f));
elseif e_cr>=e_cr_old
    f_cr=f_t*((1+(c1*e_cr/e_f)^3)*exp(-c2*e_cr/e_f)-...
        exp(-c2)*(1+c1^3)*e_cr/e_f);
    D_c=f_t*((3*c1^3*exp(-c2*e_cr/e_f)*e_cr^2/e_f^3)-...
        ((1+c1^3)*exp(-c2)/e_f)-(c2*exp(-c2*e_cr/e_f)*...
        (1+c1^3*e_cr^3/e_f^3)/e_f));
end

end
```